1-1-1997

Spectroscopic studies of short/long range ordering in polymers.

Bert Chien
University of Massachusetts Amherst

SPECTROSCOPIC STUDIES OF SHORT/LONG RANGE ORDERING IN POLYMERS

A Dissertation Presented

by

BERT CHIEN

Submitted to the Graduate School of the
University of Massachusetts Amherst in partial fulfillment
of the requirements for the degree of

DOCTOR OF PHILOSOPHY

September 1997

Department of Polymer Science and Engineering

SPECTROSCOPIC STUDIES OF SHORT/LONG RANGE ORDERING IN POLYMERS

A Dissertation Presented

by

BERT CHIEN

Approved as to style and content by:

Shaw Ling Hsu, Chair

C. Peter Lillya, Member

William J. MacKnight, Member

Howard D. Stidham, Member

Richard J. Farris, Department Head
Polymer Science and Engineering

ACKNOWLEDGMENTS

I would like to acknowledge the support and guidance provided by my advisor, Professor Shaw Ling Hsu, throughout the course of my research. I am very grateful to him for the opportunity provided to me. I would also like to thank my other committee members Professor C. Peter Lillya, Professor William J. MacKnight and Professor Howard D. Stidham.

I am especially thankful to all of the members of my research group. In particular, I express appreciation to Thomas Hahn, Gregory Martin, Yuan Ren, Sophie Riou, Zhaohui Su, Hun-Jan Tao and Dorie Yontz for the many helpful scientific discussions and experimental assistance. I would also like to give special thanks to Georg Maxein from the University of Mainz for his many suggestions.

Many people in and outside of the polymer science department have made my stay in Amherst very enjoyable. I would especially like to mention Michael Chen, Darius Deak, Wendy Petka, Darrin Pochan, Shalabh Tandon and Meredith White. They have been great friends and have really made things fun.

Lastly, I am indebted to my family for their love and support throughout the years. They have always been a great source of encouragement and inspiration.

ABSTRACT

SPECTROSCOPIC STUDIES OF SHORT/LONG RANGE ORDERING IN POLYMERS

SEPTEMBER 1997

BERT CHIEN, B.S., UNIVERSITY OF MICHIGAN

Ph.D., UNIVERSITY OF MASSACHUSETTS AMHERST

Directed by: Professor Shaw Ling Hsu

The work presented in this thesis is divided into three chapters. In Chapter 1 a general overview is presented of short/long range ordering in polymers. Chapter 2 then discusses the use of vibrational spectroscopy to probe the short range conformational order present in a series of Langmuir films at the air-water interface. Finally, the use of vibrational spectroscopy to probe the long range conformational order in a bulk polymer, poly(β-hydroxybutyrate) is presented in Chapter 3.

Using external reflection infrared spectroscopy, we were able to directly characterize the structure of series of "hairy-rod" polymers at the air-water interface. The overall structure of the films were related to the short range conformational order of long side groups attached to the rigid-rod backbones. The structure of the films were also studied as a function of surface packing density at the air-water interface by the use of a Langmuir trough coupled directly to the external reflection infrared spectroscopy setup.

A Raman active longitudinal acoustic mode capable of probing the long range conformational order associated with crystalline regions was discovered for the biodegradable thermoplastic, poly(β-hydroxybutyrate). The dependence of this mode on the fold length of crystalline lamella was clearly established. The annealing behavior of single crystals of poly(β-hydroxybutyrate) was also studied.

TABLE OF CONTENTS

LIST OF TABLES

LIST OF FIGURES

CHAPTER 1

INTRODUCTION

1.1 Short Range/Long Range Chain Segmental Order

Given that the macroscopic properties of polymers are often directly related to their chemical structure and the subsequent levels of microstructural organization, microstructural characterization at the molecular chain segmental level can often be of both fundamental and practical importance. Two examples illustrative of this are highly drawn fibers of polymers such as polyethylene, and ionically conductive polymer electrolytes. For highly drawn polyethylene fibers, performance is dependent on the length and perfection of extended chain segments where in the ideal case the modulus along the fiber axis would correspond with the theoretical modulus of an extended chain.[1-3] For some ionically conductive polymer electrolytes, on the other hand, it is not the long range chain segmental order which is important but instead the short range chain structure that is important for the conduction mechanism.[4-6] In both examples the chain segmental structure is important in determining macroscopically observed properties, high modulus in the first case and ionic conductivity in the other. However, both examples are also illustrative of the different length scales of chain order, long range versus short range structure, that can be important for different polymer systems. The focus of this work addresses this issue and involves the microstructural characterization of two systems, one exhibiting long range order and the other short range order.

Vibrational spectroscopy is an ideal technique with which to make such studies. To begin with, vibrational spectroscopy is extremely sensitive to the molecular structure of polymers. As such, it can provide information on both the long range chain segmental order present for some systems, e.g. highly ordered systems, as well as the short range

chain segmental order in more disordered systems. Orientational order may also be obtained. Additionally, due to the specificity of bands in the vibrational spectra of a given system, analysis can often be focused on specific functional groups as well as chain segments, e.g. main chain versus side groups. Given this type of structural information, it is also important to point out that vibrational spectroscopy is a versatile technique capable of characterizing a wide range of samples. Systems can range from polymers in solution, to bulk polymers to polymer thin films and polymer interfaces. Part of this can be attributed to the fact that vibrational spectroscopy is adaptable to a number of experimental geometries. Specific techniques include standard transmission infrared spectroscopy[7] and Raman scattering geometries,[7] attenuated total reflection infrared spectroscopy (ATR),[7,8] surface enhanced Raman scattering,[8] and external reflection infrared spectroscopy at air-solid interfaces[9-11] as well as more recently air-liquid interfaces.[12-17]

Using vibrational spectroscopy as the primary tool, the two polymer systems studied were a series of "hairy-rod" polymers (Chapter 2) and a biodegradable thermoplastic polyester, poly(β-hydroxybutyrate) (Chapter 3). For Langmuir films of "hairy-rod" polymers, it will be shown that the short range conformational structure of long linear side groups is important in controlling the overall ordering of the "hairy-rod" molecules at the air-water interface. A recently designed experimental technique in our laboratory combining external reflection infrared spectroscopy and a Langmuir trough was used to study the films directly at the air-water interface. For the biodegradable thermoplastic polyester, a low frequency Raman technique using longitudinal acoustic modes is first established as a unique means to directly probe the long range conformational order associated with poly(β-hydroxybutyrate) chain folded lamella. An analysis of its chain folded structure and annealing behavior is then presented.

1.2 "Hairy-Rod" Langmuir Films

The Langmuir-Blodgett technique has received attention for quite a number of years since it was first developed and studied in the 1930s.[8,18] This attention has increased particularly in the last couple decades as the demands for highly ordered ultrathin films, particularly in the microelectronics and optoelectronics fields, has also increased. Polymers exhibiting a "hairy-rod" molecular architecture have shown the most potential for forming well ordered and controllable Langmuir-Blodgett films.[19-29] A schematic of a "hairy-rod" polymer is shown in Figure 1.1.

However, a quantitative understanding of the factors which actually control the quality of these films is far from complete. Although numerous studies have focused on the characterization of Langmuir-Blodgett films utilizing techniques such as neutron reflectivity,[21,23] x-ray reflectivity,[21,23] atomic force microscopy,[22,30] transmission electron microscopy,[31] surface plasmon spectroscopy[32] and waveguide spectroscopies,[27,28,33] studies of film microstructure directly at the air-water interface prior to Langmuir-Blodgett deposition have been very rare. This deficiency has greatly limited advances in Langmuir-Blodgett film technology. For films at the air-water interface, it is well known that their transferability onto solid substrates is greatly dependent on their surface packing density and subsequent structure at the air-water interface.[29] A quantitative understanding of the molecular design parameters and surface packing density of Langmuir films necessary to optimize the quality of transferred Langmuir-Blodgett films has therefore been difficult to achieve.

For "hairy-rod" polymers in particular, it has been proposed that the transferability and subsequent quality of such Langmuir and Langmuir-Blodgett films is dictated by the relative amount of conformational disorder present in the long *n*-alkyl side groups at the air-water interface.[19,20,29] In other words, the structure of these films has been predicted to be dependent on the short range chain segmental structure of the side groups. This, however, has been impossible to substantiate up until this present study. The reasons for

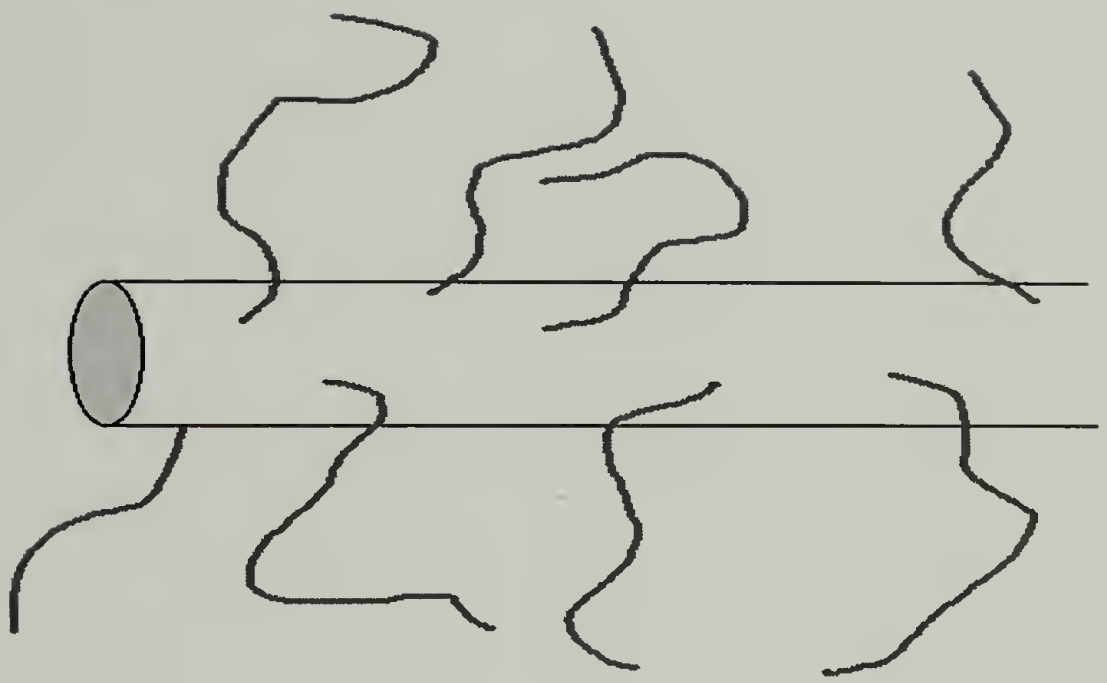

Figure 1.1 Schematic representation of a "hairy-rod" polymer.

this are the inherent difficulties associated with the study of films directly at the air-water interface. Techniques such as grazing incidence x-ray diffraction,[34] x-ray specular reflectivity,[35] neutron reflectivity[36] and fluorescence microscopy[37] while suitable for the study of some types of molecules at the air-water interface are insufficient for the study of most such films. None provide direct information on the relative amount of conformational order of polymer films, particularly for films not exhibiting crystalline order.

Being sensitive to chain segmental conformational structure, whether ordered or disordered, external reflection infrared spectroscopy at an air-water interface is not limited in this way. As a technique, it is capable of probing very small amounts of material, usually even monolayer films with surface packing densities less than that of a condensed or close packed monolayer.[38,39] Additionally, in our laboratory we have been able to couple such an external reflection infrared spectroscopy setup with a Langmuir trough. In Chapter 2 it will be described how the short range structure of *n*-alkyl side groups for a series of "hairy-rod" polymers affects the overall ordering of these Langmuir films. Using this experimental technique, the structure of the films will also be analyzed as a function of surface packing density at the air-water interface. A brief comparison of their microstructure at the air-water interface will then be made with studies on the microstructure of transferred Langmuir-Blodgett films of "hairy-rods" by other research groups.

1.3 Biodegradable Thermoplastic: Poly(β-hydroxybutyrate)

As was mentioned previously, vibrational spectroscopy is a technique that is not only sensitive to short range chain segmental structure. Using longitudinal acoustic modes which are present in the Raman spectra of some polymers, one can directly probe the long range conformational structure of ordered chain segments. Longitudinal acoustic modes are sensitive to the length of conformationally ordered chain segments.

Specifically, in the ideal case one can explicitly measure the ordered segment length distribution associated with polymers exhibiting longitudinal acoustic modes. From a morphological and experimental standpoint, this type of direct structural information on ordered chain segments provided by this Raman technique is unique from other experimental techniques presently available and has been especially useful in the study of crystalline regions (e.g. crystallite size and distribution, chain folding behavior, annealing) of chain folding semicrystalline polymers.[40-42]

However, the primary difficulty associated with longitudinal acoustic modes lies in the fact that until this study, longitudinal acoustic modes were only found in polymers exhibiting simple structures. Subsequently, although its potential as a unique morphological tool is great, the actual use of this Raman technique had been limited to a relatively small number of polymers with *polyethylene-like* structures. In Chapter 3, it will then be discussed how a longitudinal acoustic mode is established for the first time in a polymer, poly(β-hydroxybutyrate), with a structure significantly more complicated that other polymers previously found to exhibit a longitudinal acoustic mode (Figure 1.2).[40] This is significant not only from the aspect of better understanding longitudinal acoustic modes, but also because poly(β-hydroxybutyrate) is biodegradable and of commercial interest. These Raman studies were carried out in conjunction with small-angle x-ray experiments. This discussion will then be followed by a brief analysis of the annealing behavior of poly(β-hydroxybutyrate).

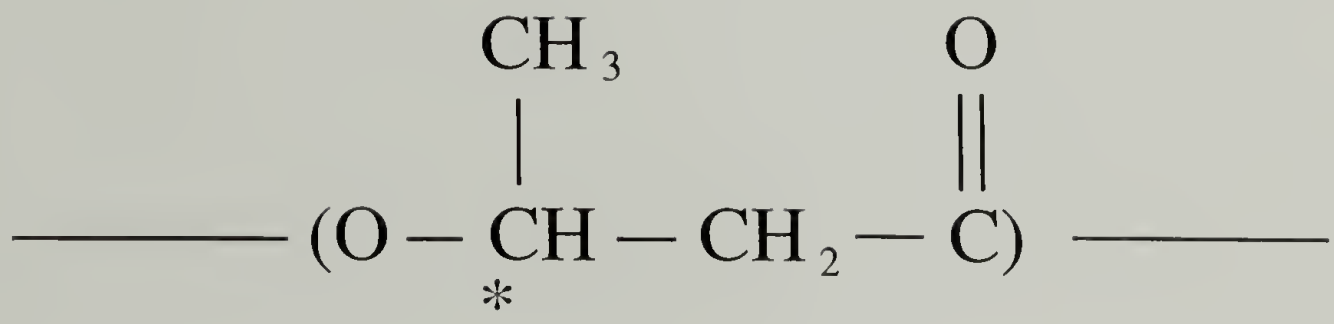

Figure 1.2 Chemical structure of poly(β-hydroxybutyrate).

References

(1) Porter, R. S.; Wang, L. *J. Macromol. Sci.-Rev.* **1995**, *C35(1)*, 63.

(2) Zachariades, A. E.; Mead, W. T.; Porter, R. S. *Chem. Rev.* **1980**, *80*, 351.

(3) Wang, Y.; Waldman, D.; Lasch, J.; Stein, R. S.; Hsu, S. L. *Macromolecules* **1982**, *15*, 1452.

(4) Frech, R.; Manning, J.; Teeters, D.; Black, B. E. *Polymer* **1988**, *60*, 1785.

(5) Schantz, S.; Torell, L. M.; Stevens, J. R. *J. Appl. Phys.* **1988**, *64*, 2038.

(6) Yoon, S. Thesis, University of Massachusetts, 1995.

(7) Bower, D. I.; Maddams, W. F. *The Vibrational Spectroscopy of Polymers*; Cambridge Univeristy Press: Great Britain, 1989.

(8) Ulman, A. *An Introduction to Ultrathin Organic Films*; Academic Press: Boston, 1991.

(9) Allara, D. L.; Nuzzo, R. G. *Langmuir* **1985**, *1*, 45.

(10) Allara, D. L.; Nuzzo, R. G. *Langmuir* **1985**, *1*, 52.

(11) Mumby, S. J. *Macromolecules* **1986**, *19*, 1054.

(12) Buontempo, J. T.; Rice, S. A. *J. Chem. Phys.* **1993**, *98*, 5835.

(13) Buontempo, J. T.; Rice, S. A.; Karaborni, S.; Siepmann, J. I. *Langmuir* **1993**, *9*, 1604.

(14) Buontempo, J. T.; Rice, S. A. *J. Chem. Phys.* **1993**, *98*, 5825.

(15) Dluhy, R. A.; Wright, N. A.; Griffiths, P. R. *Appl. Spectros.* **1988**, *42*, 138.

(16) Dluhy, R. A.; Mitchell, M. L.; Pettenski, T.; Beers, J. *J. Appl. Spectrosc.* **1988**, *42*, 1289.

(17) Gericke, A.; Simon-Kutscher, J.; Huehnerfuss, H. *Langmuir* **1993**, *9*, 2119.

(18) Roberts, G. *Langmuir-Blodgett Films*; Plenum Press: New York, 1990.

(19) Wegner, G. *Thin Solid Films* **1992**, *216*, 105.

(20) Wegner, G. *Ber. Bunsenges. Phys. Chem.* **1991**, *95*, 1326.

(21) Vierheller, T. R.; Foster, M. D.; Schmidt, A.; Mathauer, K.; Knoll, W.; Wegner, G.; Satija, S.; Majkrzak, C. F. *Macromolecules* **1994**, *27*, 6893.

(22) Tsukruk, V. V.; Foster, M. D.; Reneker, D. H.; Schmidt, A.; Wu, H.; Knoll, W. *Macromolecules* **1994**, *27*, 1274.

(23) Schmidt, A.; Mathauer, K.; Reiter, G.; Foster, M. D.; Stamm, M.; Wegner, G.; Knoll, W. *Langmuir* **1994**, *10*, 3820.

(24) Schwiegk, S.; Vahlenkamp, T.; Xu, Y.; Wegner, G. *Macromolecules* **1992**, *25*, 2513.

(25) Menzel, H.; Weichart, B.; Hallensleben, M. L. *Thin Solid Films* **1993**, *223*, 181.

(26) Menzel, H.; Hallensleben, M. L.; Schmidt, A.; Knoll, W.; Fischer, T.; Stumpe, J. *Macromolecules* **1993**, *26*, 3644.

(27) Mathy, A.; Mathauer, K.; Wegner, G.; Bubeck, C. *Thin Solid Films* **1992**, *215*, 98.

(28) Mathauer, K.; Mathy, A.; Bubeck, C.; Wegner, G. *Thin Solid Films* **1992**, *210/211*, 449.

(29) Duda, G.; Schouten, A. J.; Arndt, T.; Lieser, G.; Schmidt, G. F.; Bubeck, C.; Wegner, G. *Thin Solid Films* **1988**, *159*, 221.

(30) Tsukruk, V. V.; Foster, M. D.; Reneker, D. H.; Schmidt, A.; Knoll, W. *Langmuir* **1993**, *9*, 3538.

(31) Yase, K.; Schwiegk, S.; Lieser, G.; Wegner, G. *Thin Solid Films* **1992**, *213*, 130.

(32) Menzel, H.; Hallensleben, M. L. *Polym. Bull.* **1991**, *27*, 89.

(33) Hickel, W.; Duda, G.; Jurich, M.; Krohl, T.; Rochford, K.; Stegeman, G. I.; Swalen, J. D.; Wegner, G.; Knoll, W. *Langmuir* **1990**, *6*, 1403.

(34) Weissbuch, I.; Leveiller, F.; Jacquemain, D.; Kjaer, K.; Als-Nielsen, J.; Leiserowitz, L. *J. Phys. Chem.* **1993**, *97*, 12858.

(35) Schwartz, D. K.; Schlossman, M. L.; Pershan, P. S. *J. Chem. Phys.* **1992**, *96*, 2356.

(36) Henderson, J. A.; Richards, R. W.; Penfold, J.; Thomas, R. K.; Lu, J. R. *Macromolecules* **1993**, *26*, 4591.

(37) Weis, R. M. *Chem. Phys. Lipids* **1991**, *57*, 227.

(38) Ren, Y.; Shoichet, M. S.; McCarthy, T. J.; Stidham, H. D.; Hsu, S. L. *Macromolecules* **1995**, *28*, 358.

(39) Ren, Y.; Meuse, C. W.; Hsu, S. L. *J. Phys. Chem.* **1994**, *98*, 8424.

(40) Chien, B. T.; Hsu, S. L.; Stidham, H. D. *Macromolecules* **1996**, *29*, 4247.

(41) Hsu, S. L.; Krimm, S.; Krause, S.; Yeh, G. S. Y. *J. Polym. Sci. Polym. Lett. Ed.* **1976**, *14*, 195.

(42) Schaufele, R. F.; Shimanouchi, T. *J. Chem. Phys.* **1967**, *47*, 3605.

CHAPTER 2

MICROSTRUCTURE OF "HAIRY-ROD" POLYMER FILMS AT THE AIR-WATER INTERFACE

2.1 Introduction

2.1.1 "Traditional" Langmuir-Blodgett Films

The Langmuir-Blodgett technique provides a relatively unique means by which supramolecular architectures of highly ordered layered assemblies of organic molecules may potentially be formed. Originally designed as a method to build up layered assemblies of simple long chain aliphatic carbonic acids and their salts, it was later extended as a means to produce supramolecular architectures useful for the study of intermolecular interactions and various photophysical and photochemical processes.[1,2] In those studies Langmuir-Blodgett films served as ordered matrices for probing the interactions between molecules via photon, electron, and proton transfer. A variety of other types of more fundamental research utilizing the supramolecular structure of Langmuir-Blodgett films have also been carried out. Another example is of Langmuir-Blodgett films of polymerized liposome structures which were studied as models for cell membranes[3] and as potential drug carriers.[4]

More recently with the heightened demand for well controlled ultrathin films from a variety of technologically important fields, Langmuir-Blodgett films have gained new prominence. Some potential applications that have been envisioned for Langmuir-Blodgett films include use as waveguides, insulators (e.g. in capacitor-type applications and as electrically insulating coatings for semiconductor device fabrication), chemical/biological sensors and membranes, resists for microlithography, for optical information storage and switches (e.g. using photochromic dyes which can be altered by

photochemically induced isomerization), piezoelectric, pyroelectric, and optoelectronic devices, in photonics, and to control the tribology of surfaces (e.g. in magnetic disks).[1-3,5-8]

The general principles of the Langmuir-Blodgett technique are relatively simple.[1,2] First, a monolayer film must be spread at the air-water interface of a Langmuir trough. Such a Langmuir film, as opposed to a transferred film called a Langmuir-Blodgett film, forms the basic unit of the building-up of the final multilayer film. "Traditional" Langmuir-Blodgett materials, as are shown schematically in Figure 2.1, derive their surface activity which allows them to be spread, compressed, and subsequently organized at the air-water interface, from their amphiphilic character; i.e., they are composed of a polar head group and a hydrophobic tail and are, in general, water insoluble. Prior to the actual deposition process, the monolayer at the air-water interface is compressed from the as-spread state where in general the film may be described as an expanded monolayer, i.e. large surface areas where the monolayer film resembles a two-dimensional gas. A general schematic of the various regions associated with a film at the air-water interface is shown in Figure 2.2. Idealized regions describing two-dimensional "solid", "liquid" and "gas"-like states are illustrated. It is upon the formation of a condensed monolayer, i.e. monolayer film resembling a two-dimensional liquid/solid, that the actual deposition step is usually carried out.

The most common form of Langmuir-Blodgett film deposition, called Y type deposition, is shown in Figure 2.3.[2] In this idealized schematic the substrate is hydrophilic and the first monolayer is transferred as the substrate is raised through the subphase (b). The substrate may either be placed in the subphase before the monolayer is spread, or following spreading lowered into the subphase through the compressed monolayer. As might be expected, the adhesion of the first layer to the substrate is particularly important for the production of multilayer films. A monolayer is subsequently deposited on each traversal of the surface (c). As shown in d, the

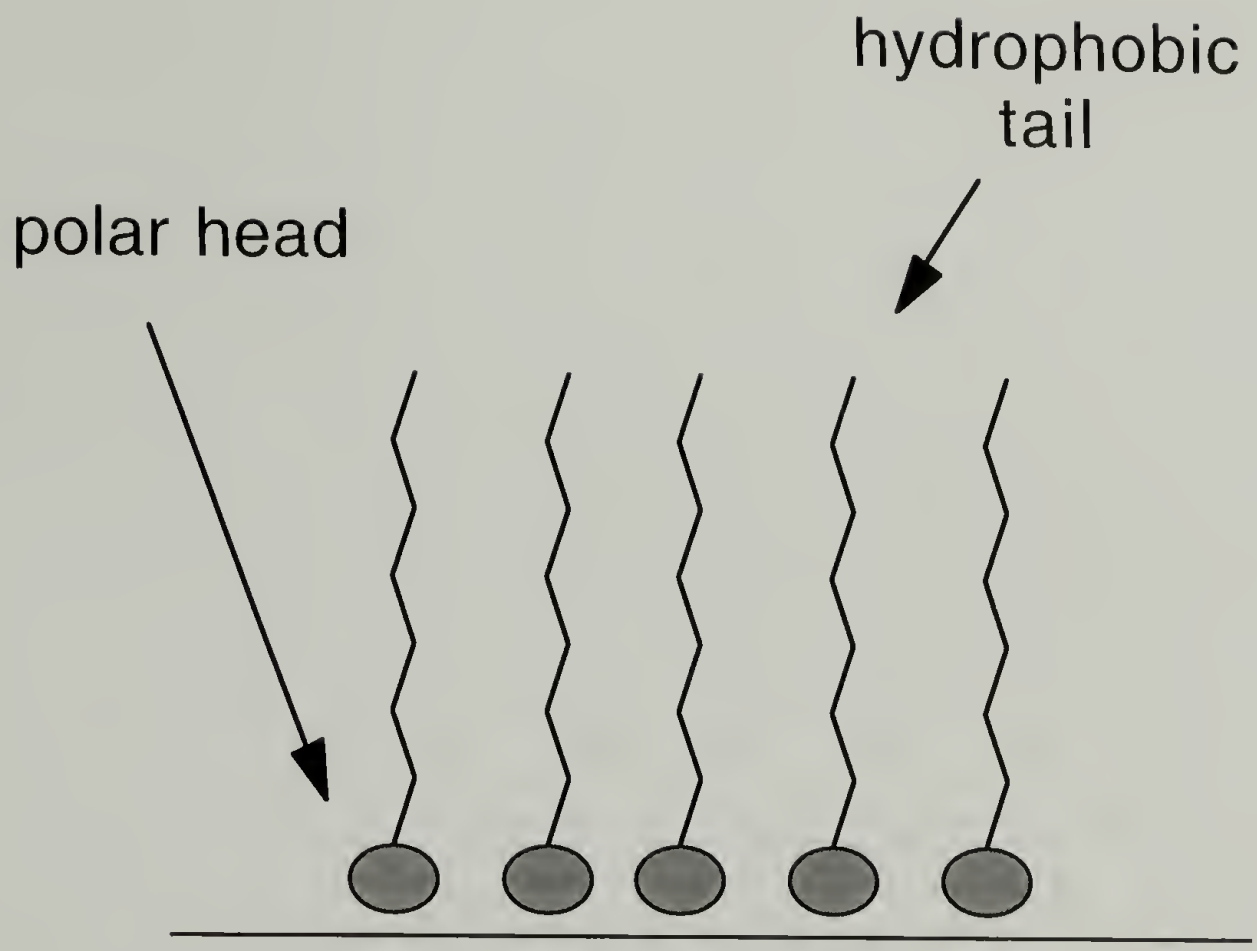

Figure 2.1 "Traditional" small molecule amphiphile at the air-water interface.

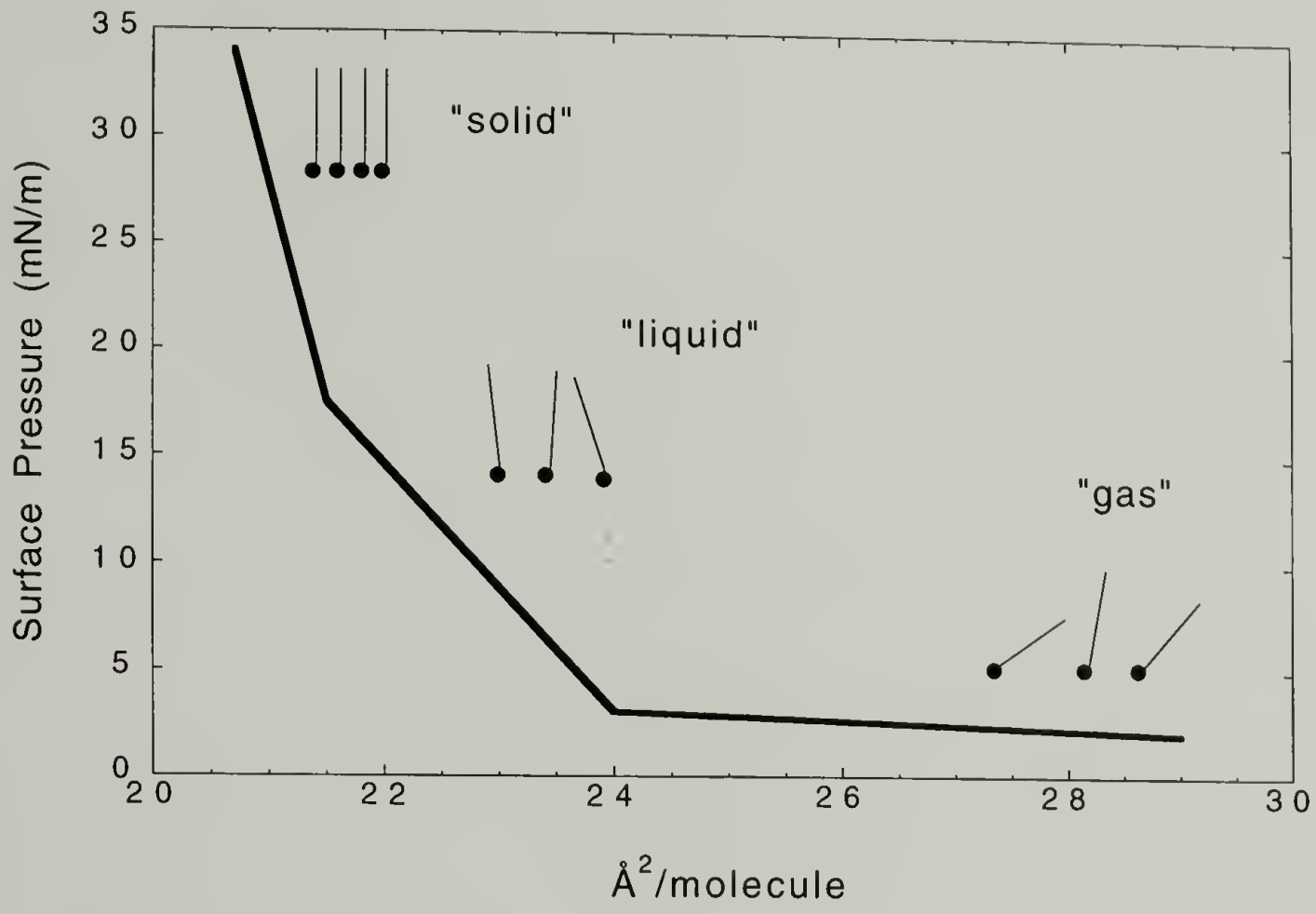

Figure 2.2 Schematic illustration of a surface pressure/area isotherm showing the idealized structure of a film at the air-water interface.

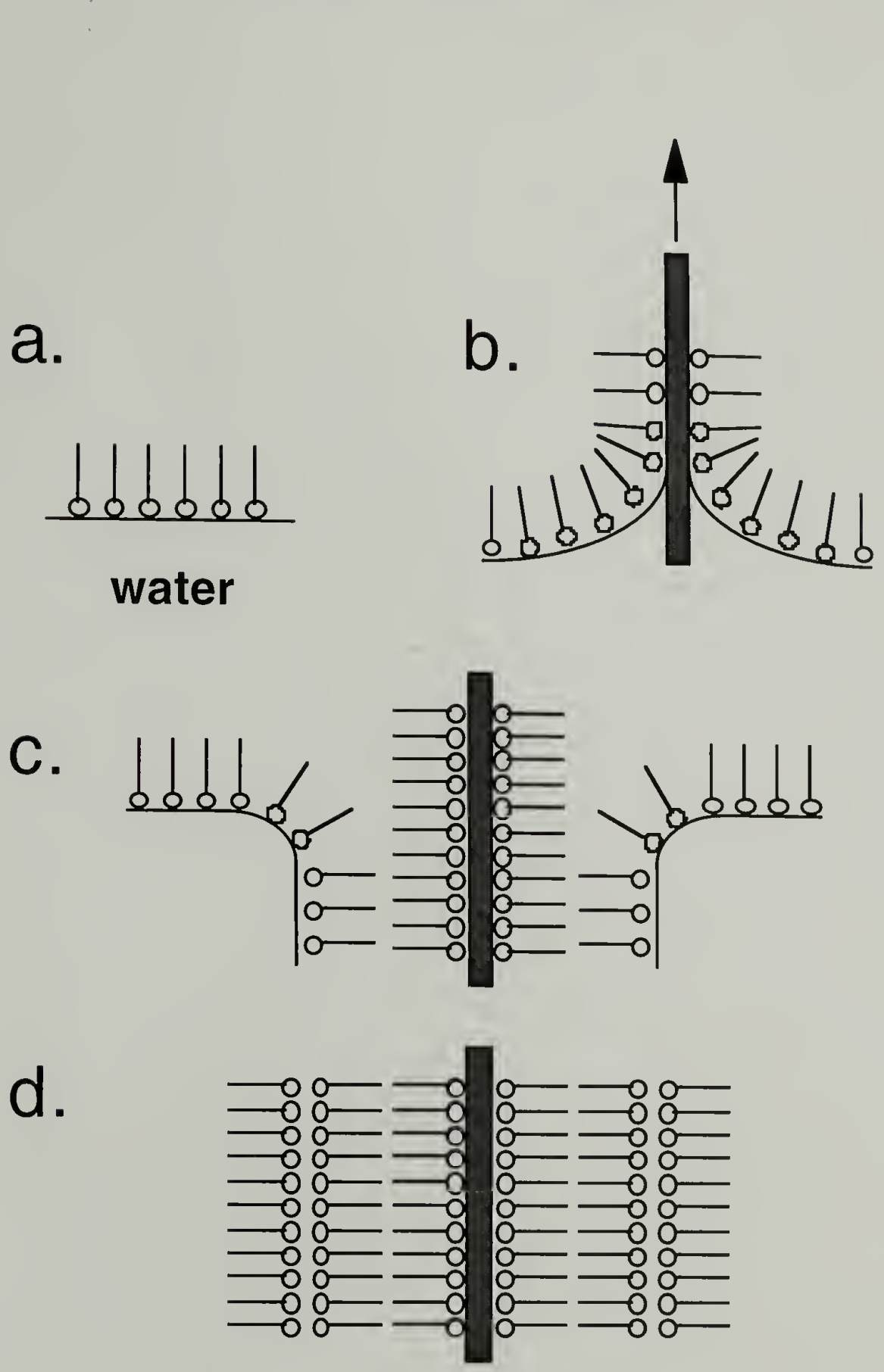

Figure 2.3 Langmuir-Blodgett transfer: Y-type deposition.

transferred layers ideally stack in a head-to-head and tail-to-tail configuration. If the solid substrate is hydrophobic a monolayer will be deposited as it is first lowered into the subphase; thus a Y type film containing an even number of monolayers can be fabricated.

Although films transferring in a Y-like deposition mode are the most common, monolayers which deposit only as the substrate is being inserted into the subphase or only as the substrate is being removed have been reported. These deposition modes are referred to as X type and Z type, respectively. Schematic diagrams for the deposition and the expected molecular arrangement for the two types of layers in X and Y type deposition are shown in Figure 2.4. Mixed deposition modes have also been defined where XY deposition refers to complete transfer of the monolayer as the substrate is being lowered into the subphase, but only partial transfer as the substrate moves up through the monolayer-air interface.[2]

Langmuir-Blodgett film deposition is often characterized by the deposition or transfer ratio, τ, given by

$$\tau = A_L/A_S$$

where A_L is the decrease in the area occupied by the monolayer on the water surface held at a constant surface pressure, and A_S is the coated area of the solid substrate. Another parameter, p, has also been used to quantify the various deposition modes and is given by

$$p = \tau_u/\tau_d$$

where τ_u and τ_d are the deposition ratios on the upward and downward passages, respectively of the substrate.[2]

The deposition mechanism of Langmuir films described in Figure 2.3 and 2.4 depicts a simple means by which films may be transferred. However, in actuality the

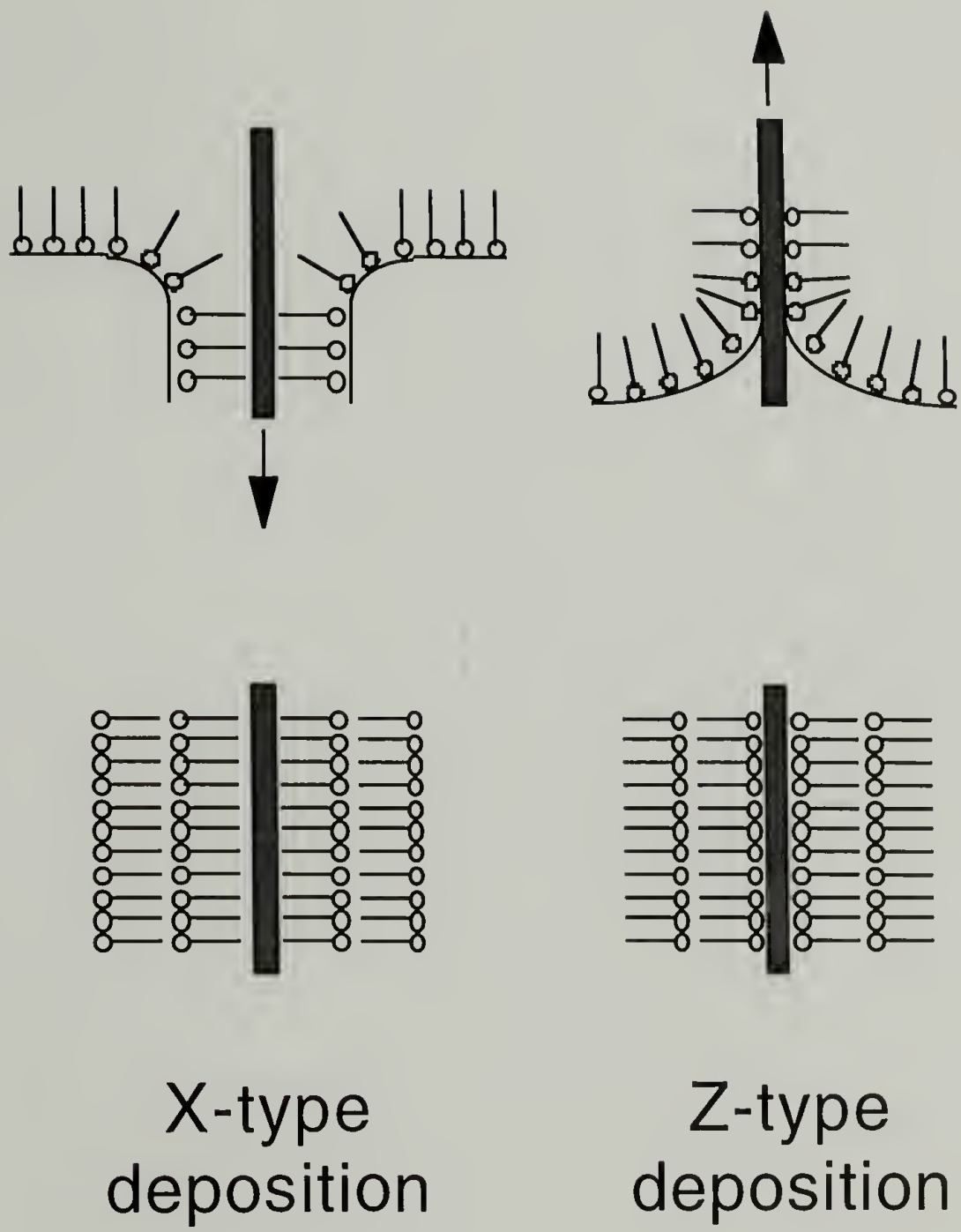

Figure 2.4 Langmuir-Blodgett transfer: X-type and Z-type deposition.

detailed mechanism and dynamics by which floating monolayers are transferred onto solid substrates are much more complex and still poorly understood. Relatively little is known beyond the crude and idealized Y, X and Z type deposition models. Moreover, films rarely transfer in the ideal manner discussed previously. Specifically, multilayer films having the order represented in Figures 2.3 and 2.4 are almost never obtained. As a result, Langmuir-Blodgett films have had difficulty particularly with respect to practical applications. In fact, from this technological standpoint, Langmuir-Blodgett films have not to this point found any practical applications.

In addition to the lack of a quantitative understanding of the transfer process itself, problems have also been associated with the design of molecules suitable for forming highly ordered Langmuir-Blodgett films. Traditional amphiphilic molecules, e.g. long chain fatty acids, have many difficulties.[9,10] The main problem lies in the inherent instability of Langmuir-Blodgett films composed of such low molecular weight amphiphilic molecules. The stability of the layered assemblies of such films is dependent on the crystallization and packing of the long chain hydrophobic tails. However, reorganization processes and a lack of temperature stability often lead to a complete destruction of the film structure over extended periods of time. Specifically, the lifetime of the layered structure which may initially be present rarely exceeds a few days at room temperature. High temperature stability is limited by the low melting points of most long-chain hydrocarbon derivatives.

A further complication arises from the grainy texture exhibited by these films (Figure 2.5). It is believed that upon spreading at the air-water interface, monolayers of these molecules rapidly form islands of quasi-two-dimensional crystals. Upon compression, the islands form what can essentially be viewed as a two-dimensional continuous solid composed of many individual domains. Fluorescence microscopy studies in fact suggest that a rich variety of lateral structures may exist at the air-water interface. This may further complicate transfer. Subsequently during deposition of the

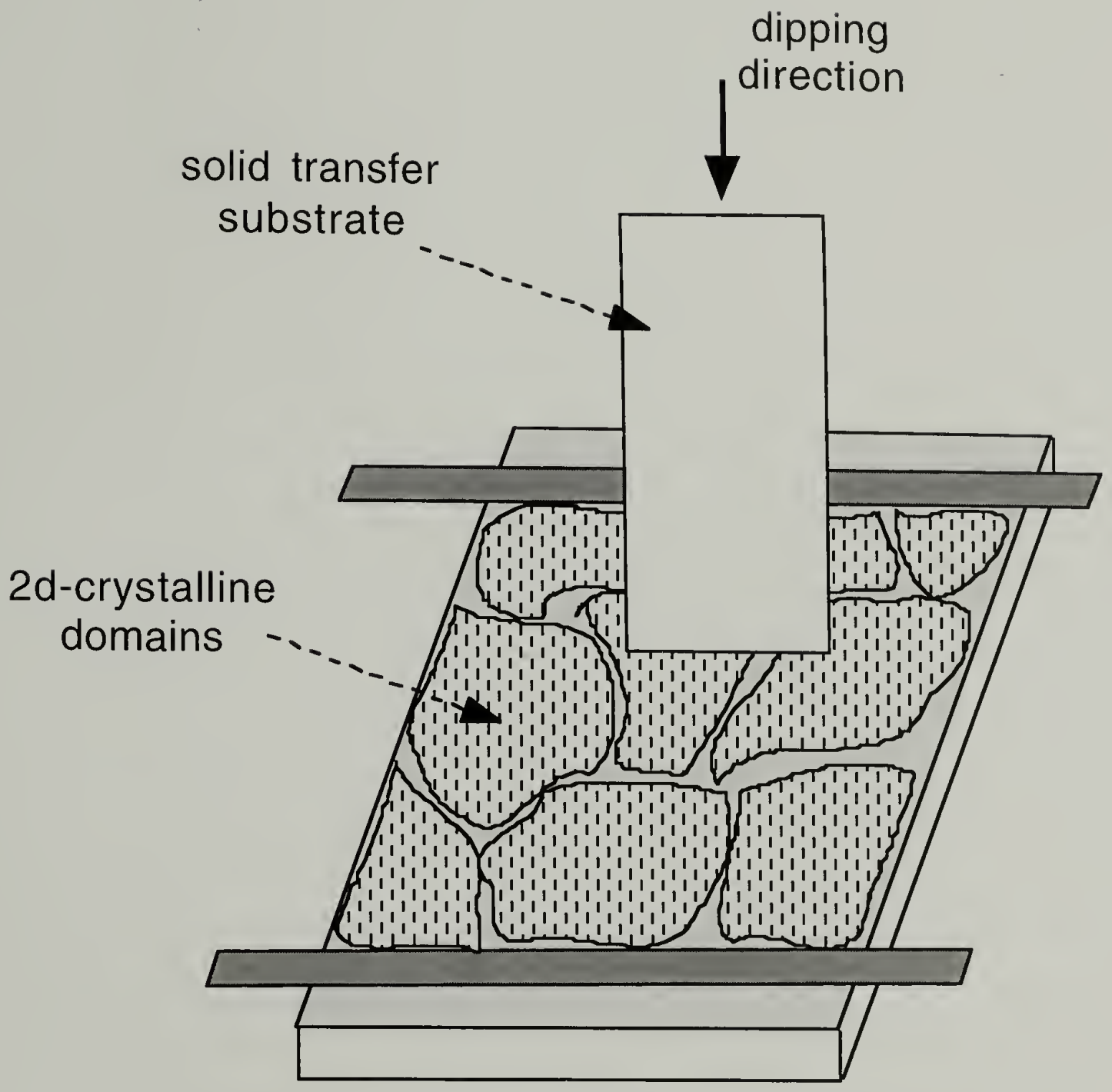

Figure 2.5 Schematic of two-dimensional "grainy" texture for monolayers composed of low molecular weight amphiphiles at an air-water interface.

film, it has been hypothesized that the grainy texture at the air-water interface is distorted by shear and flow forces introduced by the substrate at the water surface.[9-11] As a result, highly ordered layered assemblies with few defects are difficult to achieve. In addition, the transport properties of such transferred films are likely to be strongly influenced by grain boundaries and defects. These grain boundaries in transferred films present a problem for optical applications such as planar waveguides where losses were found to be no better than 10 dB/cm due to the scattering of light. Attempts to improve the structural quality of transferred films of small molecule amphiphiles by annealing expansion-compression cycles or by heat treatment of the monolayer to produce large single crystalline monodomains samples have met with limited success.[8,12,13]

The use of polymers to enhance film stability has also been studied.[9,10,14] Initially polymerization of monolayers or multilayers of deposited functional monomers was suggested as a means to produce a stable film while also preserving the layered structure of the monomers. This technique has had some success but is more complex and is limited to specific systems. The solid state polymerization of Langmuir-Blodgett films of diacetylenes by ultraviolet or high energy irradiation or, after doping with sensitizers, exposure to visible light is one such system.[15] Issues which must be addressed are internal stresses which are often generated following polymerization. These stresses can result in films with large cracks or fissures.

As an alternative to the more limited scope of polymerizing preformed layers of monomers, the spreading and subsequent transfer of amphiphilic polymers using the Langmuir-Blodgett technique has been investigated extensively in recent years. Here homopolymers or copolymers composed of long hydrophobic side chains and a hydrophilic main chain (e.g. poly(octadecyl methacrylate), poly(octadecyl acrylate)) have commonly been spread to the air-water interface. In most cases transfer is only possible once the film is compressed to a condensed monolayer state where it is believed the long hydrophobic side chains form a solid analogue phase similar to the structure small

molecule amphiphiles form. Problems associated with the formation of a grainy texturc and defects again arise. Moreover, the layered structure initially formed by Langmuir-Blodgett films of such polymers, i.e. layers of ordered/crystallized side chain segmcnts alternating with layers of essentially amorphous main chain, is stabilized predominantly by the ordering/crystallization of the linear side chains. The limits of the thermal stability are again determined by the melting range of the side chain segments.

Fundamentally, the difficulty associated with the molecular design of amphiphilic molecules lies in the fact that for a monolayer film to be transferred from the air-water interface, the monolayer must be compressed. However, compression induces what is believed to be an ordering of the long hydrophobic groups and the formation of a two-dimensional polycrystalline texture that is not amenable to the dynamics associated with the transfer process. On the other hand, the ordering of the long hydrophobic groups following transfer is what provides for the stability of the films. Due to this problem between balancing film stability and transferability, amphiphilic molecules have inherent limitations with respect to forming high quality Langmuir-Blodgett films.

2.1.2 "Hairy-Rod" Polymers

In light of the shortcomings of traditional Langmuir-Blodgett materials (e.g. small molecule amphiphiles, polymerization of transferred layers of monomers, amphiphilic polymers) and the idea that the Langmuir-Blodgett method is still a technique with the potential to produce well defined superstructures of molecules with practical applications, a newer type of molecular design, "hairy-rod" polymers, was introduced in the late 1980s (Figure 2.6). The idea was to design molecules that would not only be transferablc, i.e. films amenable to the dynamics associated with transfer, but also stable following deposition.[6,9,10,12,13,16-22] The general architecture of “hairy-rod” polymers consists of a long rigid rod-like backbone decorated with long flexible hydrocarbon side chains. From a design standpoint, the concept was to provide the rigid-rod backboncs with a

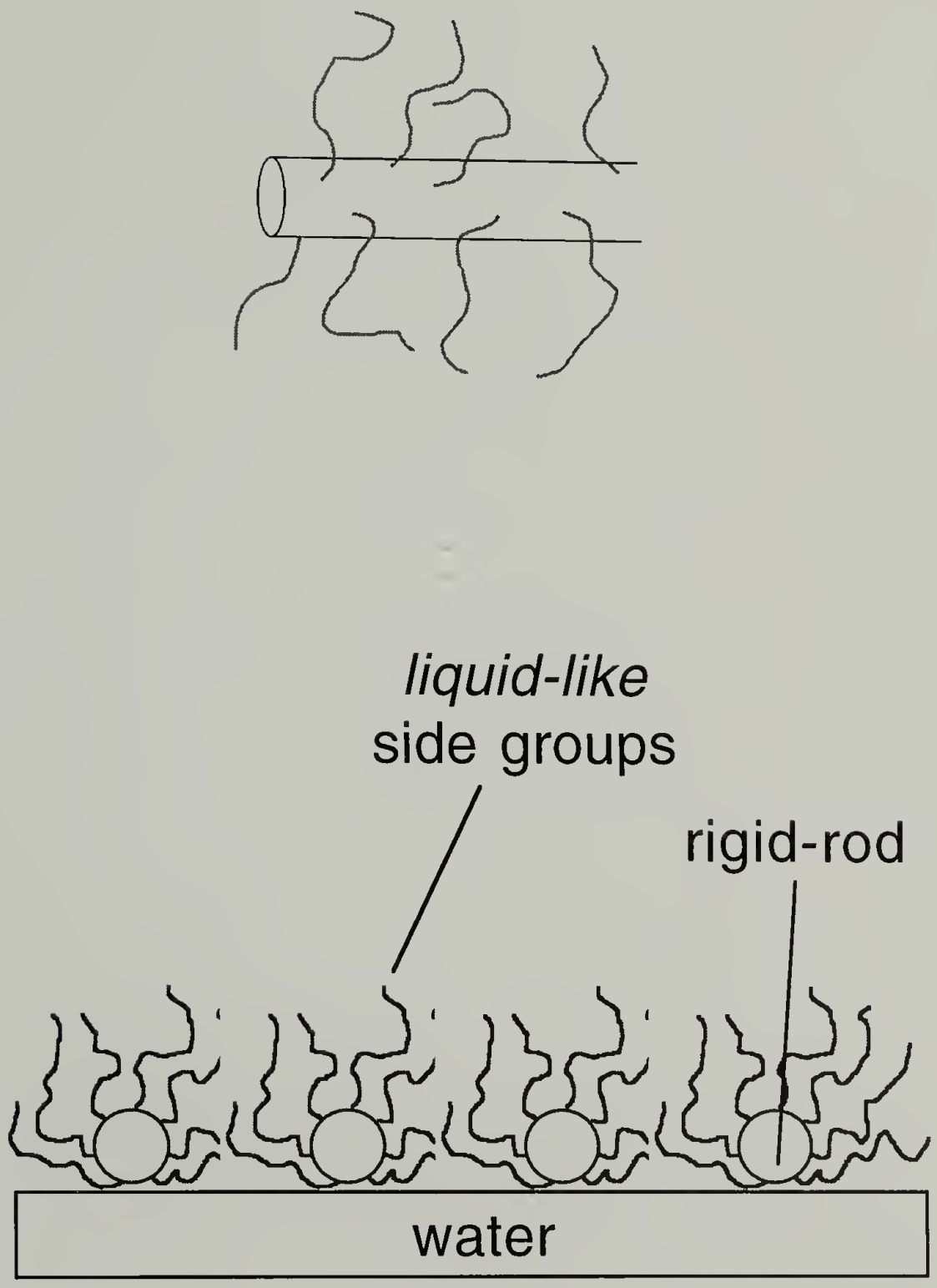

Figure 2.6 Schematic of a "hairy-rod" polymer composed of *liquid-like* side groups and a rigid-rod backbone. The rigid-rods lie flat at the air-water interface.

molecularly defined skin of *solvent-like* or *liquid-like* segments.[9,10] A film exhibiting these characteristics at an air-water interface would then address difficulties traditional Langmuir-Blodgett materials have during transfer. By embedding the rods in a continuous matrix of flexible *liquid-like* side groups, it was felt that transferability would be enhanced, i.e. decreased number of defects and fewer grain boundary effects. As was mentioned earlier, it has been proposed that the fluid dynamics of a monolayer on the water surface can greatly affect transfer due to a flow field at the surface during transfer.[11] In theory, the *liquid-like* matrix would impart the rigid-rods with greater mobility during transfer. The rigid-rods on the other hand would provide structural stability for such a transferred Langmuir-Blodgett film. Many such "hairy-rod" polymers have been known to form liquid crystalline phases in the bulk.[23-27]

Present studies have thus far shown that Langmuir-Blodgett films of polymers with a "hairy-rod" architecture are much improved over traditional Langmuir-Blodgett materials. Under certain conditions it has been found that upon transfer "hairy-rod" polymers can form highly ordered supramolecular structures with relatively few defects. The quality of these deposited films depend on the molecular surface packing density at the air-water interface during transfer and the length and number of *n*-alkyl side groups attached to the rigid main chain. The stability of transferred films has also been found to be enhanced relative to other Langmuir-Blodgett materials. The multilayer structures typically last over a period of at least several months. In addition, transfer ratios can approach unity at transfer speeds up to several centimeters per minute. This allows for the rapid build-up of multilayers. Films composed of greater than 1000 layers have been achieved with surface smoothness' better than 0.6 to 0.8 nm.[9,10] In x-ray and neutron reflectivity studies it has been shown that such films can form well defined double layers, shown schematically in Figure 2.7 (i.e. alternating backbone-backbone layer, hydrocarbon-hydrocarbon side chain layer).[16,20] In these studies on polyglutamate

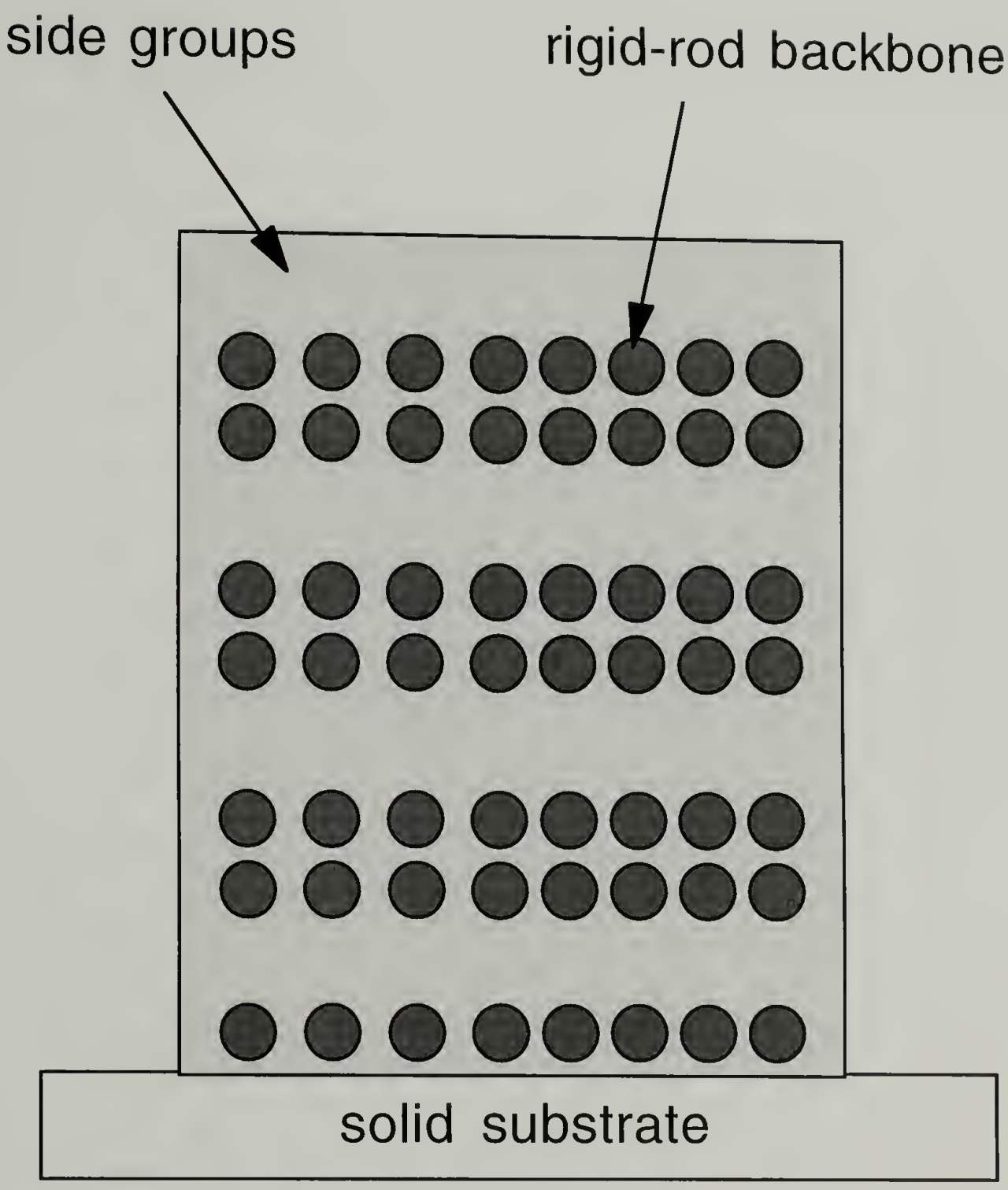

Figure 2.7 Schematic illustration of double layer structure of deposited Langmuir-Blodgett "hairy-rod" films.

"hairy-rod" polymers, it was found that although annealing at ~80° C causes the backbone positions to relax slightly, no interlayer diffusion occurs and the double layer structure continues to persist.

Under the previously mentioned conditions, it has also been found that following transfer there can be a preferential orientation of the rigid-rods parallel to the dipping direction of the substrate (Figure 2.8). Any grainy texture which may be present at the air-water interface is for the most part not present in the transferred film. For "hairy-rod" Langmuir-Blodgett films of polyglutamates, waveguide mode-loss measurements yielded values in the range of 2.5-5.5 dB/cm.[8,12,13] As was mentioned previously, Langmuir-Blodgett films of amphiphilic molecules exhibiting the typical grainy texture had losses of no better than 10 dB/cm. In addition, Brillouin spectra obtained from these oriented "hairy-rod" Langmuir-Blodgett films have allowed for the evaluation of the tensor elements of the elastic modulus of the film. These results have shown that C_{33} (to a good approximation, Young's modulus measured along the helical axis, i.e. the dipping direction) has a value of 12.2 GPa whereas C_{13} is 4.2 GPa.[28] Noting that little is quantitatively known about the structure of these films directly at the air-water interface, it has been proposed that the *liquid-like* character of the long *n*-alkyl side chains is responsible for this observed alignment of the rigid-rods. This will be more fully discussed in the following section.

The design principles for "hairy-rod" polymers are shown in Figure 2.9 with several specific examples.[9,10] The first is a polymer based on phthalocyaninato-polysiloxane (PCPS) as the parent compound. Polymers of this type are substituted with alkoxy chains at the perimeter of the phthalocyanine moieties represented in the Figure 2.9 as disks. The rigidity of these molecules arises from the complete steric hindrance of any bending motion by the dense stacking of the disc-like phalocyanine moieties. Cellulose derivatives also are intrinsically stiff or more exact worm-like macromolecules as a consequence of their stereochemistry. Upon functionalization with alkoxy groups, they

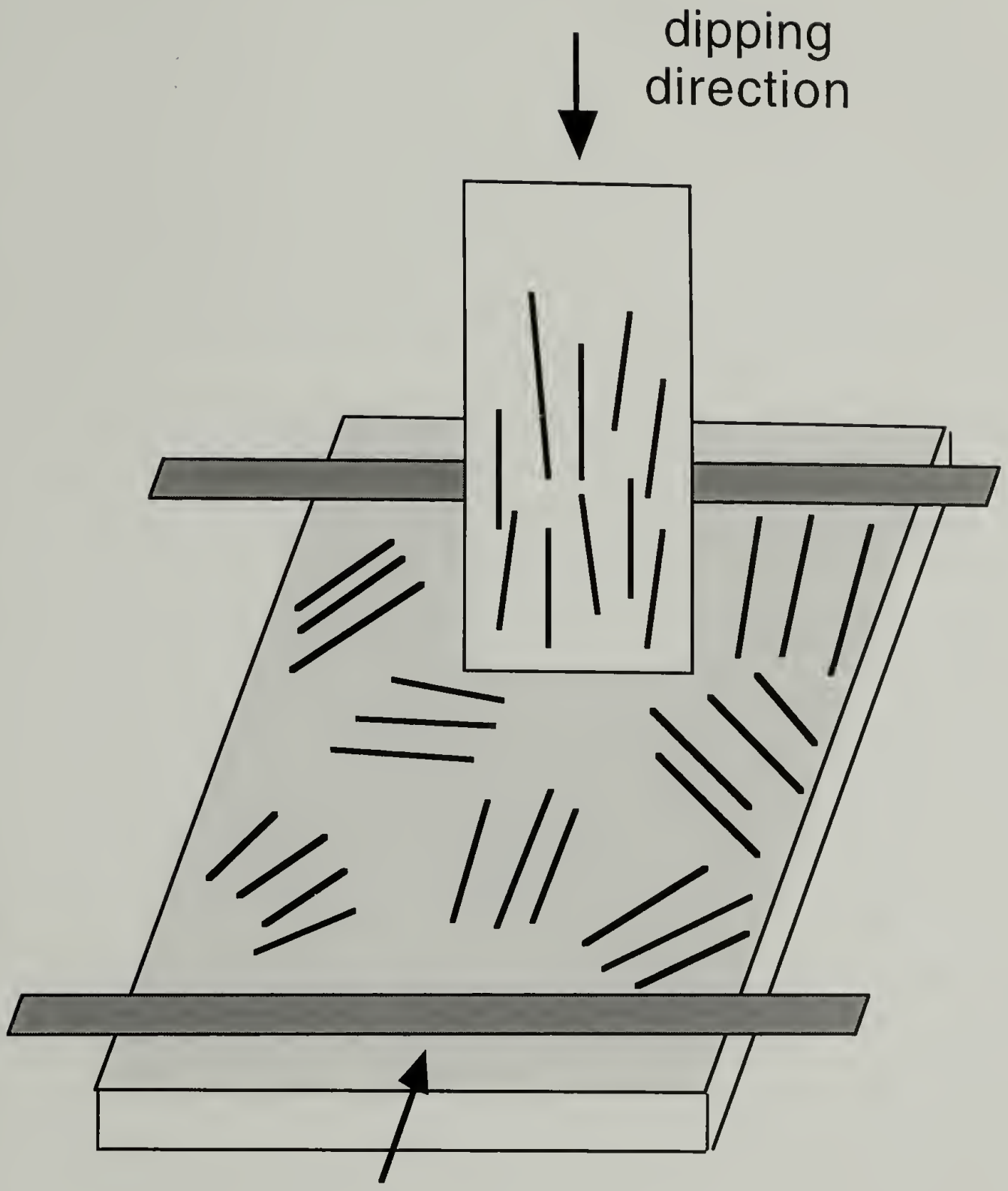

Figure 2.8 Nematic-like domains at the air-water interface and their preferential alignment upon deposition using the Langmuir-Blodgett technique. The rigid-rods lie flat at the air-water interface.

"Hairy-Rod" Polymers

I.

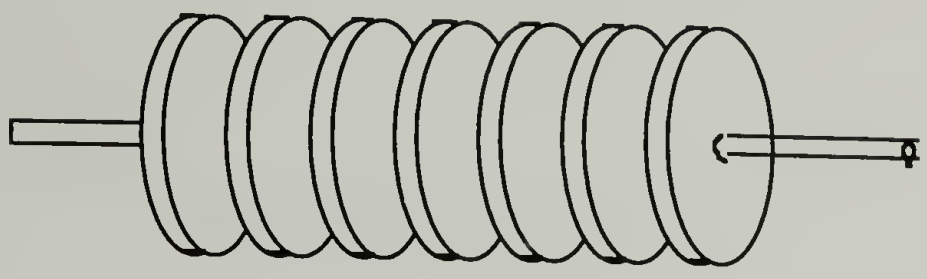

II.

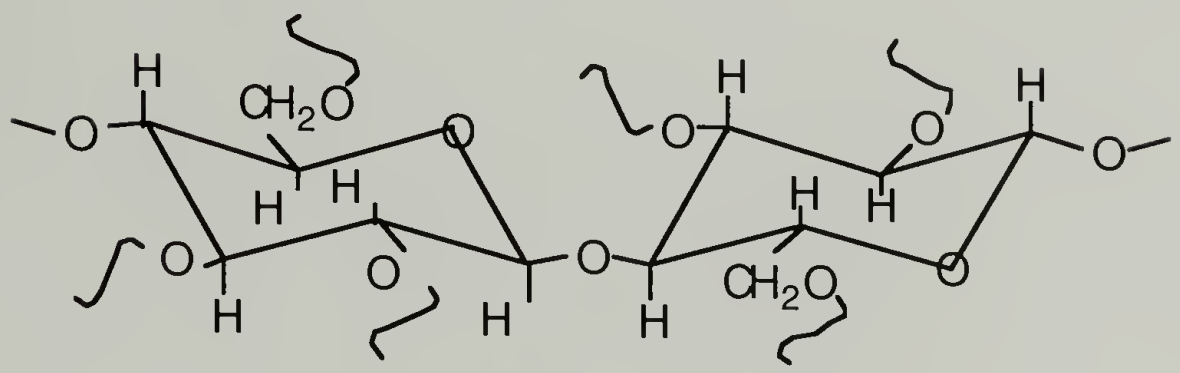

III.

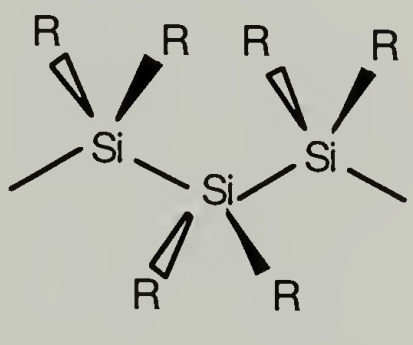

IV.

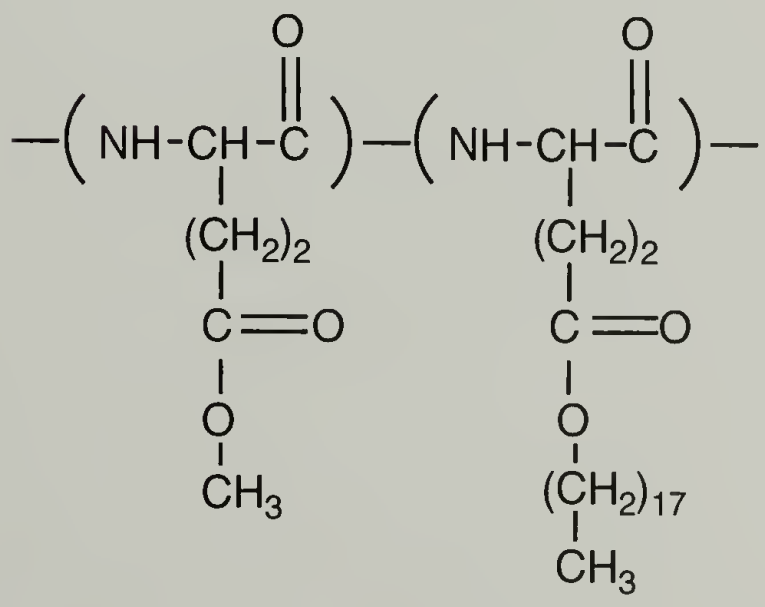

Figure 2.9 Schematic illustration of several types of "hairy-rod" polymers.

become soluble in common solvents making them suitable to be spread at an air-water interface. Polysiloxanes, although not inherently rigid, can be made "hairy-rod" polymers if the side groups are designed to introduce both steric hindrance with regard to bending of the main chain and at the same time flexible groups at the outer perimeter of the molecule. Some other polymers which can also form "hairy-rod" architectures are polyisocyanates,[23,24,29] polyisocyanides,[30] phthalocyaninato-polygermoxanes,[31] hemiporphyrazin-polygermoxans[32] and poly(1,4-phenylenes).[33]

However, the "hairy-rod" polymers which have received the most attention recently as Langmuir-Blodgett materials are *n*-alkyl side chain substituted polyglutamates.[6-8,10,12,13,17,20-22,28,34-37] Studies in the bulk have shown that these synthetic polypeptides exist in a stable α-helix conformation even when their side chains are altered.[25-27] The rigid-rod character of the α-helices arises from the strong intermolecular hydrogen bonding between the amide groups of the backbone segments. Given this rigid backbone, it has also been found that in the bulk state, the properties of these "hairy-rod" polymers are strongly influenced by *n*-alkyl side chains. Properties vary both as a function of side chain length as well as degree substitution. Specifically, with a sufficient number of long side chains these polymers have been found to form liquid crystalline phases (cholesteric and columnar hexagonal liquid crystal phases) above the melting temperature, T_m, of the side chains.[26,27] Although technically described as thermotropic liquid crystals, these "hairy-rod" polymers can be viewed as being analogous to lyotropic liquid crystals were the paraffinic side chains essentially serve as a *solvent-like* matrix for the rigid-rod backbones. Below T_m the molecules form a structure composed of interdigitated crystalline side groups sandwiched between layers of peptide backbones.

2.1.3 Current Understanding of Langmuir Film Structure

Given the effect long *n*-alkyl side chains have in modifying the bulk structure of "hairy-rod" polymers, part of the motivation in using these materials at the air-water interface was to transfer this control over structure and properties to Langmuir-Blodgett films. As mentioned previously, the goal was to enhance the transferability and ordering of the rigid-rods at the air-water interface by controlling the *solvent/liquid-like* quality of side groups. However, even though the quality and structure of transferred Langmuir-Blodgett films of "hairy-rod" polymers have been widely studied using a number of techniques (e.g. x-ray scattering and reflectivity,[16,17,20] neutron reflectivity,[16,20] infrared spectroscopy,[35] uv-visible spectroscopy,[6,7] atomic force microscopy,[17,18] transmission electron microscopy,[38] surface plasmon spectroscopy[39] and waveguide spectroscopies[8,12,13]), little is quantitatively known about the structure of Langmuir films at the air-water interface prior to and during deposition. Specifically, little is directly known about the relationship between the microstructure of a Langmuir film and its transferability. Moreover, transfer studies have shown that the quality of a transferred Langmuir-Blodgett film is highly dependent on the surface packing density of the film at the air-water interface during transfer. It can be readily inferred that the structure of a Langmuir film varies with surface packing density. Some structural parameters likely to affect transfer are molecular orientation, molecular packing and conformational order. Presently, much of what has been assumed about the structure of films at the air-water interface has been drawn from the shape of surface pressure/area isotherms as well as from films removed from the air-water interface.[14,20,38,40-44] For studies on films removed from the air-water interface, however, transfer indubitably changes the structure of the film. A more direct and quantitative understanding of the microstructure of films at the air-water interface would help in determining the molecular design parameters and transfer conditions important for making high quality Langmuir-Blodgett films.

The main difficulty associated with this problem lies in the fact that, relative to studies on transferred films, obtaining direct structural information of films at the air-water interface has been difficult. The use of x-ray reflection and scattering techniques[45,46] are limited due to the low scattering volume of the low density films at the air-water interface. Additionally, although a technique such as grazing incidence x-ray diffraction has been useful for the study of crystalline monolayers at the air-water interface (e.g. crystalline structure and tilt of small molecule amphiphiles in particular), it is less useful for monolayers not exhibiting crystalline order. The use of fluorescence microscopy on the other hand, aside from providing images of lateral structures does not provide direct information on the molecular structure of a monolayer.[47] UV-visible spectroscopy has also been used to study the aggregation and orientation of specific functional groups exhibiting absorption bands in the uv-visible spectra for particular monolayers at an air-water interface, but is limited to monolayers with such functional groups.[7]

Overall, there have essentially been no direct studies on the microstructure of "hairy-rod" films at the air-water interface. As a result, Langmuir-Blodgett transfer experiments on these films have proceeded largely in the dark with respect to the film being transferred. In addition, the formation of highly ordered "hairy-rod" multilayer films greatly depends, as discussed previously, on the molecular surface packing density of the film at the air-water interface during transfer and the length and number of *n*-alkyl side groups attached to the rigid main chain.

A schematic description of what has been proposed to occur at the air-water interface for "hairy-rod" polymers during transfer is shown in Figure 2.8 from the previous section, 2.1.2. Initially when the film is spread at the air-water interface, it is believed that the rigid-rods form a two-dimensional nematic liquid crystal-like phase composed of domains of random in-plane orientation. The side chains are presumed to be flexible and form a continuous *liquid-like* matrix in which the rigid-rods are dispersed.

As the film is compressed prior to the deposition process, the domains impinge and a grainy texture much like that described for amphiphilic molecules is the result. During transfer, however, the *liquid-like* matrix allows the rigid-rods to flow on the water surface in a direction parallel to the dipping direction of the substrate. Thus the grainy texture at the air-water interface is largely eliminated following transfer and the rigid-rods become preferentially aligned as has been observed. It should again be pointed out that there has been no direct proof of this proposed behavior of "hairy-rod" films at the air-water interface.

Thus, as a first step in understanding the actual molecular design parameters and transfer conditions (i.e. surface packing density of the film at the air-water interface) important for making Langmuir monolayers with microstructures conducive to forming highly ordered Langmuir-Blodgett films, the following sections will describe studies on two types of "hairy-rod" polymers directly at the air-water interface. In particular, the "hairy-rod" polymers studied were a series of copolyglutamates and a copolyisocyanate. The technique used to directly characterize these films at the air-water interface was external reflectance infrared spectroscopy. Having found success in the characterization of thin films on metallic substrates (e.g. gold),[14,48,49] external reflection infrared spectroscopy has more recently been used to study films on nonmetallic substrates such as air-water interfaces.[50-57] In addition, the external reflection reflectance infrared spectroscopy setup in our laboratory has also been coupled with a Langmuir trough. Thus, the surface area at the air-water interface could be accurately controlled and the surface tension of films could be measured.

The focus of the research was specifically on the role of *n*-alkyl side groups as *liquid-like* groups and how their *liquid-like* character may vary as a function of degree side group substitution and surface packing density at the air-water interface. As was mentioned previously, the *liquid-like* character of the side groups at the air-water interface has been presumed to be an important factor in increasing transferability. There have

been no direct studies to corroborate this. Questions to be addressed are: how *liquid-like* are the long alkyl side groups and do they really serve as a *liquid-like* matrix for the rigid-rod main chain at the air-water interface? If so, how might this affect any subsequent ordering of the rigid-rod backbones? This is especially relevant given the known liquid crystalline behavior of both types of samples in the bulk.

Some other questions to be addressed are the following: (1) does the orientation of the side chains change with respect to the plane of the air-water interface as a function of surface packing density, (2) do the rigid-rods align preferentially during compression in the trough. Several other studies have indicated that during compression in a Langmuir trough, "hairy-rod" polymers with their large axial ratio may preferentially align parallel to the compression barriers. In none of these studies, however, was the degree of alignment which may have been present at the air-water interface quantitatively determined.

Overall, since transfer of Langmuir films is dependent on their structure at the air-water interface, a better understanding of that structure and the factors that affect it (e.g. rigid-rods, side chains, surface packing density etc) would improve the understanding behind making highly ordered Langmuir-Blodgett films.

2.2 External Reflection Infrared Spectroscopy/Langmuir Trough

The coupling of an external reflection infrared spectroscopy setup with a Langmuir trough provides a potentially powerful tool for the study of films at air-water interfaces. By precisely controlling the surface packing density of films spread at the air-water interface, it is possible with external reflection infrared spectra obtained directly at the air-water interface to relate structural changes in the film to changes in surface pressure. Only a few other research groups, however, have coupled these two techniques.[50,53-56] Where this has occurred the specifics of the coupling, which are important, have often varied. In the following, a description of external reflection

infrared spectroscopy will be given after which the coupling of the technique with a Langmuir trough in our laboratory will be discussed.

2.2.1 External Reflection Infrared Spectroscopy: Theory

The use of infrared spectroscopy to study water supported Langmuir monolayers was originally pioneered by Dluhy.[51,52] In principle, the infrared spectrum of a monolayer contains direct information about molecular orientation, molecular packing as well as the conformational order of chain segments and thus is a powerful technique for the study of such systems. A spectrum is obtained by reflecting an infrared beam from an air/film/substrate interface, measuring the reflected intensity as a function of wavelength, and ratioing this signal with the reflected intensity as a function of wavelength obtained from the uncovered substrate. However, although external reflection infrared spectroscopy has long been successful in the study of thin films on metallic substrates as was mentioned previously, it has been utilized much less for films at air-water interfaces. This is due to difficulties associated with the reduced signal level and the complex boundary conditions governing electromagnetic waves interacting with dielectric surfaces (e.g. water) that make the details of the experimental geometry (i.e. reflection geometry, state of polarization) more demanding. In our experiments these difficulties which have limited some previous studies, have been minimized and in turn high quality spectra have been obtained even for low surface concentration monolayer films. In the following, an overview of the physics associated with reflection/absorption at an air/film/substrate interface will be presented along with some model calculations showing how reflection/absorption varies as a function of the reflection geometry (i.e. incident angle of infrared beam), the state of polarization of the incident beam, and the substrate.

The general configuration for reflection at an air/film/substrate interface is shown in Figure 2.10 for an ideal three phase system. The incident electric field, E, can be resolved into two components, one oriented perpendicular to the scattering plane (i.e. the

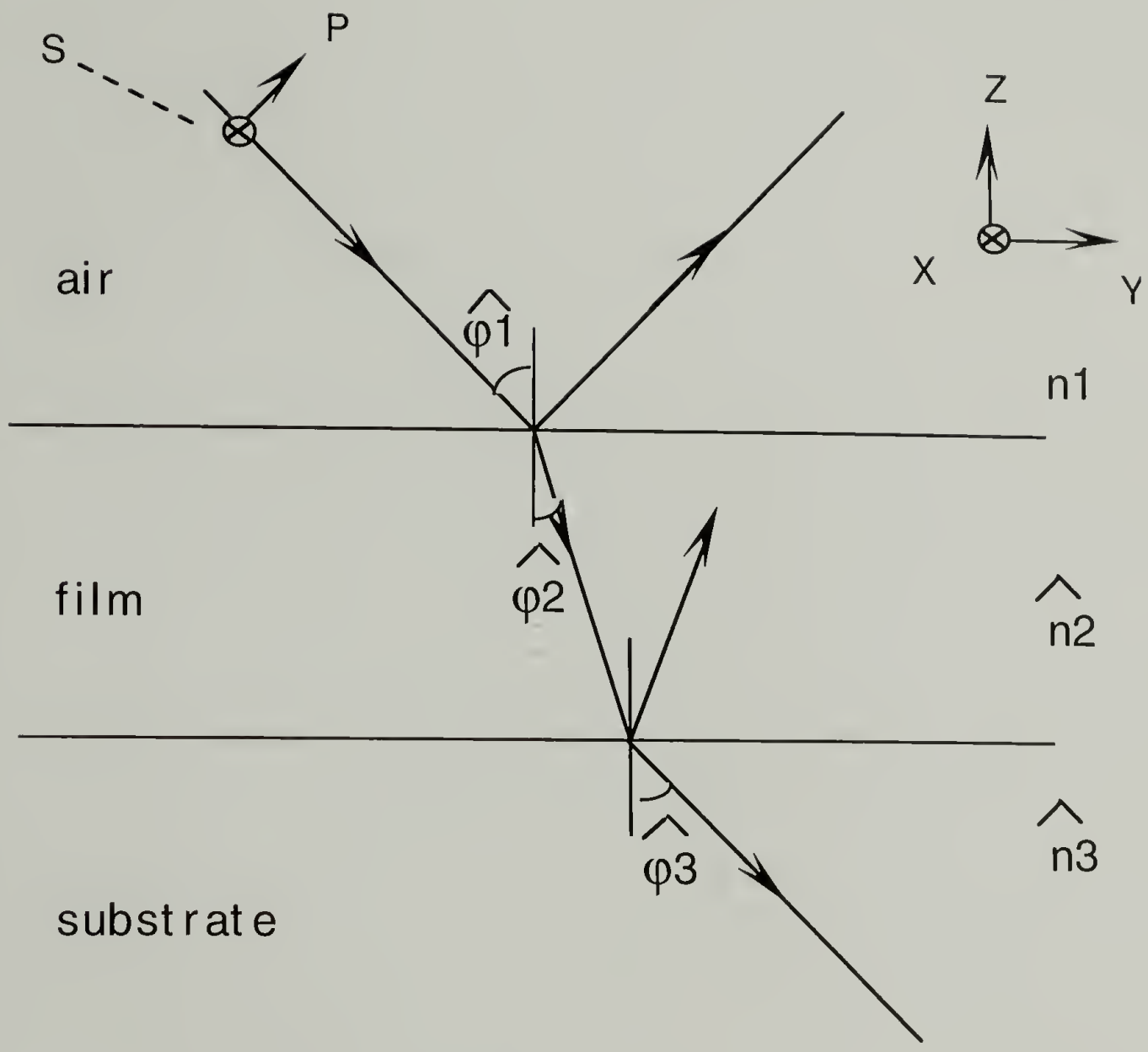

Figure 2.10 Generalized three phase schematic for a film on a substrate. n1, n2, and n3 are the refractive indices of air, the film, and the substrate, respectively.

y-z plane) and the other oriented parallel. These components are the s and p polarized waves respectively. The optical properties are in turn governed by the boundary conditions for the electromagnetic wave at the interfaces and the refractive indices of air, the film, and the substrate. If these parameters are known and if the film and substrate are assumed to be optically isotropic, the reflected spectra can then be readily calculated.[57-60] Of particular interest in our case is how spectra vary as a function of the incident angle of the infrared beam. These calculations are important for determining the optimal reflection geometry that will yield the best signal/noise ratio. Using the following general equations, the computed spectra shown in this section were made by Yuan Ren using the application Mathcad by MathSoft Inc.[58,61]

The amplitude of the reflectivity for the two polarized components of the electromagnetic field at each interface is given by the following equations:

$$\hat{r}_{12}(p) = \frac{(n_1\cos\varphi_2 - \hat{n}_2\cos\varphi_1)}{(n_1\cos\varphi_2 + \hat{n}_2\cos\varphi_1)} \tag{2.1}$$

$$\hat{r}_{12}(s) = \frac{(n_1\cos\varphi_1 - \hat{n}_2\cos\hat{\varphi}_2)}{(n_1\cos\varphi_1 + \hat{n}_2\cos\hat{\varphi}_2)} \tag{2.2}$$

$$\hat{r}_{23}(p) = \frac{(\hat{n}_2\cos\hat{\varphi}_3 - \hat{n}_3\cos\hat{\varphi}_2)}{(\hat{n}_2\cos\hat{\varphi}_3 + \hat{n}_3\cos\hat{\varphi}_2)} \tag{2.3}$$

$$\hat{r}_{23}(s) = \frac{(\hat{n}_2\cos\hat{\varphi}_2 - \hat{n}_3\cos\hat{\varphi}_3)}{(\hat{n}_2\cos\hat{\varphi}_2 + \hat{n}_3\cos\hat{\varphi}_3)} \tag{2.4}$$

In these equations, the complex refractive index for each medium I is

$$\hat{n} = n + i\hat{k} \tag{2.5}$$

where n is the real part of the index of refraction and k is the extinction coefficient, ϕ_1 is the angle of incidence, and ϕ_2 and ϕ_3 are the angles of refraction as defined by Snell's law:

$$\hat{\varphi}_2 = \sin^{-1}\left(\frac{\sin\varphi_1}{\hat{n}_2}\right) \tag{2.6}$$

$$\hat{\varphi}_3 = \sin^{-1}\left(\frac{\hat{n}_2\sin\hat{\varphi}_2}{\hat{n}_3}\right) \tag{2.7}$$

The reflectivity, R, can then be calculated by taking the square of the amplitude reflection coefficient r ($R = r \cdot r^*$, where r^* is the complex conjugate of r) which for this three phase system may be expressed as

$$\hat{r} = \frac{\hat{r}_{12} + \hat{r}_{23} \cdot \exp(2i\hat{\beta})}{1 + \hat{r}_{23} \cdot \hat{r}_{12} \cdot \exp(2i\hat{\beta})} \tag{2.8}$$

In this equation, β is the phase shift and is defined as

$$\hat{\beta} = \frac{\omega \hat{n}_2 d\cos(\hat{\phi}_2)}{c} \tag{2.9}$$

where d is the film thickness, c is the speed of light, and ω is the angular frequency of the incident infrared beam. With the reflectivity of the air/film/substrate system, the

absorbance defined as $-\log(R/R_0)$ can be determined where R_0 is the reflectivity of the pure air/substrate surface, or in other words the background/reference state.

Given that polarization of the incident infrared can provide insight into the orientation of specific chain segments and/or functional groups with defined dipole moments within a film, the mean square electric fields for both s and p polarizations can also be determined[62] with the following relations in a (x,y,z) coordinate system as defined by Figure 2.10:

$$\langle E_{s1}^2 \rangle = (1 + R_s) + 2R_s^{1/2}\cos\left(\beta_s - 4\pi\left(\frac{z}{\lambda}\right)n_1\cos\phi_1\right) \tag{2.10}$$

$$\langle E_{p,y}^2 \rangle = \cos^2\phi_1\left[(1 + R_p) - 2R_p^{1/2}\cos\left(\beta_p - 4\pi\left(\frac{z}{\lambda}\right)n_1\cos\phi_1\right)\right] \tag{2.11}$$

$$\langle E_{p,z}^2 \rangle = \sin^2\phi_1\left[(1 + R_p) + 2R_p^{1/2}\cos\left(\beta_p - 4\pi\left(\frac{z}{\lambda}\right)n_1\cos\phi_1\right)\right] \tag{2.12}$$

In these relations, β_s and β_p are the phase shifts of the electric fields for the s and p polarizations respectively due to reflection at the interfaces.

Taking representative values for the refractive indices of the various phases, model calculations for were then carried out for a polymer film on a metallic (non-dielectric) substrate and a polymer film on a water substrate (dielectric). As was mentioned above, these calculations provide a good insight into the factors which affect reflection/absorption associated with real air/polymer film/substrate systems. Beginning first with the calculations for a polymer film on a metallic substrate, the input parameters chosen were as follows. The polymer film is taken to be 33 Å thick and has a refractive index of 1.5 + (0.10)i. The refractive index of the metallic substrate, which is also a complex value, is chosen to be 2.5 + (30.0)i corresponding to gold. The refractive index of air is 1. Also, the calculation was made at a frequency of 2920 cm^{-1}.[58]

With these parameters, the calculated mean square electric field for the two polarizations is shown in Figure 2.11 as a function of the angle of incidence of the infrared beam. At all angles, the s and py components are essentially zero. On the other hand, at grazing incident angle the pz component has a very large value. What this effectively leads to is a system where the mean square electric field only has a component in the z direction perpendicular to the plane of the film and substrate. This is important from the point of determining molecular orientation in that for such films only dipole moments which have some component perpendicular to the interface can absorb and subsequently be probed with the incident radiation. Termed the "surface selection rule", this provides a means of determining molecular orientation relative to the plane of the interfaces and is well established in traditional external reflectance infrared spectroscopy for films at metallic substrates. The loss of the s polarized component of the mean square electric field is evident from the plots of the phase shift and reflectivity versus the angle of incidence as shown in Figure 2.12 and Figure 2.13. Here it can be seen that this component experiences a phase shift of about 180° with a reflectivity of about one irrespective of incident angle. This leads to a state where the incident and reflected light fields interfere to produce a resultant standing wave field with a node at the surface. Conversely, the p polarized component depends strongly on the angle of incidence and can have very high values. The variation of the calculated absorbance with incident angle is shown in Figure 2.14. It can be seen that the absorbance of the s polarized component of the infrared beam remains at zero. The p component of the absorbance varies with the incident angle, however, and reaches very high absorbance values near the grazing incident angle (~88°) before sharply falling off. These calculations show why grazing incidence external reflection infrared spectroscopy has been successful in characterizing films at on such substrates (i.e. high pz mean square electric field and absorbance)

Using the same approach as for the model metallic substrate with the previous equations, model calculations of a polymer film at an air-water interface were made using

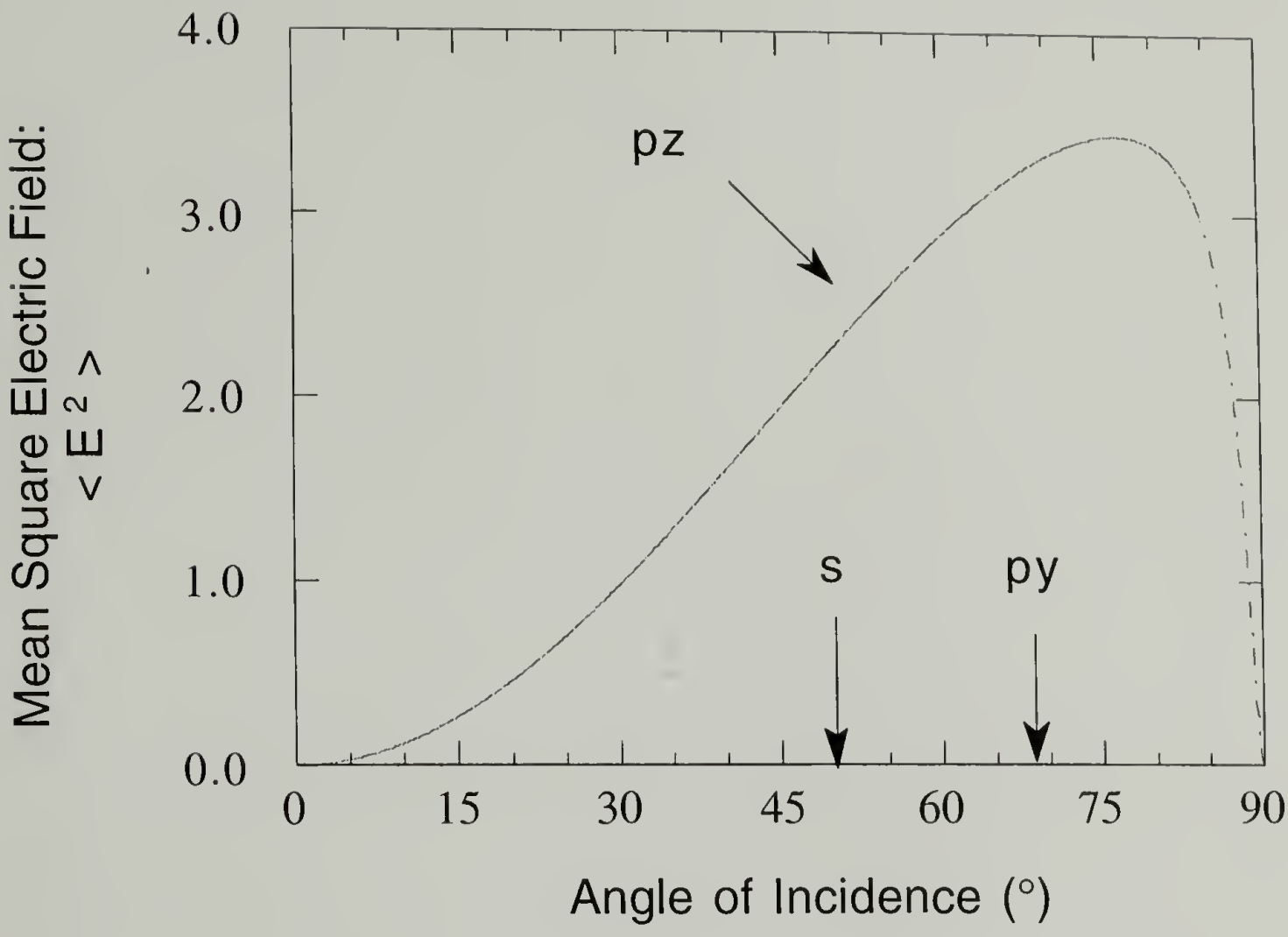

Figure 2.11 Mean square electric field of both polarizations for a film at an air-metal surface.

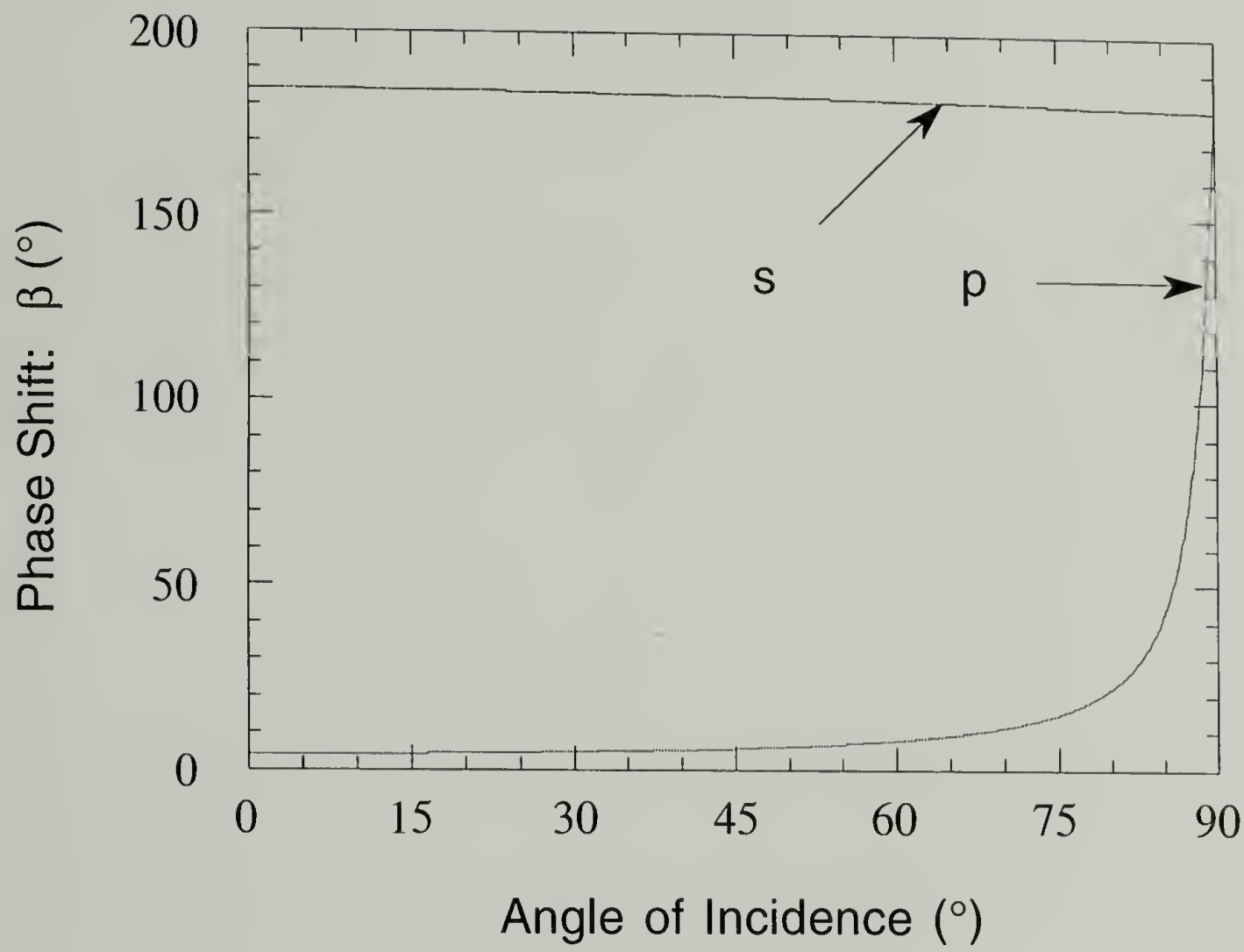

Figure 2.12 The variation of the phase shift for both s and p polarizations for a film at an air-metal surface.

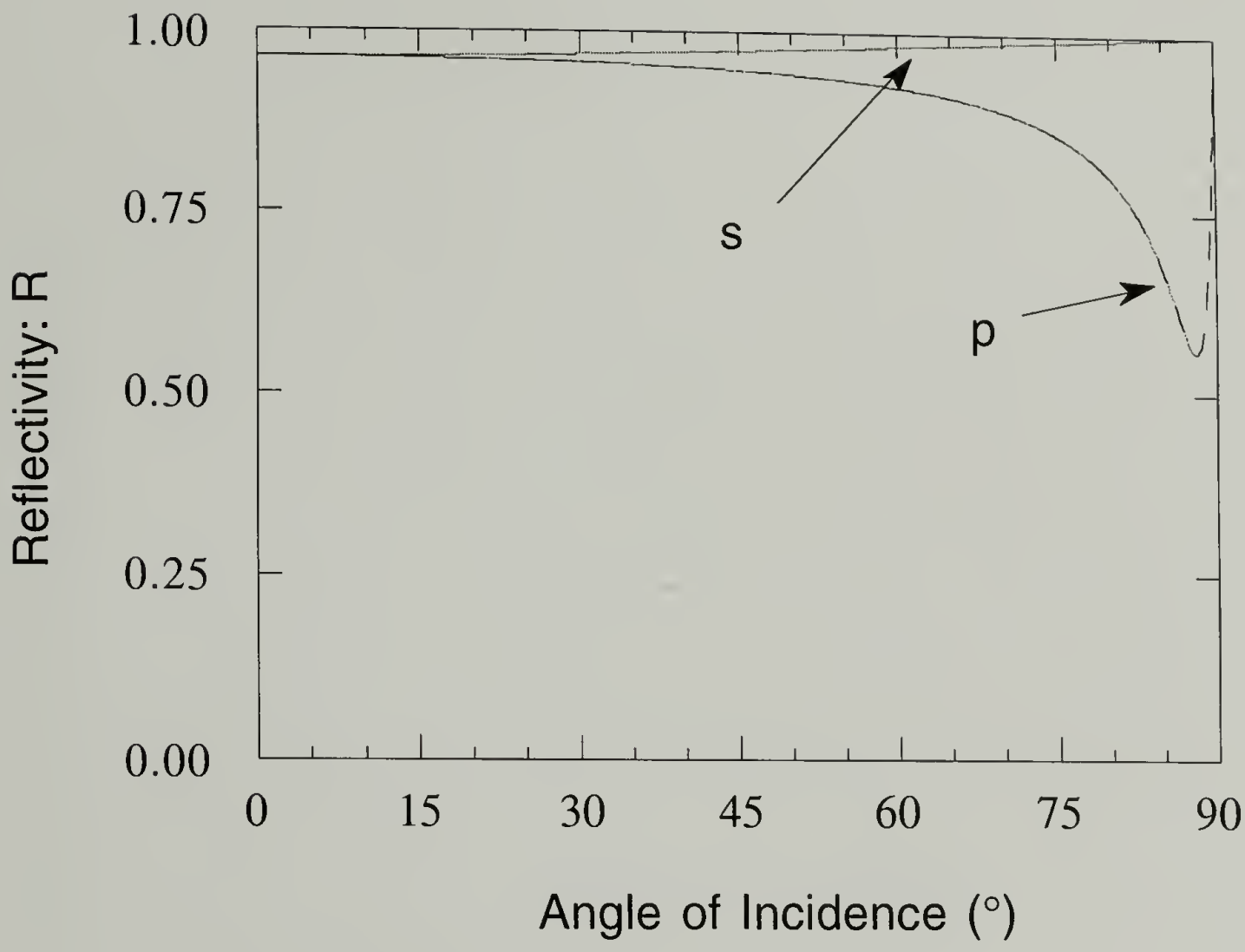

Figure 2.13 Variation of the reflectivity for both s and p polarizations of a film at an air-metal surface.

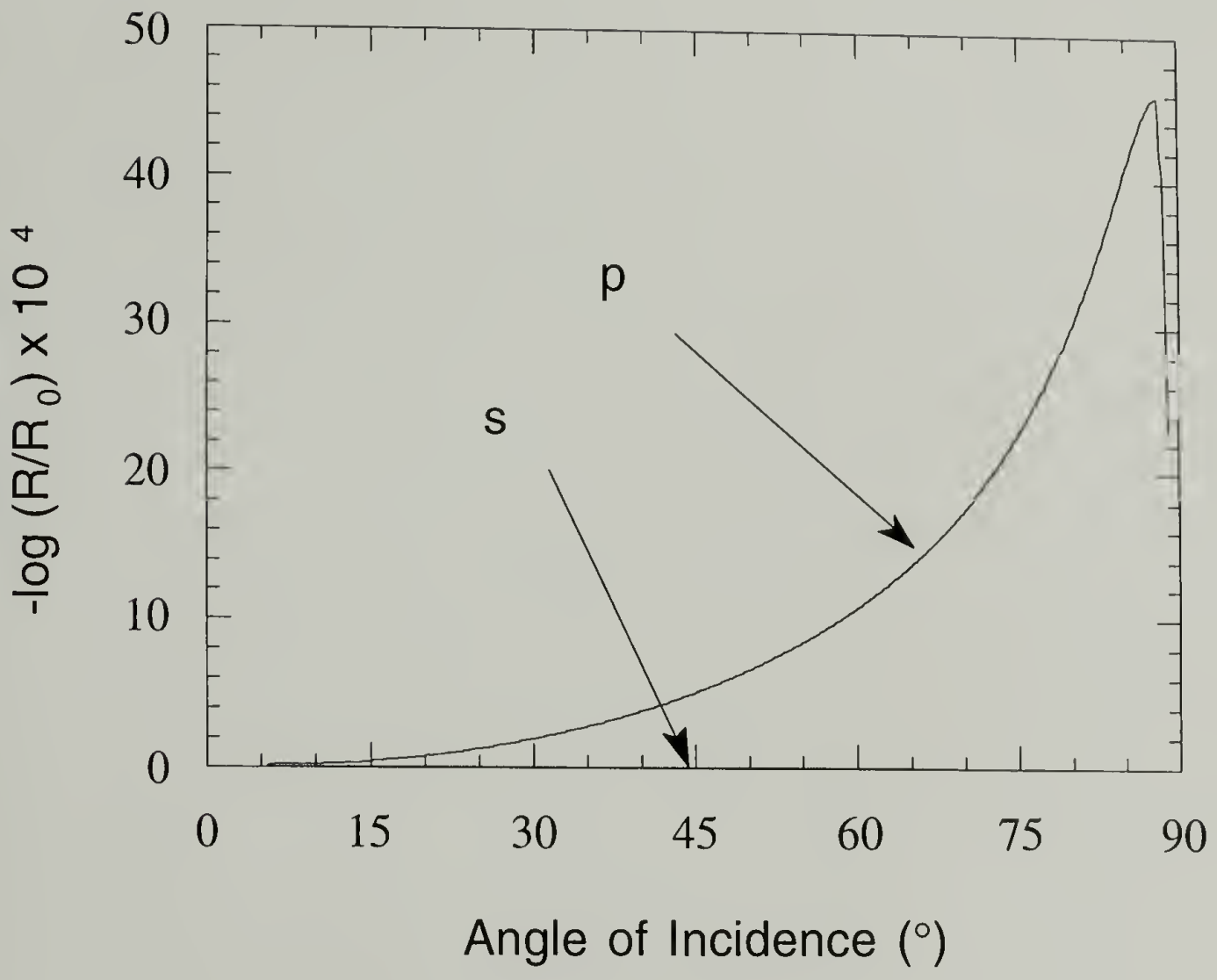

Figure 2.14 Absorbances for s and p polarizations for a film at an air-metal surface.

the same representative input parameters with the exeeption of n for the substrate. In these ealculations the input value for the refractive index of water, a dieleetric media, was 1.441 + (0.0297)i.[58] It can be seen that the caleulated results vary greatly from those obtained with a metallic substrate. Figure 2.15 shows the mean square electrie fields for the s and p polarizations. The most obvious difference from the ealculations with a metallic substrate is that in this ease, all of the eomponents of the mean square electrie field vary with the incident angle of the infrared beam. What this essentially means is that as opposed to reflection from a metallie substrate, with reflection from a water substrate or subphase it is potentially possible with s and p polarized beams to eharaeterize dipole moment orientation not only relative to the z direction, but also along the x and y directions. By varying the incident angle of the infrared beam, the mean square electric field in each of the x (i.e. the s polarized eomponent), y, and z direetions could in theory be maximized. It should be noted, though, that for a p polarized incident beam it is difficult to achieve a relatively pure mean square electrie field in the z direetion perpendicular to the interfaees since there is always some component in the y direction (py component) parallel to the plane of the interfaces at virtually all angles. However, a drawback which is apparent in this plot, is that the mean square electric field intensities are low relative to the pz component of the mean square electrie field for refleetion on a metallic substrate at grazing incident angle. Thus the interaction between the absorbates and the electric field are weaker. Therefore, for experiments at the air-water interface to be successful, the associated optics, interferometer, deteetor, and incident angle must be optimized to give the best signal/noise ratio possible as was alluded to earlier.

Plots of the reflectivity and absorbance versus incident angle are shown in Figure 2.16 and Figure 2.17 respectively. In Figure 2.16, it can be seen that the reflectivity of the s polarized eomponent increases with the angle of incidence. The p polarized component, however, exhibits a dip to zero reflectivity at the angles near the Brewster angle. This is as expeeted sinee at the Brewster angle, the p polarized component of the

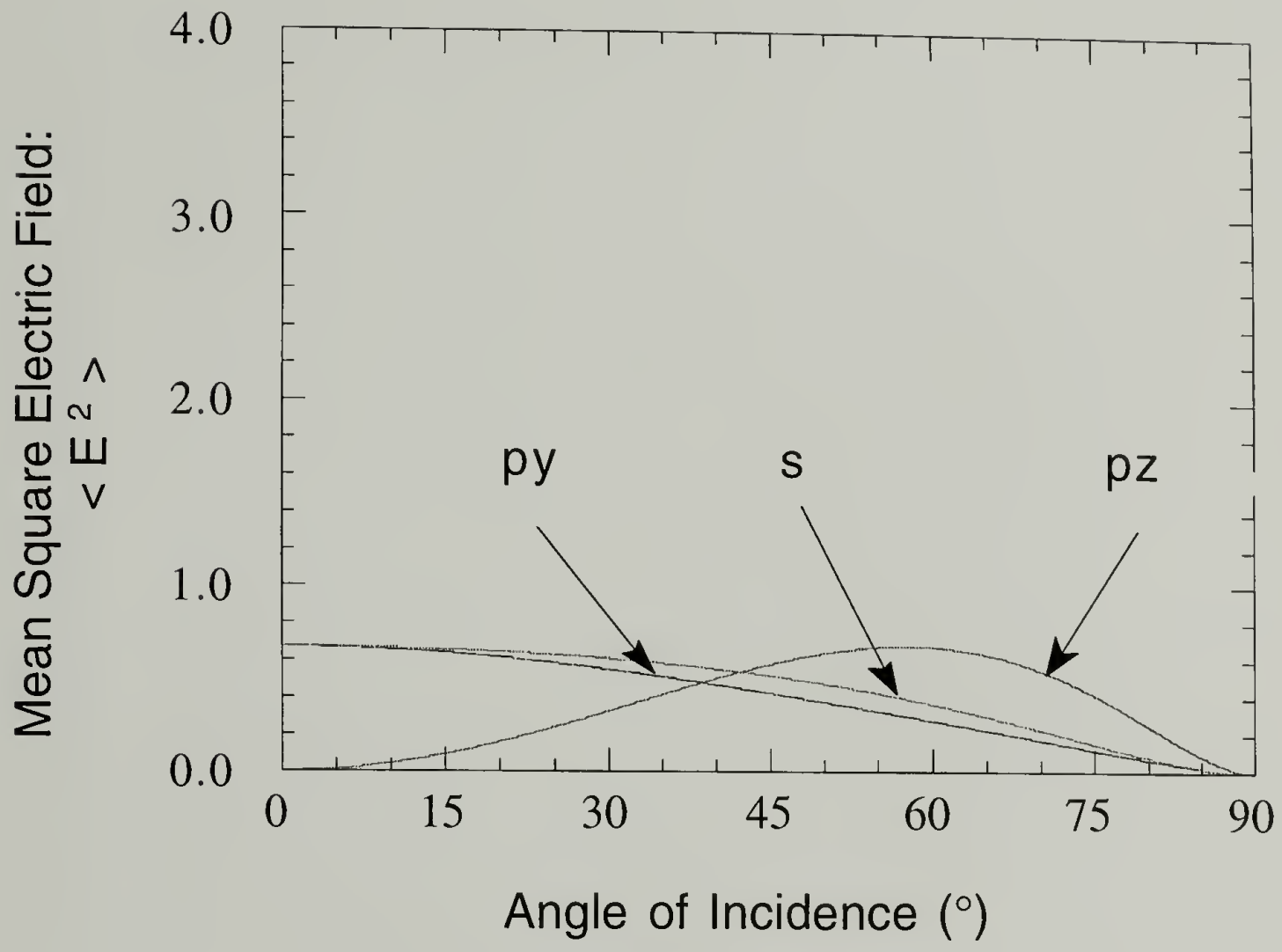

Figure 2.15 Mean square electric field of both polarizations for a film at the air-water interface.

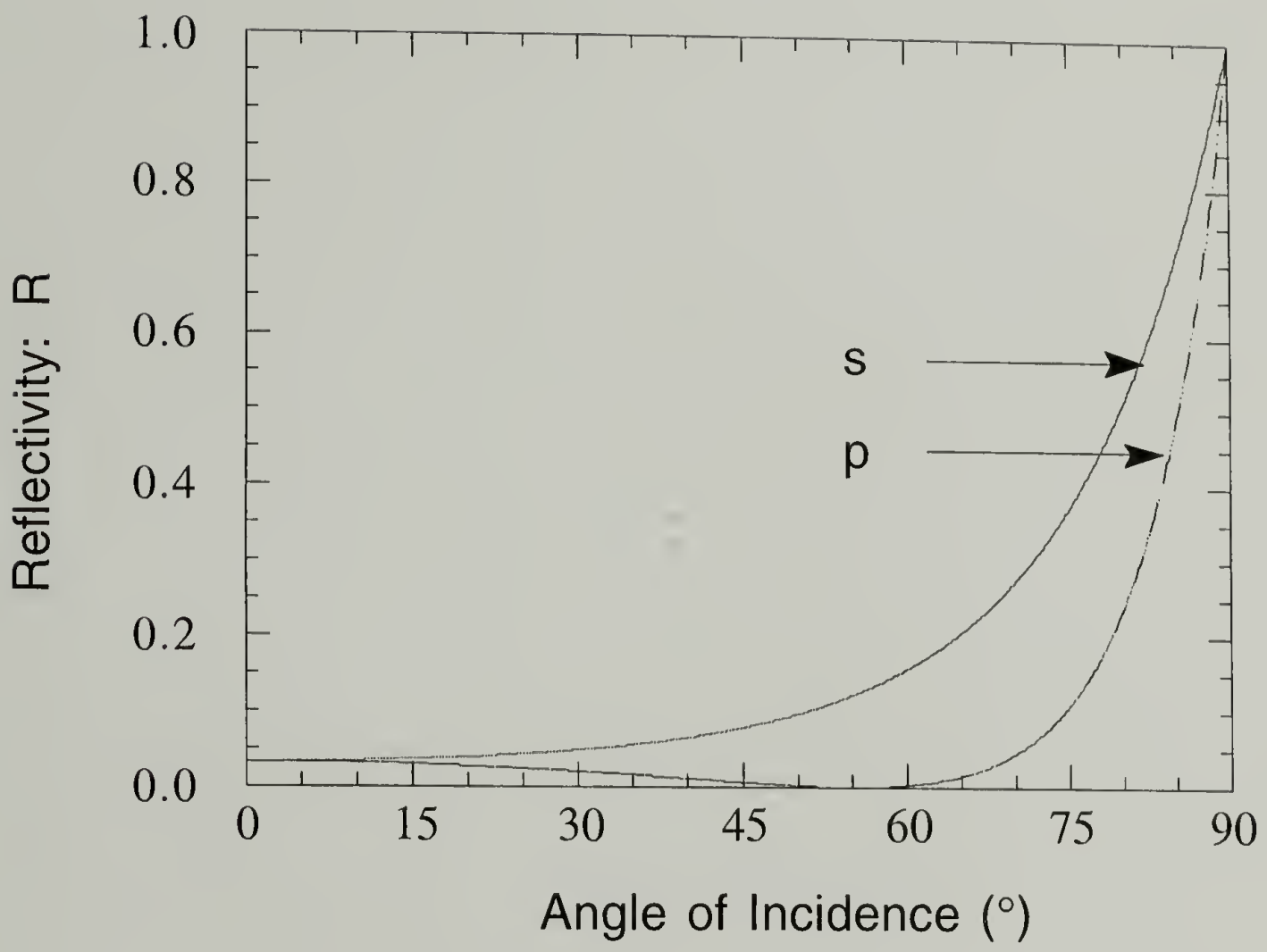

Figure 2.16 Variation of the reflectivity for both s and p polarizations of a film at the air-water interface.

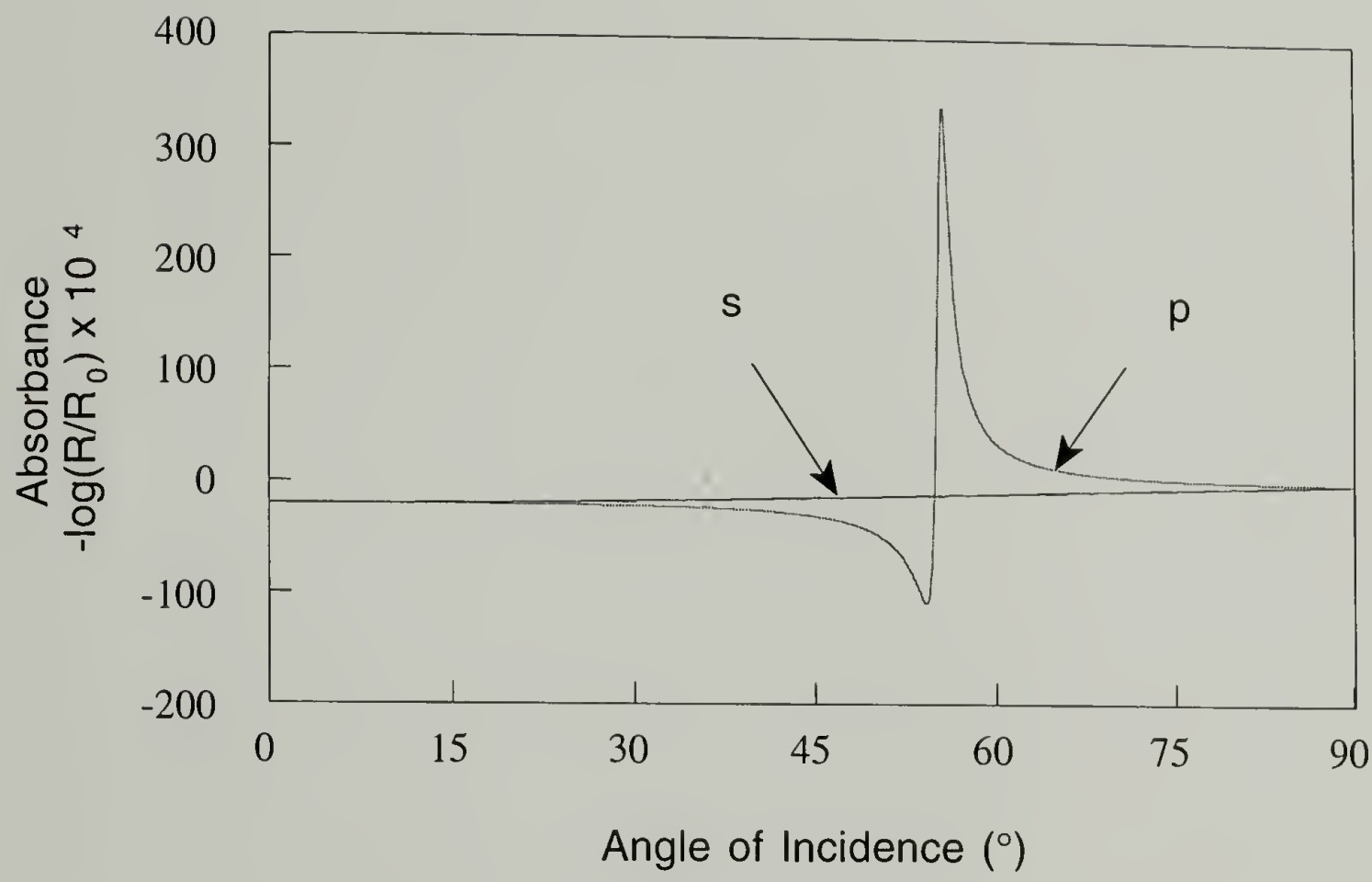

Figure 2.17 Absorbances for s and p polarizations for a film at the air-water interface.

electric field is not reflected. Looking at Figure 2.17, it can be seen that the angular dependence of the absorbance of the s and p components are very different. For the s component, the calculated absorbance is negative for most angles and has a maximum absolute value at angles approaching 0°. This shows that the reflectivity of the air/polymer film/water system is for most angles greater than the reflectivity for the pure two phase air-water interface. The s component of the absorbance is also small relative to the calculated p component absorbance with a metallic substrate at grazing incident angle. The dependence of the p component of the absorbance, although initially similar to the s component at lower angles, has a large enhancement and subsequent change in sign at angles near the Brewster angle where the absorbance changes from negative values to positive values with increasing incident angle. Even with the large enhancement in the theoretical absorbance of the p component at angles near the Brewster angle, from a practical standpoint reflection/absorption at such angles is not optimal due to the poor signal/noise ratio. The poor signal/noise ratio is caused by the fact that although the change in reflectivity due to presence of the film at the air-water interface is large, producing high absorbances, the reflectivity of the air/film/water system itself is very near zero. Reflection/absorption at other angles yields spectra with smaller absorbances due to the smaller difference in reflectivity between the air/film/water state versus the pure air-water state, but of greater importance have a much better signal/noise ratio. Nevertheless, angles of incidence near the Brewster angle have at times been chosen for experiments at the air-water interface by other researchers.

Overall, however, the reflectivities for both components are small relative to the pz polarized component for metallic substrates. This leads to lower instrumental throughput and lower signal/noise ratios. The calculated plots in Figures 2.15, 2.16 and 2.17 illustrate the greater overall demands required for infrared reflection experiments of polymer films at air-water interfaces versus polymer films at air-metal interfaces. Lastly,

Figure 2.18 shows the phase shift associated with the s and p components of the electric field where it can be seen that the p component undergoes a 180° change in phase at the Brewster angle.

2.2.2 Coupling of Langmuir Trough and External Reflection Infrared Spectrometer

In order to precisely control the surface packing density of polymer films spread at an air-water interface while simultaneously measuring both the external reflectance infrared spectra and the surface pressure of the spread film, a Langmuir trough was designed and coupled with a Fourier transform infrared instrument. The design and construction of the setup was done by Sophie Riou. A schematic of this experimental setup is shown in Figure 2.19 where the entire setup (trough, interferometer, detector and associated optics) is mounted on a floating optical table. The general design of the experimental setup was patterned after earlier designs by Dluhy among other groups.[51,52,55,56] In the following, the specifics of the Langmuir trough itself will first be described. A description of the actual coupling between the trough and the Fourier transform infrared instrument will then be presented.

In designing the trough, several factors were of particular importance. First, the trough had to be large enough so that edge and meniscus effects would be minimized. Additionally, the size of the trough had to be large enough to accommodate both the reflected infrared beam at the film surface and the Wilhelmy plate associated with surface pressure measurements. Specifically, there had to be enough space near the center of the trough so that both meniscus effects from the edges of the trough on the Wilhelmy plate and the reflected infrared beam and meniscus effects from the Wilhelmy plate itself on the reflected infrared beam would be negligible. With this in mind, the trough, machined from a solid piece of Teflon™, had a length of 450 mm and a width of 153 mm. By moving the compression barriers of the Langmuir trough, the surface area at the air-water interface could be varied from 540 cm^2 to 125 cm^2. The depth of the bath was 5 mm.

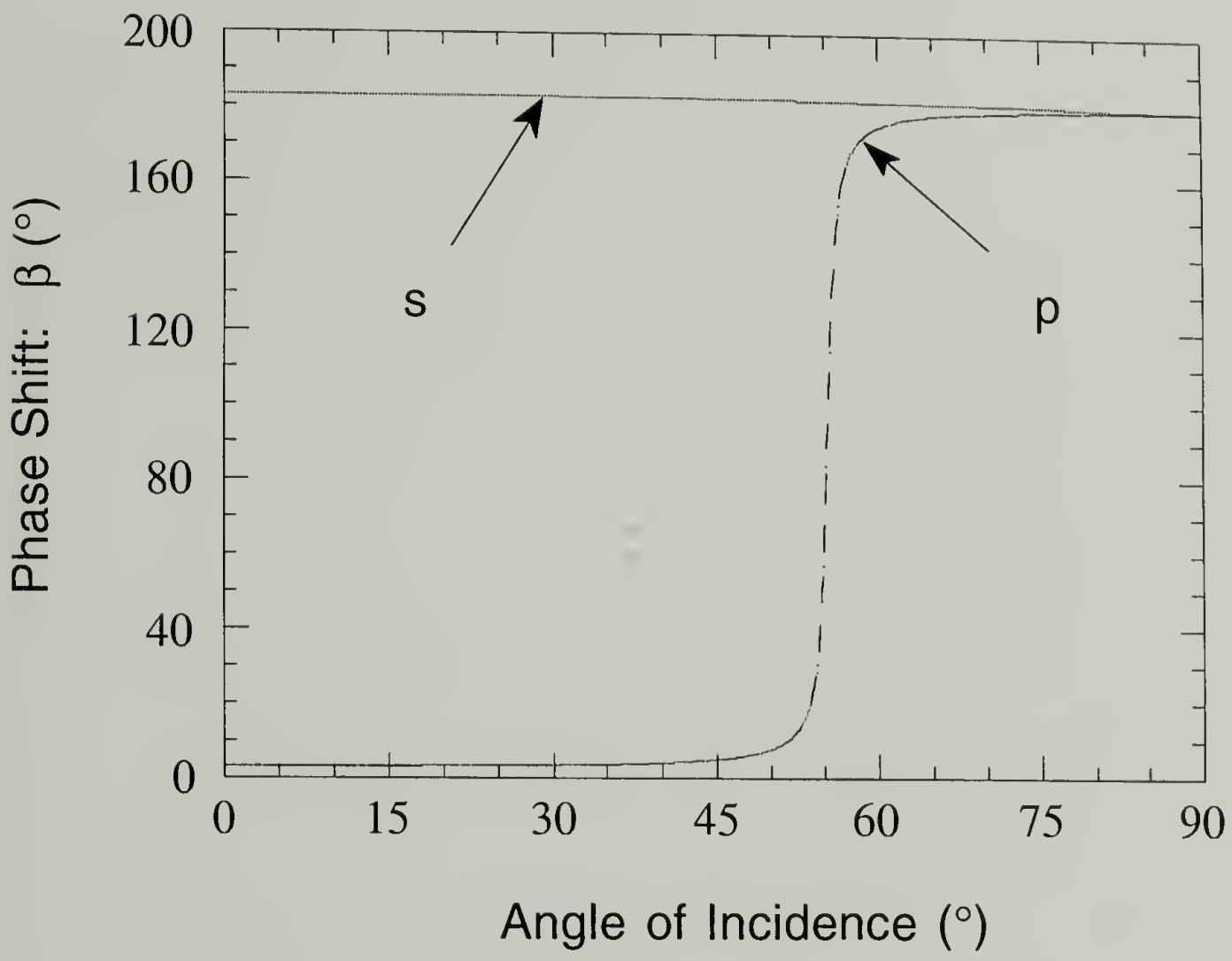

Figure 2.18 The variation of the phase shift for both s and p polarizations for a film at the air-water interface.

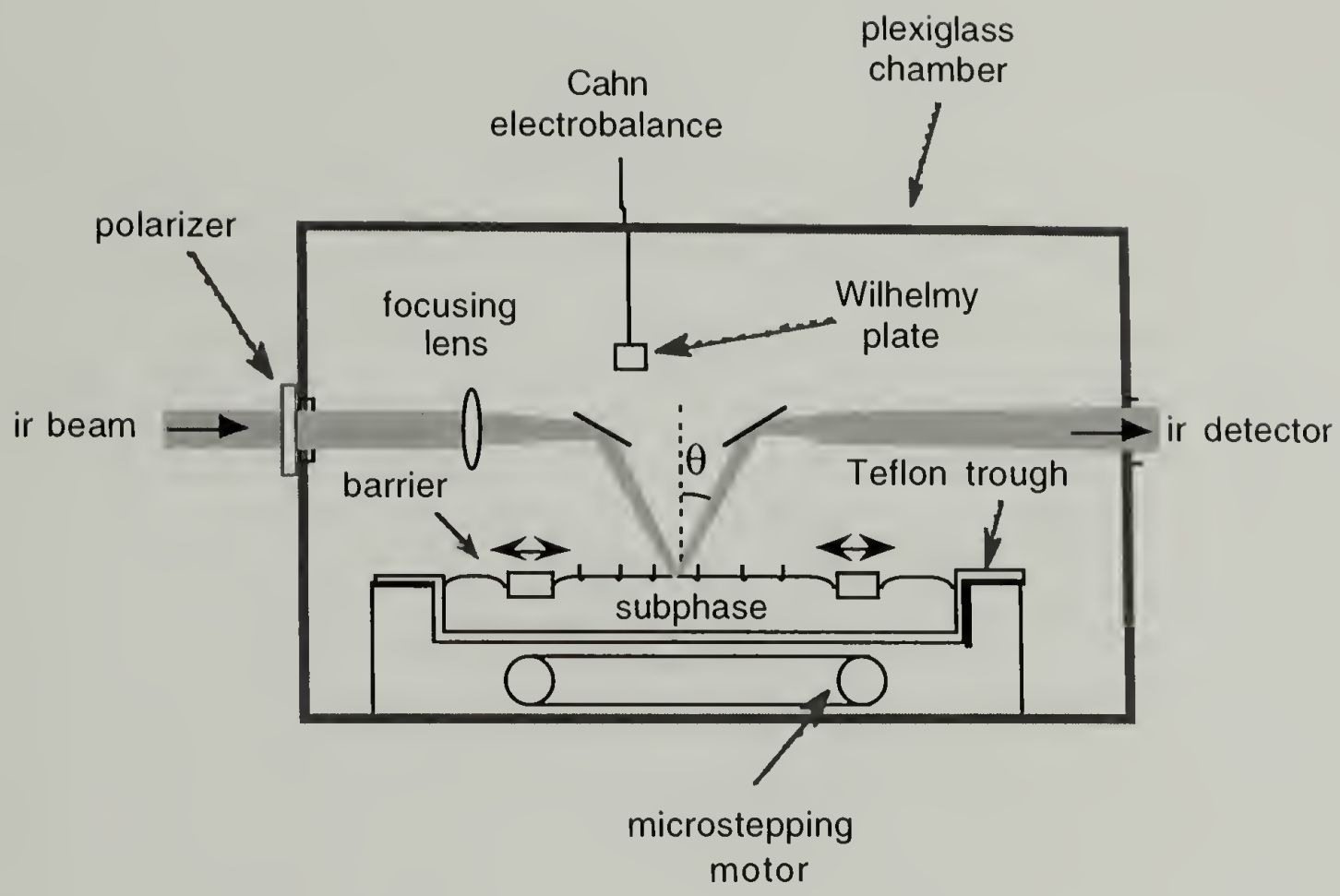

Figure 2.19 A schematic of the coupling of external reflection infrared spectroscopy and a Langmuir trough.

In addition, the entire Teflon™ trough was mounted on a solid anodized aluminum baseplate and enclosed in a Plexiglass chamber. Within the baseplate were several channels in which fluid could be circulated for temperature control of the trough. The Plexiglass chamber, on the other hand, served to isolate the trough environment from contaminants (e.g. dust) as well as to allow for the control of the relative humidity of the trough environment. The relative humidity in the trough chamber was controlled by slowly purging the chamber with either nitrogen gas or carbon dioxide-free dry air.

Another important factor in the design of the Langmuir trough was the use of a microstepping motor for the accurate control of the compression barriers of the trough. Such a motor was chosen for its ability to operate smoothly without perturbing the water surface, and for its ability to operate at extremely low speeds. The specific motor used in driving the compression barriers of the trough was a Parker Hannifin Corporation OEM 57-51 single shaft microstepping motor actuated by a Parker Hannifin Corporation OEM 650 driver. The microstepping motor operated at a 25 000 steps/revolution resolution. The barriers of the trough, in use driven simultaneously toward the center of the trough in the lengthwise direction of the trough, were made from two flat movable 200 x 25 x 5 mm Teflon™ strips. To prevent leakage of the film being compressed between the barriers at the air-water interface, the barriers were designed such that they fit tightly across the rim of the trough. Subsequently, the barrier compression rate could be varied continuously from 0.6 cm^2min^{-1} to 60 cm^2min^{-1} with great precision and accuracy.

The surface pressure of films spread in the trough was measured with a Cahn Balance 2000 (ATI Instruments) electrobalance enclosed in the Plexiglass chamber with the trough. Specifically, a 15 mm x 10 mm x 0.18 mm Wilhelmy paper plate (Whatman Chromatographic paper n°1) in contact with the film-water surface was connected by a thin wire to the electrobalance. The electrobalance was calibrated with a series of known weights and surface tension measurements were also made on several different solvents of known surface tension to check the accuracy of the measurement. Prior to the

spreading of a sample at the air-water interface, the surface tension of the pure water subphase was set to zero. Surface tension measurements could be measured with an accuracy of roughly +0.2 mNm^{-1}. Also, the Wilhelmy paper plate was oriented parallel to the compression barriers of the Langmuir trough.

The Fourier transform infrared interferometer and detector associated with external reflection infrared spectroscopy were coupled externally to the Plexiglass enclosed Langmuir trough in the following manner. First, the collimated infrared beam produced by the interferometer (Perkin-Elmer System 2000 Fourier transform infrared interferometer) was either passed directly into the enclosed chamber of the trough, or if polarization experiments were desired (i.e. s polarized or p polarized infrared beam) was passed through a polarizer (Brewster's angle double diamond infrared polarizer) and then into the chamber. The beam then was passed through a focusing lens after which it was reflected off of a flat gold coated mirror (Edmund Scientific) and brought into focus at the film-water surface. The focusing lens, specifically, was a 200 mm focal length f/8 Zinc Selenide lens purchased from Ealing Optical. The angle of incidence of the infrared beam at the air-water interface could be adjusted with the flat gold coated mirror. For these experiments, the angle of incidence of the infrared beam was always set at $30 \pm 4°$. The reason this particular angle of incidence was selected is due to the fact that at this angle the absorbance and signal/noise ratio for both s and p polarized beams are reasonable for reflection/absorption on polymer films at the air-water interface. This is shown in Figure 2.17 (discussed previously in section 2.2.1) with a plot of the calculated absorbance (s polarized and p polarized components) versus incident angle for such a system. In the experiments discussed in this chapter, however, no experiments were carried out with a p polarized incident beam for reasons which will be explained later. All experiments were done with a s polarized beam. It should also be pointed out that because of the chosen incident angle, all infrared bands in the measured external reflectance infrared vibrational spectra were negative. In terms of the analysis of such negative bands (i.e. peak position,

intensity, band shape etc.), however, the analysis does not change from that of standard transmission infrared vibrational spectra with positive absorbances.

Following reflection/absorption of the infrared beam at the air/film/water interfaces, the infrared beam is then reflected off of another flat gold coated mirror (Edmund Scientific) and then sent to the detector. It should also be mentioned here that the trough is oriented such that the compression direction of the barriers is parallel to the plane formed by the incident and reflected infrared beams. This geometry makes it such that for a s polarized infrared beam, the polarization direction, in addition to being in the plane of the air-water interface, is perpendicular to the compression direction. External detector optics then focus the infrared beam onto a ~1.0 mm^2 active area of the detector. The detector, was a narrow-band mercury-cadmium-telluride (EG&G Judson J15D) detector equipped with a Zinc Selenide window which had to be cooled with liquid nitrogen. To prevent water from condensing on the detector window, the detector and its associated optics were isolated in a small chamber which was constantly purged with either nitrogen or carbon dioxide-free dry air. This type of detector has a cut-off frequency at ~750 cm^{-1} (no detection < 750 cm^{-1}) and has a peak sensitivity of $D\lambda^* = 4.10 \times 10^{10}$ $cmHz^{1/2}W^{-1}$ at 10 kHz. The signal/noise ratio in transmittance mode at 2000 - 2200 cm^{-1} was $\Delta T = 0.021\%$.

Finally, the Langmuir trough and external reflection infrared spectroscopy setup was tested with several well studied small molecule amphiphiles such as phosphocholine. It was found that the surface pressure/area isotherms for monolayer films of these molecules were in good agreement with previously published isotherms. The spectra obtained of these monolayer films at the air-water interface were also in good agreement with what has been reported by others.[56] These results demonstrated that our Langmuir trough and external reflection infrared spectroscopy setup could both produce high quality spectra as well as accurately control the molecular surface area of films spread at the air-water interface.

2.3 Instrumentation and Methods

Due to the fact that small amounts of contaminants can affect the behavior of films spread at an air-water interface, extreme care was taken to assure that the Langmuir trough was clean before each experiment. In addition to keeping the Plexiglass™ enclosure closed as often as possible to minimize dust, the Teflon™ trough itself as well as the Teflon™ compression barriers were cleaned before each run with chloroform. Also, on a very regular basis, both the Teflon™ trough and barriers were immersed in solutions of water and KOH. Following such a soaking, the trough and barriers were thoroughly rinsed with distilled and then deionized water.

In preparing the trough for an experiment, the trough was first filled with deionized water to a level moderately above both the edges of the trough and the barriers. The surface of the water between the barriers was then aspirated with a clean glass pipet to remove any trace contaminants adsorbed to the water surface. A Wilhelmy plate was then placed in contact with the water surface allowing for the plate to wet. Upon stabilization of the electrobalance, the barriers of the trough were then slowly closed and opened while monitoring the voltage output of the electrobalance. If a change in voltage was observed indicating surface contaminants, the water surface was again aspirated and the process repeated until a change in voltage was not observed. Attention also had to be taken to make sure that the level of the water surface remained above the compression barriers following aspiration.

With the compression barriers open to their maximum surface area, a single beam external reflectance infrared spectrum of the pure water surface was then obtained. This spectrum would be used as a reference state to ratio with sample single beam spectra. The polymer solution was then spread. The amount of polymer spread at the air-water interface was always chosen such that the as-spread uncompressed film would form a very expanded monolayer (i.e. large surface area per molecule at the air-water interface where the surface pressure is constant at zero). Spreading was specifically done using a

100 µl Hamilton graduated glass syringe equipped with a Teflon™ tipped plunger in a dropwise manner. By carefully placing the syringe needle tip close to the water surface, drops were slowly applied. The film was then allowed to equilibrate for at least 1 hour before the barriers were compressed. The compression speed for all experiments was 2.77 cm^2min^{-1} (150 min for a full range compression experiment). Additionally, experiments were done with the water subphase maintained at room temperature.

The external reflectance infrared spectra collected for films spread at the air-water interface were obtained with the incident beam polarized in the s direction, parallel with the plane of the interface (Figure 2.20). As was mention previously, no p polarized spectra were collected. The reason for this is due to the fact that while the s polarized component can readily be used to probe dipole moment orientation since it is defined within the plane of the interface, the p polarized component does not have a well defined polarization direction with respect to the air-water interface. In addition, it should be pointed out that the polarization direction of the s polarized infrared beam in our experimental setup was also perpendicular to the axis of compression as defined by the moving barriers. As was shown in section 2.2.1, a p polarized infrared beam has components both in the plane of the interface (i.e. specifically the py component of the p polarized beam which is perpendicular to the s polarization) as well as perpendicular to the air-water interface (i.e. pz component). Although the relative amounts of each component can be varied by changing the angle of incidence of the infrared beam as was shown with the calculated mean square electric field intensities (Figure 2.15), it is difficult nevertheless to get a relatively pure p polarized component perpendicular to the surface of the air-water interface. Moreover, practically speaking the accurate control of the relative amounts of each of the two components would also be quite hard to achieve.

External reflection infrared spectra were collected under the following conditions. Due to the relatively small signal, the J-stop collimator of the interferometer was set to a resolution of 4 cm^{-1} with the largest aperture, 12.5 mm, so as to give the highest energy.

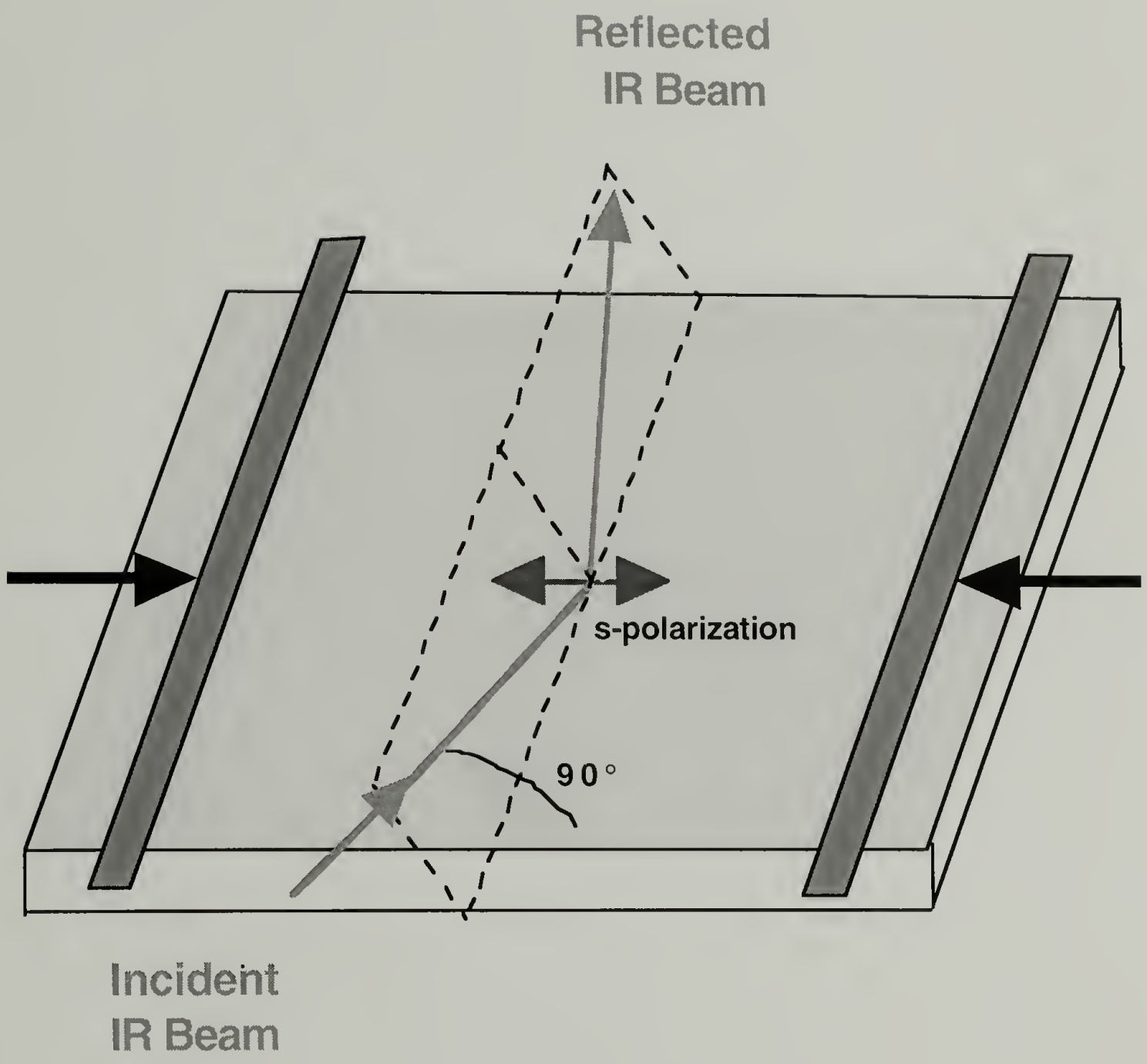

Figure 2.20 Reflection geometry and polarization direction of infrared beam at the air-water interface of the Langmuir trough.

The gain was set at 8. A triangular apodization function was also selected to modify the Fourier transformation of double sided interferograms. The number of coadded scans for each spectrum varied between 100 and 512 and was collected at a resolution of 4 cm^{-1}. For compression experiments, the scan time was sufficiently fast relative to the compression speed of the barriers; each spectrum could be considered to have been collected at a constant surface area. The data were collected at a 0.2 cm^{-1} interval. As mentioned previously, infrared absorbances are defined by the relation $-\log(R/R_0)$ where R and R_0 are the reflectivities of the water surface with the polymer film and without the polymer film, respectively.

An important issue that had to be addressed in the collection of sample spectra was the difficulty of water vapor bands (~2000 cm^{-1} to 1400 cm^{-1}) present to varying degrees in the ratioed sample spectra. Typically, in the collection of infrared spectra for most types of samples this not a problem; the sample chamber for the background single beam spectra and for the sample single beam spectra are both purged with either dry air or nitrogen for sufficient periods of time. However, for external reflection infrared spectroscopy at an air-water interface such a complete purge of the trough chamber cannot be done for obvious reasons. Thus there can large mismatch between the external reflection infrared single beam spectra for the background, i.e. the pure water surface, and the sample single beam spectra. In the ratioed spectra, this can make the analysis of bands from the sample difficult in regions which overlap with water vapor bands. To deal with this, the humidity level of the trough chamber was controlled by varying the nitrogen/dry air purge as spectra were being collected. The spectrometer software package (PE-Grams/2000™ Version 2.03, Galactic Industries Corporation) allows for the realtime viewing of ratioed spectra during scanning. Thus by carefully regulating the humidity level in accordance with the observed real time spectra during scanning, oftentimes the water vapor bands could be minimized from sample spectra making analysis of bands in these regions possible.

An additional feature in the external reflection infrared spectra which should also be discussed is a distortion in the baseline at roughly 1650 cm^{-1} present in some spectra. This distortion could not be removed as with water vapor bands and is caused by the large change in the complex refractive index of the water subphase. The distortion appears as a rise in the baseline in a direction opposite to that of the negative absorbances from a polymer film. It is present to varying extents for different samples. However, it was observed that in spectra collected for a given sample spread at the air-water interface, the shape of this distortion in the baseline did not change during compression. Thus the analysis of peaks in this region for a series of spectra collected during compression was done by making the same baseline correction in each spectrum.

Transmission infrared spectra were obtained using a Bruker IR98 FT-IR instrument. The detector was a liquid nitrogen cooled narrow-band mercury-cadmium-telluride (MCT) detector. Films were cast on polished CaF_2 disks (25 mm x 2 mm). Individual spectrum were obtained by coadding 256 scans at a resolution of 2 cm^{-1}.

The analysis of peaks in infrared spectra (i.e. peak position, peak height, peak area) obtained at the air-water interface and by standard transmission infrared spectroscopy was done using Lab Calc by Galactic Industries Corporation, a data analysis software package.

Differential scanning calorimeter scans were done using a DSC 2910 instrument by DuPont Instruments. Upon initially cooling with liquid nitrogen -30° C, heating runs for the various samples made at 10° C per minute.

2.4 Polyglutamates

As was mentioned previously, a series of polyglutamates were studied at the air-water interface. The goal was to understand the affect of long *n*-alkyl side groups on the structure of polyglutamate "hairy-rod" Langmuir films as a function of surface packing density and *n*-alkyl side group content. The specific polymers studied were two random

copolyglutamates, poly(γ-methyl-L-glutamate-*co*-γ-*n*-octadecyl-L-glutamate)s with varying *n*-alkyl side group content (20% and 50% *n*-octacecyl-L-glutamate groups) (Figure 2.21) and a pure poly(γ-methyl-L-glutamate) without *n*-alkyl side groups. All three samples are insoluble in water.

2.4.1 Materials

Poly(γ-methyl-L-glutamate-*co*-γ-*n*-octadecyl-L-glutamate) random copolymers can be synthesized in two ways; either by the copolymerization of the N-carboxy anhydrides of γ-methyl-L-glutamate and γ-*n*-octadecyl-L-glutamate, or by ester interchange reaction of poly(γ-methyl-L-glutamate) with *n*-octadecyl alcohol.[25-27] In our experiments, the latter method was used. Poly(γ-methyl-L-glutamate) purchased from Sigma Co. of $MW_{[VIS]}$ = 37 000 and stearyl alcohol (99.0%) purchased from Aldrich Co. were used without further purification. The ester interchange reactions were performed at ~80° C with 0.5 g of poly(γ-methyl-L-glutamate) and 20 g of stearyl alcohol dissolved in 50 mL of 1,2-dichloroethane (99.8%, Fisher Scientific) with 1.2 g of *p*-toluenesulfonic acid as a catalyst. After an arbitrary reaction time (~14 hours or less), the polymers were isolated by precipitation from solution into methanol (99.9%, Fisher Scientific). They were then purified several times by fractional precipitation from solution in chloroform-methanol mixed solvent and dried under vacuum at ~100° C.

The composition of the copolymers was determined by ^{1}H NMR spectroscopy (d-chloroform/copolymer solution). The ^{1}H NMR spectra for the two copolymers made are shown in Figure 2.22 and Figure 2.23 for the samples of 20% and 50% γ-*n*-octadecyl-glutamate composition, respectively. The assignments for the peaks in the spectra are as follows in Table 2.1.[63] The overall percentage of the *n*-octadecyl-L-glutamate groups in each of the two copolymers was then determined by taking the ratio of the intensity of a given side group proton from a *n*-octadecyl group divided by the number of such protons in a repeat unit, and the intensity of the backbone C<u>H</u> proton. The two random

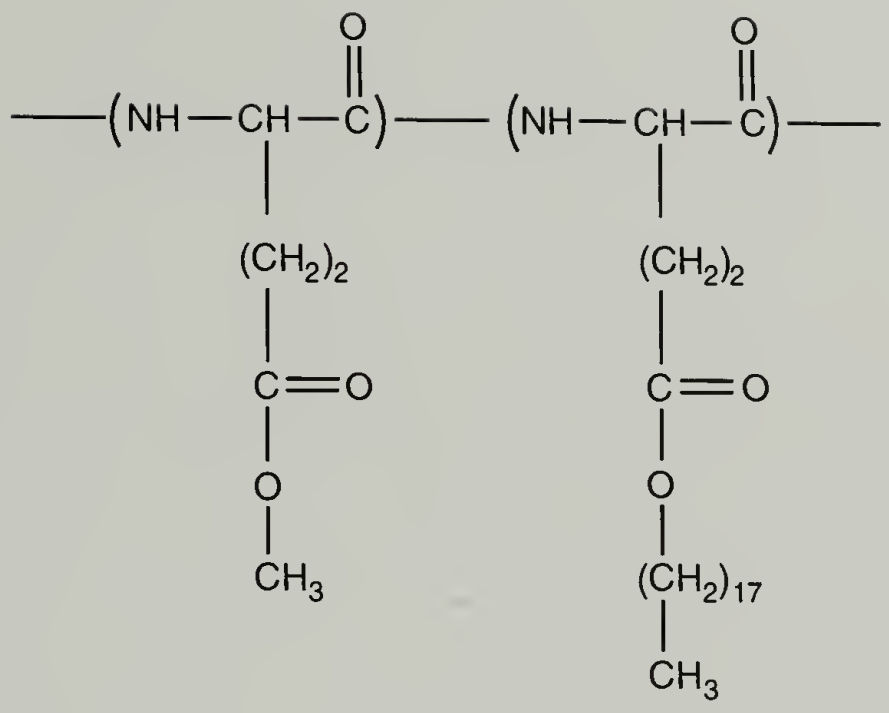

Figure 2.21 "Hairy-rod" poly(γ-methyl-L-glutamate-*co*-γ-*n*-octadecyl-L-glutamate).

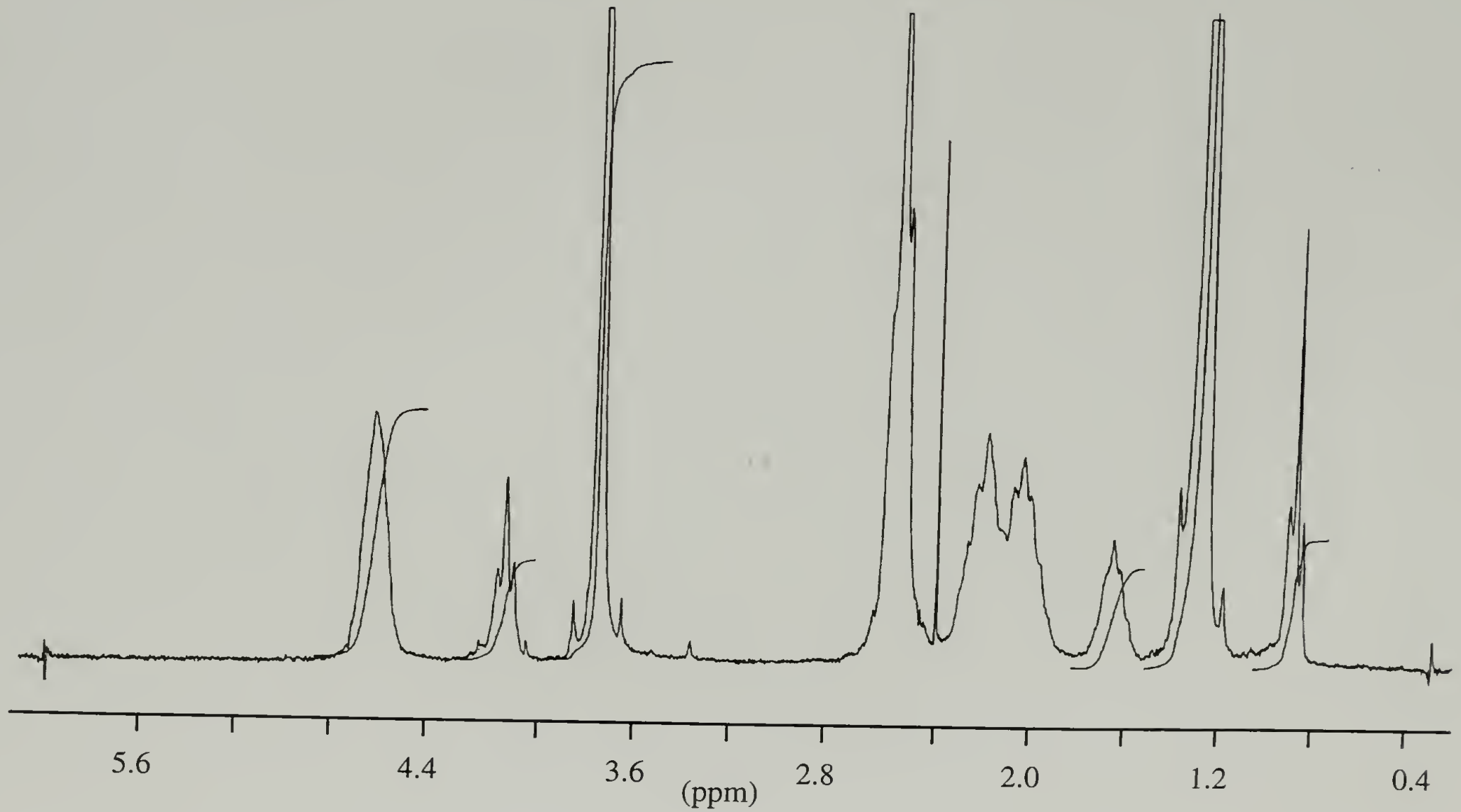

Figure 2.22 ^{1}H NMR spectrum of copolyglutamate of 20% γ-*n*-octadecyl-L-glutamate composition.

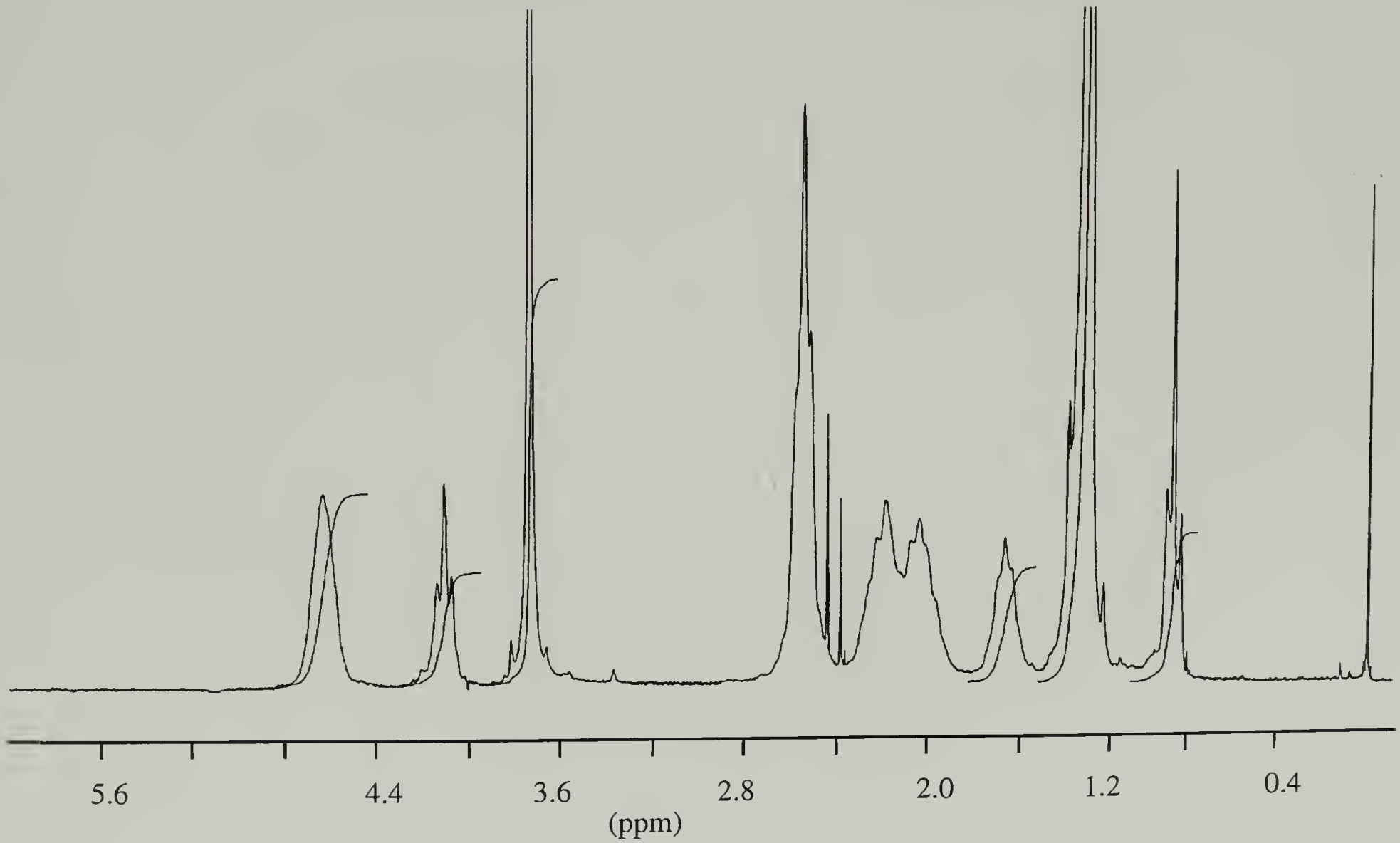

Figure 2.23 ^{1}H NMR spectrum of copolyglutamate of 50% γ-*n*-octadecyl-L-glutamate composition.

Table 2.1 ^{1}H NMR Peak Assignments for Copolyglutamates.

^{1}H Assignment	Chemical Shift (ppm)
a) backbone C<u>H</u>	4.63
b) side group COO-C<u>H</u>$_3$	3.726
c) side group COO-CH$_2$-C<u>H</u>$_2$-	1.62
d) side group COO-CH$_2$-CH$_2$-(C<u>H</u>$_2$)$_{15}$-	1.267
e) side group COO-CH$_2$-CH$_2$-(CH$_2$)$_{15}$-C<u>H</u>$_3$	0.87

copolymer samples were calculated to have 20% and 50% *n*-octadecyl-L-glutamate repeats respectively.

Poly(γ-methyl-L-glutamate) without the long *n*-octadecyl side groups was purchased from Sigma Co. and was used as received. The viscosity average molecular weight ($MW_{[VIS]}$) of the sample, as listed on the container, was 307 000.

The solvents used for the spreading of polymer monolayers on the Langmuir trough were 99:1 mixtures of chloroform (99.0+%, Fisher Scientific) and dichloroacetic acid (99.0+%, Fisher Scientific). These solvents were used as received. Solutions were made at 0.1 mg/ml polymer/solvent respectively. The solutions were stored in the dark at +5° C and were allowed to equilibrate to room temperature before use.

The water used for the subphase of the Langmuir trough was distilled water treated by filtration with a Milli-Q purification system yielding deionized water of a nominal resistivity (18.2 $M\Omega cm^{-1}$).

2.4.2 Results and Discussion

The results and subsequent discussion of polyglutamates will be divided into several sections. In the first section (2.4.2.1), the surface pressure/area isotherms for each of the three types of samples studied will be discussed. The discussion will be limited mostly to the analysis of the isotherms along the lines of what others have often concluded about the structure of films based on these plots. Since isotherms provide limited structural information in themselves, some of the analysis will therefore be speculation and will serve as a precursor to the more quantitative analysis that will follow. A more quantitative analysis of the isotherms and the structure of the films at the air-water interface will then begin with results obtained from external reflectance infrared spectra. Section 2.4.2.2 will focus on the structure of the *n*-octadecyl side groups and their *liquid-like/solvent-like* quality and section 2.4.2.3 on the subsequent ordering of the rigid-rod main chains with compression. In the following sections, the results at the air-water

interface will also be related to their predicted effect on the Langmuir-Blodgett transfer process and Langmuir-Blodgett film structure.

2.4.2.1 Surface Pressure/Area Isotherms

The surface pressure/area isotherms for the poly(γ-methyl-L-glutamate) sample, the poly(γ-methyl-L-glutamate-*co*-γ-*n*-octadecyl-L-glutamate) of 20% γ-*n*-octadecyl-L-glutamate composition, and the poly(γ-methyl-L-glutamate-*co*-γ-*n*-octadecyl-L-glutamate) of 50% γ-*n*-octadecyl-L-glutamate composition are all shown in Figure 2.24.

Beginning first with poly(γ-methyl-L-glutamate), it can be seen that the shape of the isotherm can be characterized as roughly having four regions: a) a region at large surface areas greater than 21 $Å^2$/chemical repeat where the surface pressure remains constant at zero, b) a region characterized by a steep rise in the surface pressure to 22 mNm^{-1} between ~19.5 and 17.0 $Å^2$/chemical repeat, c) a plateau region where the surface pressure levels off, d) a final rise in the surface pressure starting gradually at ~12.5 $Å^2$/chemical repeat and later gaining in slope. This surface pressure/area isotherm is in agreement with what has been previously reported.[64-67]

In these previous studies it has commonly been assumed that at an air-water interface, Langmuir films of these hydrophobic synthetic polypeptides adopt a stiff rod-like α-helical conformation which is stabilized by strong intramolecular hydrogen bonds along the helix axis.[43,44,65,68] In some studies, indirect measurements have also been interpreted as indicating the α-helical conformation (e.g. usually films transferred onto solid substrates[43] or deuteration exchange experiments[64,66]). Subsequently, it has often been stated that given such a long rigid rod-like conformation, the molecules lie flat at the air-water interface.

As will be more fully discussed in section 2.4.2.3, this helical conformation at the air-water interface has now been directly established for poly(γ-methyl-L-glutamate). Therefore, with the conformation known and given that an α-helix has a calculated

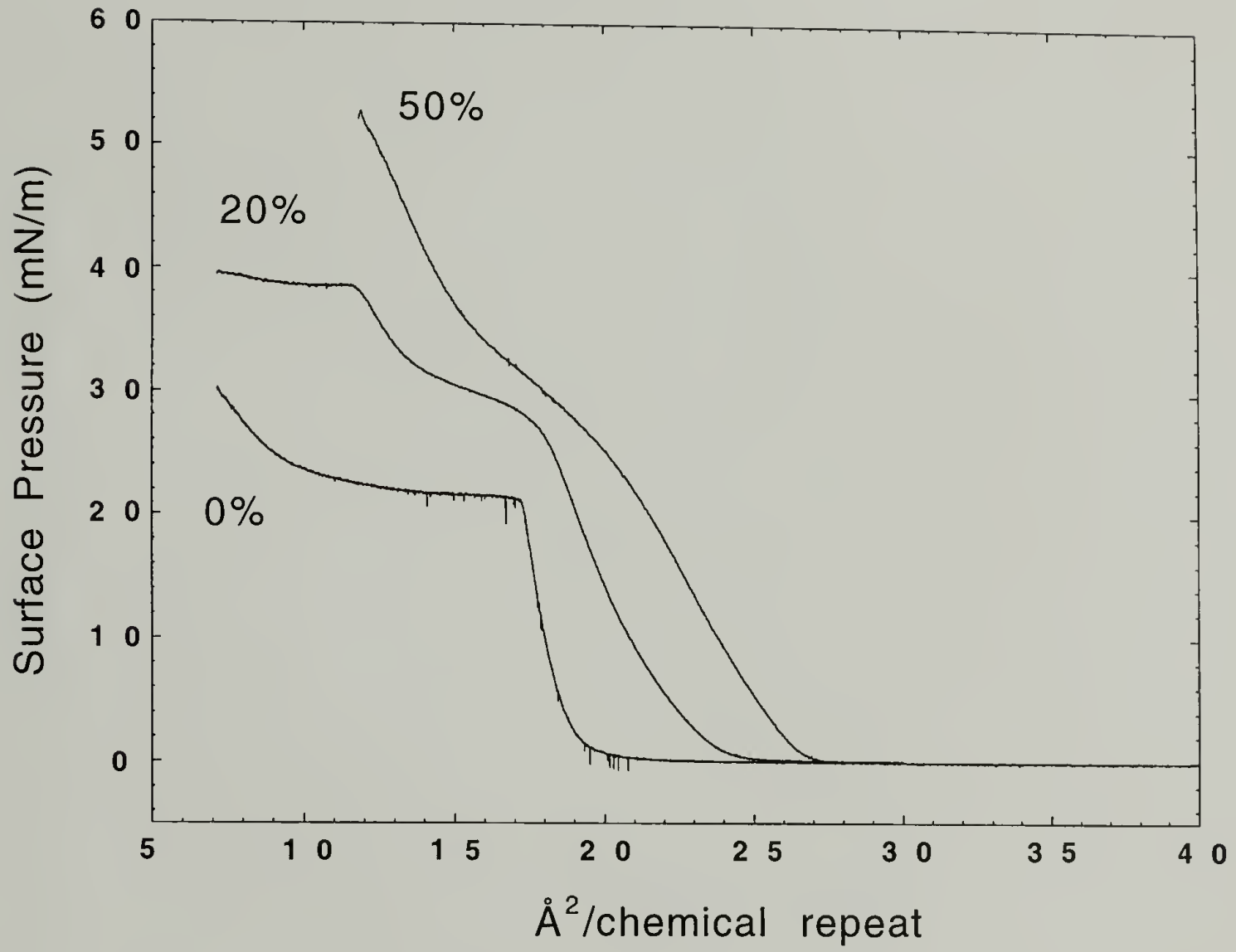

Figure 2.24 Surface pressure/area isotherms for films of poly(γ-methyl-L-glutamate), and poly(γ-methyl-L-glutamate-*co*-γ-*n*-octadecyl-L-glutamate) of 20% and 50% γ-*n*-octadecyl-L-glutamate composition at the air-water interface.

molecular diameter of ~14 Å and a length of 1.5 Å per residue along the molecular axis,[35] an area per chemical repeat of 21 $Å^2$ can be calculated for closely packed helices lying flat at an air-water interface. This value is in close agreement with the beginning of the sharp rise in the surface pressure/area isotherm. It can therefore be concluded that the molecules do in fact lie flat and upon compression pack efficiently at the interface. Additionally, given the rather large rise in the surface pressure once the monolayer becomes condensed, it is likely that the film possesses a considerable amount of intermolecular cohesion at the water surface (i.e. between polymer molecules themselves and between polymer molecules and water surface). For a less stable monolayer incapable of such close packing at an air-water interface, collapse of the film would occur at much larger surface areas and the rise in the surface pressure upon compression to a condensed monolayer state would be smaller before collapse. A reason for the stability of monolayers of poly(γ-methyl-L-glutamate) at the air-water interface can be attributed to the hydrogen bonded groups and the ester groups in the side chains which together give the molecules a slightly hydrophilic character even though overall, the molecules are hydrophobic and not soluble in water. Since the Langmuir-Blodgett transfer process usually requires transfer of a condensed monolayer, neglecting other factors (e.g. fluid dynamics of the monolayer at the water surface[9-11]) the stability of films has been interpreted as being one important factor in affecting transferability.[30]

The "yield point" of the monolayer at ~22 mNm^{-1} and the plateau region in the surface pressure/area isotherm has been commonly attributed to a transition from a monolayer composed of domains of parallel packing helices (poly(γ-methyl-L-glutamate) exhibits lyotropic liquid crystalline phase behavior[25]) to a bilayer, both with the helices lying flat relative to the air-water interface (Figure 2.25).[43,44,65,66,68,69] The explanation is that first, the surface area per molecule is too small for the all α-helices to continue packing as a monolayer. Second, for the film to maintain a constant surface pressure with decreasing surface area, the structural transition that is implied by the surface pressure

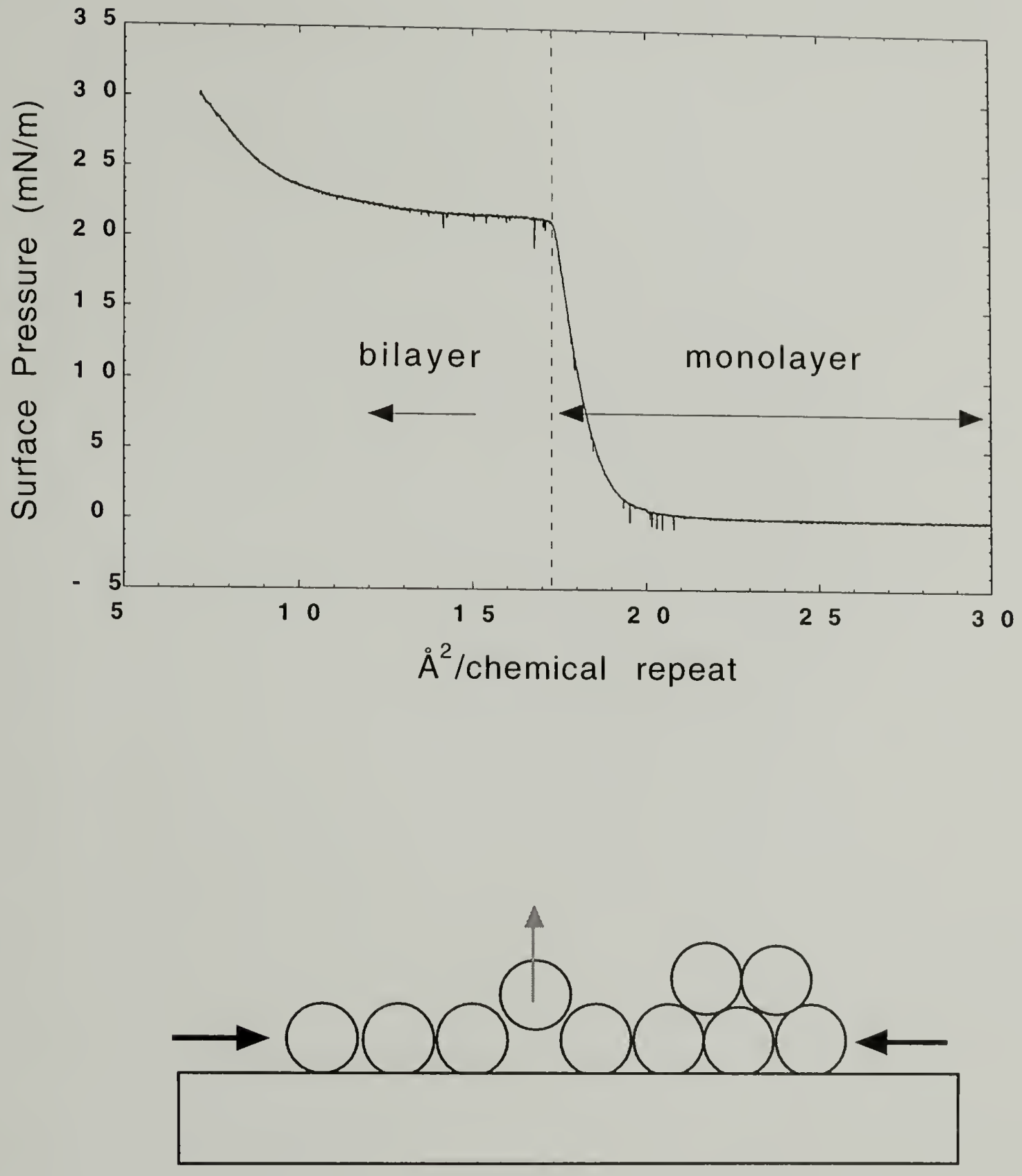

Figure 2.25 Schematic representation of the transition from a monolayer to a bilayer of rigid helices. The helices lie flat at the air-water interface.

area isotherm must be one that is well ordered. A total collapse of a film at an air-water interface (i.e. forming islands) would cause a large drop in the surface pressure. A less ordered transition (e.g. condensed monolayer to a film composed of some monolayer, some bilayer, some trilayer as well as intermediates) would have some slope in the surface pressure/area isotherm curve. Also, an orientation of the rigid-rod α-helices out of the plane of the air-water interface is unlikely given the long rigid backbone formed by the strong intramolecular bonds along the backbone axes and the partially hydrophilic quality of the polypeptide mentioned previously. Third, the rise in the surface pressure following this plateau region in the isotherm occurs at areas roughly half (~12.5 Å) that at which the first rise occurs (~19.5 Å). That the plateau region does not quite extend to half the area of the first rise may suggest that in contrast to the initial formation a bilayer, later the transition becomes less distinct. It has been proposed that this may be due to irregularities in the remaining monolayer or bilayer structure.[64-67] More of the specifics of the ordering behavior of this polymer directly measured using external reflection spectroscopy will be discussed in section 2.4.2.3.

The addition of *n*-octadecyl side groups randomly substituted off of the main chain backbone greatly changes the shape of the surface pressure/area isotherm. For the isotherm of poly(γ-methyl-L-glutamate-*co*-γ-*n*-octadecyl-L-glutamate) of 20% *n*-octadecyl-L-glutamate composition, the initial rise in the surface pressure occurs at a slightly larger surface area (~24.5 $Å^2$/chemical repeat) upon forming a condensed monolayer. This can be explained by the larger diameter of the molecules, again verified as α-helical (2.4.2.3), due to the long *n*-octadecyl side groups. The rise in surface pressure, although still relatively sharp, is less so compared to poly(γ-methyl-L-glutamate) and extends to 18.0 $Å^2$/chemical repeat. The rise reaches a final value of ~28.0 mNm^{-1} after which there are two plateau regions. The first is slightly sloped and ends at ~13.0 $Å^2$/chemical repeat. The second is very flat and begins at 12.0 $Å^2$/chemical repeat. This isotherm is similar to one reported previously by Wegner for a copolyglutamate of

35% γ-*n*-octadecyl-L-glutamate residues.[35] In that report it was proposed that the first plateau region in the surface pressure/area isotherm corresponds to a transition associated with an ordering of the long *n*-alkyl side chains induced by the closer packing of the molecules at the air-water interface. However, in section 2.4.2.2 this is shown not to be the case. Given the molecular area at which the first plateau region begins, it is reasonable instead to assign this region of the isotherm to a monolayer-bilayer transition similar to the one in poly(γ-methyl-L-glutamate) films. The presence of the side chains, however, appears to make the transition less distinct, i.e. slope in plateau. The area at which this plateau region ends, ~13.0 Å^2/chemical repeat, is again roughly half the area of the initial rise in surface pressure, ~24.5 Å^2/chemical repeat. The same type of an incremental thickening of the film (i.e. bilayer to trilayer) can perhaps be assigned to the second plateau region in the isotherm.

As was shown in Figure 2.24, with an increase in the *n*-octadecyl-L-glutamate composition to 50%, both plateau regions in the isotherm disappear. The isotherm instead exhibits a gradually rising surface pressure beginning at a surface area of ~27.0 Å^2/chemical repeat. In addition, the plot of the surface pressure versus area exhibits an inflection beginning at ~17.0 Å^2/chemical repeat. As will be more fully explained in the following sections, the disappearance of the flat plateaus corresponding to well defined monolayer-bilayer transitions in the previous samples, can here be directly attributed to the changing structure of the long *n*-alkyl side groups. The surface pressure/area isotherm indicates that the transition from a monolayer to a multilayer film is less ordered/distinct and can probably be associated with the onset of the inflection point in the isotherm. It can be added that in another study at the air-water interface involving a fully side chain substituted polyglutamate, poly(γ-*n*-octadecyl-L-glutamate), the isotherm was found to exhibit only a single gradual rise in the surface pressure beginning at ~33 Å^2/chemical repeat with no inflection point.[70]

With an increased number of *n*-alkyl side groups attached to the rigid-rod backbone the isotherms clearly suggest that the three samples exhibit different structures at the air-water interface during compression. The next two sections will explain some of the reasons for the differences in the measured surface pressure/area isotherms.

2.4.2.2 Structure of *N*-Alkyl Side Chains

The structure of the *n*-alkyl side chains for the two "hairy-rod" copolyglutamates studied will be divided into two parts. First, the *liquid-like* or *solvent-like* character of the side chains at the air-water interface will be analyzed. The discussion will focus particularly on how the *liquid-like* character of the *n*-alkyl side groups changes with compression at the air-water interface for each of the two samples with long side groups. As was mentioned previously, the initial goal of "hairy-rod" polymers was provide the rigid-rod main chains with a *solvent-like* matrix at the air-water interface to enhance transferability onto solid substrates. Subsequently, the transferability or non-transferability of "hairy-rod" polyglutamates has been proposed to be dependent on the *liquid-like* or *non-liquid-like* character of the long side groups at the air-water interface. In the second part, the relative change in orientation of the *n*-alkyl side chains will be analyzed as a function of compression at the air-water interface.

To start with, the *liquid-like* or *solvent-like* quality of the *n*-alkyl side groups at the air-water interface will be defined as being related to their degree of conformational order. Particularly pertinent in this analysis are the many studies which have correlated changes in phase and changes in the conformation of hydrocarbon chains with shifts in the frequencies of the CH_2 asymmetric and symmetric stretching infrared modes.[55,71] In general, it has been observed that when such a system is an isotropic liquid, the hydrocarbon chains are very disordered, i.e., containing many gauche conformers, and the frequencies of the two modes are in the ranges of 2924 cm^{-1} to 2928 cm^{-1} and 2852 cm^{-1} to 2856 cm^{-1}. Conversely, when a more ordered phase is formed where the chains

are in a predominantly all-trans conformation, e.g., paraffin crystallites, the frequencies of the CH_2 asymmetric and symmetric stretching modes shift to 2918 cm^{-1} and 2850 cm^{-1}, respectively. Therefore, by analyzing this region in the external reflection infrared spectra of the two copolyglutamates spread at an air-water interface, *n*-alkyl side chains which are found to be very conformationally disordered will be characterized as *liquid-like*. *N*-alkyl side chains which are very conformationally ordered will be characterized as *non-liquid-like*.

The CH_2 asymmetric stretching mode in the external reflection infrared spectra of the 20% γ-*n*-octadecyl-L-glutamate sample is shown in Figure 2.26 as a function of varying surface area. The corresponding surface pressure/area isotherm is shown in the upper portion of Figure 2.26. Analyzing the infrared spectra, it is apparent that the long *n*-alkyl side chains for this sample of relatively low degree side chain substitution remain conformationally disordered throughout the surface pressure/area isotherm. As was discussed previously, the absorbances for peaks in the external reflectance infrared spectra of films at an air-water interface are negative. Although of intensities indicative of the small amount of material at the air-water interface ranging from ~0.0005 to ~0.0015 absorbance units, both the half width as well as the peak frequency position of the bands can be readily analyzed. Figure 2.27 plots the peak frequency position versus the surface area as such a film is compressed.

Initially, at surface areas greater than ~25 $Å^2$/chemical repeat the CH_2 asymmetric stretching peak position remains constant at ~2928 cm^{-1}. Here the monolayer is very far from that of a close packed or condensed monolayer and the relative surface density of both the rigid-rod backbones and the *n*-alkyl side chains is small. As is reflected by the peak position, the long *n*-alkyl side chains are very *liquid-like* . In general, both the rigid-rods and the long side groups can be described as being in a two-dimensional gas-like state (Figure 2.2). Although epi-fluorescence microscopy images of fully long side chain substituted polyglutamates have indicated that domains form in this expanded region,[70]

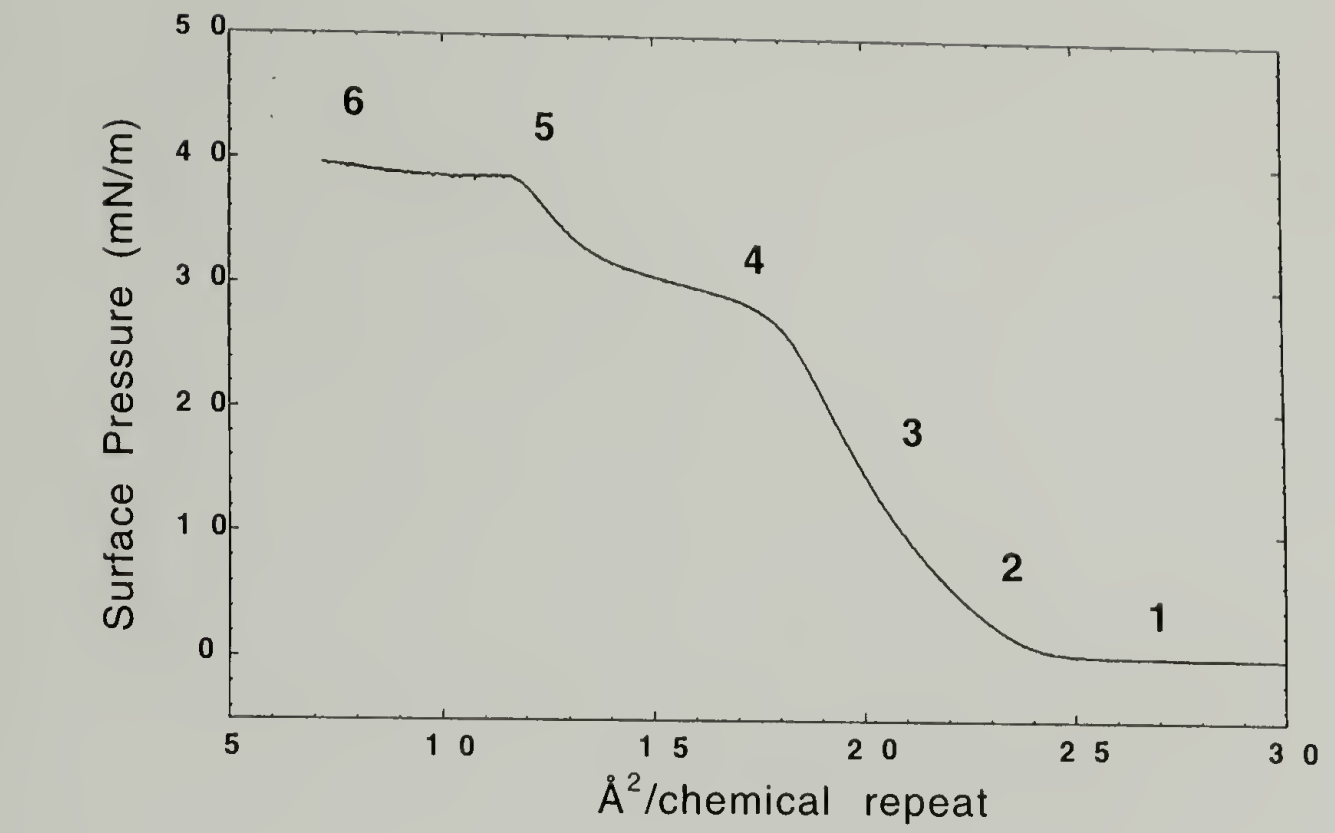

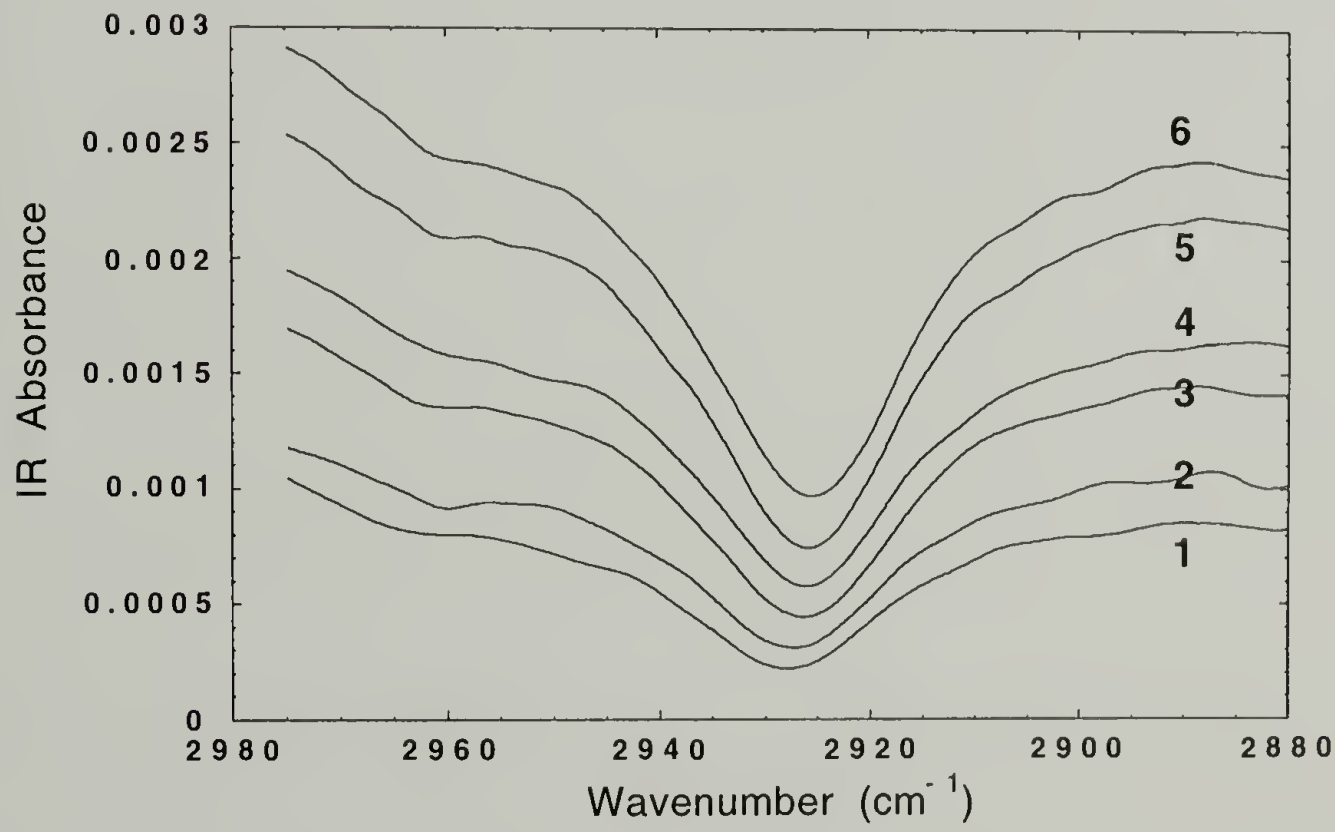

Figure 2.26 20% γ-*n*-octadecyl-L-glutamate sample: Overlay of CH_2 asymmetric stretching mode with compression at the air-water interface.

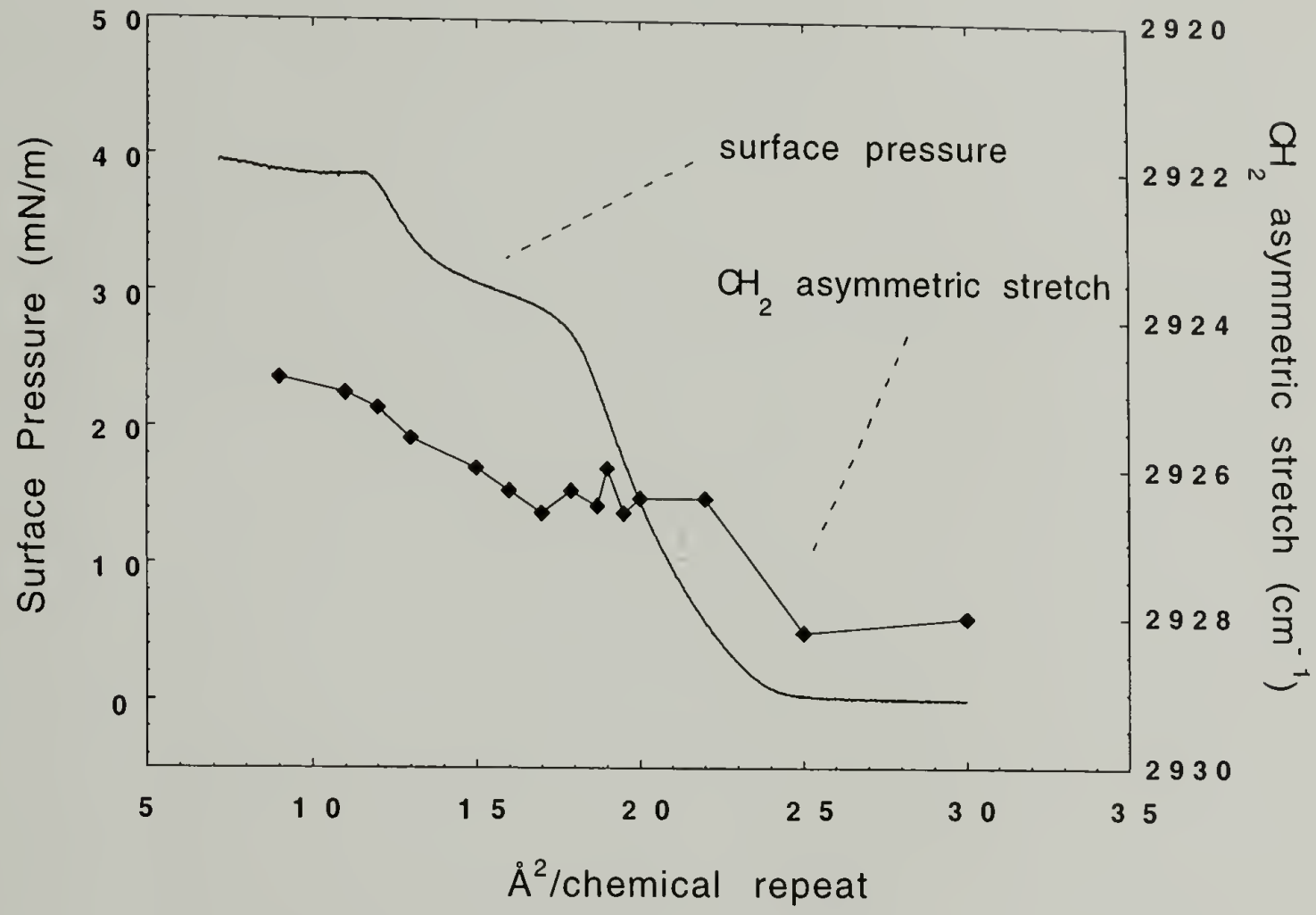

Figure 2.27 20% γ-*n*-octadecyl-L-glutamate sample: Plot of CH_2 asymmetric stretching mode peak position with compression at the air-water interface.

the packing of rigid-rods within these domains is probably not close given the CH_2 asymmetric stretching peak position. The side chains thus can be described as being analogous to a liquid paraffin. Given the large surface area per molecule, the side chains do not form a continuous matrix of *liquid-like* groups. Instead the side chains can be better characterized as forming a *liquid-like* skin on the surface of individual helices.

As the surface area at the air-water interface is further decreased, the surface pressure begins to rise corresponding with the initial formation of a condensed monolayer. As can be seen in Figure 2.27, there is also a corresponding decrease in the CH_2 asymmetric stretching peak position to a value of 2926.4 cm^{-1} indicating a small decrease in the number of gauche conformers as side groups from adjacent helices pack closer. Overall, however, the side groups can still be considered conformationally disordered. Due to the small number of *n*-alkyl side chains substituted off of the rigid-rod backbones, further ordering of the side groups is not possible even though the monolayer as a whole can be described as condensed. Treating the side groups as being decoupled from the rigid-rods, in this region the side groups can be characterized as remaining in a two-dimensional gas-like state as indicated by the CH_2 asymmetric stretching peak position. The rigid-rods, however, with a surface packing density close to the pure rigid-rod system prior to the monolayer-bilayer transition (~18.0 versus 17.0 $Å^2$/chemical repeat) are in more of a liquid-like or solid-like state at the air-water interface. This idealized description of side groups can be used to explain why the rise in the surface pressure is less steep than for the pure rigid-rod system. The gas-like side groups on the surface of the rigid-rods provide the condensed monolayer with a greater compressibility at the air-water interface.

This degree of conformational disorder of the long side groups remains relatively constant as the monolayer is further compressed through much of the plateau region associated with the formation of a bilayer. During the transition, the lateral distance between molecules likely remains relatively constant as the much of the energy exerted

during compression goes instead to forcing helices from the air-water surface during the formation of a bilayer. Thus both the packing density of the side chains and subsequently the CH_2 asymmetric stretching peak position remain relatively constant.

Upon further compression at areas corresponding to the second rise in the surface pressure and the second plateau, the CH_2 asymmetric stretching peak position very gradually decreases reaching a final measured value of 2924.8 cm^{-1} at an area of 9 $Å^2$/chemical repeat. Here, the association of *n*-alkyl side groups between layers and the formation of a multilayer film more closely resembling the structure in bulk is probably responsible for the decrease in the number of gauche conformers relative to that of the as-spread monolayer film. The peak position of the CH_2 asymmetric stretching mode from a transmission infrared spectra of a solid cast film of poly(γ-methyl-L-glutamate-*co*-γ-*n*-octadecyl-L-glutamate) of 20% γ-*n*-octadecyl-L-glutamate composition is slightly lower at 2923.8 cm^{-1}. The long side chains in this bulk state can still be considered mostly disordered. As would be expected, a differential scanning calorimeter scan of such a bulk film does not indicate any crystallization of the long *n*-alkyl side groups. Overall, with a total shift of the CH_2 asymmetric stretching peak position from 2928 cm^{-1} to 2924.8 cm^{-1} indicating a very gradual decrease in the amount of conformational disorder, the side groups can be characterized as *liquid-like* throughout the measured surface pressure/area isotherm.

The CH_2 asymmetric stretching spectra for the poly(γ-methyl-L-glutamate-*co*-γ-*n*-octadecyl-L-glutamate) of 50% γ-*n*-octadecyl-L-glutamate composition are shown in Figure 2.28. The corresponding plot of the peak frequency positions is shown in Figure 2.29. Here it can be observed that, as opposed to the 20% γ-*n*-octadecyl-L-glutamate sample, there is a large shift in the peak frequency of the CH_2 asymmetric stretching vibration as the film is compressed. Beginning at expanded surface areas between 27 mNm^{-1} and 45 mNm^{-1} where the film is an expanded monolayer, the long side chains are highly disordered and can be characterized as *liquid-like*. The CH_2 asymmetric stretching

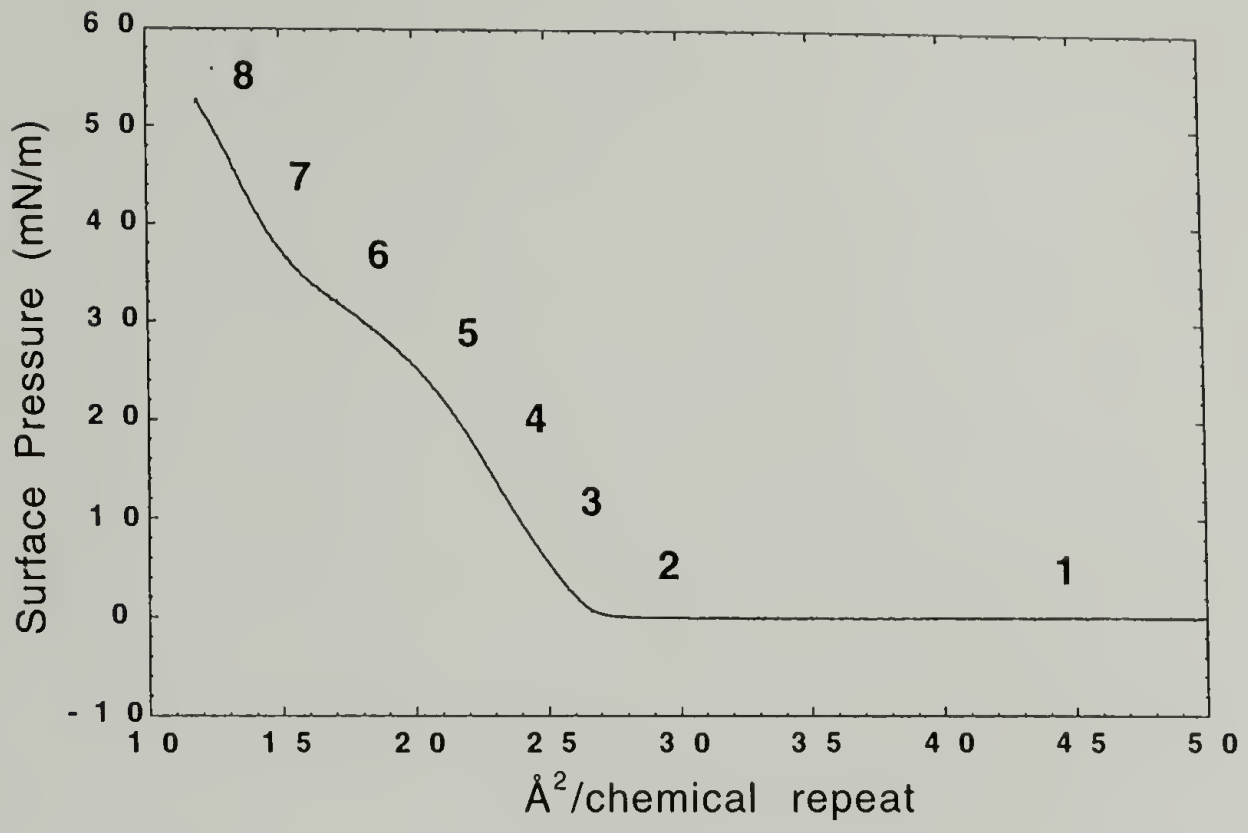

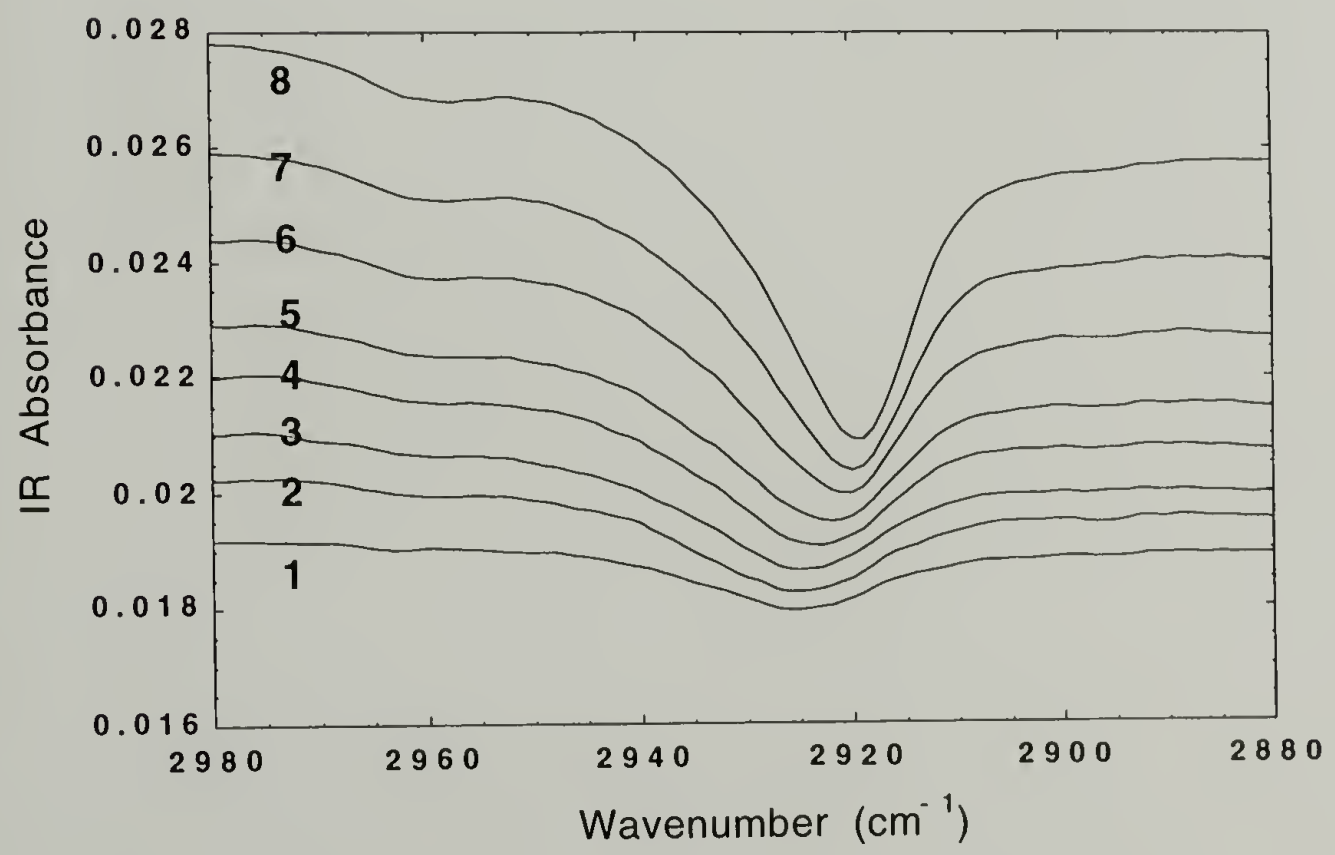

Figure 2.28 50% γ-*n*-octadecyl-L-glutamate sample: Overlay of CH_2 asymmetric stretching mode with compression at the air-water interface.

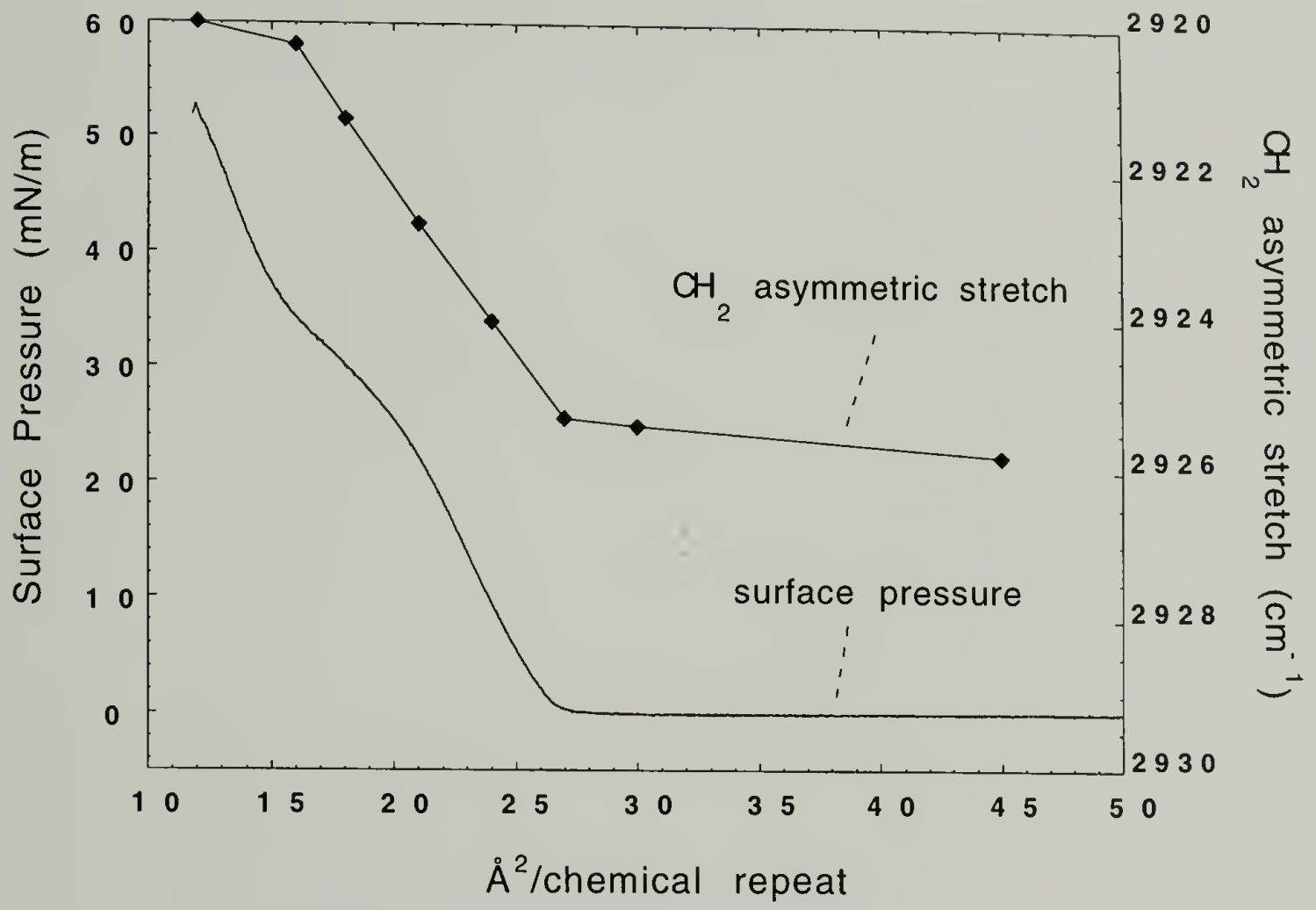

Figure 2.29 50% γ-*n*-octadecyl-L-glutamate sample: Plot of CH_2 asymmetric stretching mode peak position with compression at the air-water interface.

peak position remains at ~2925.5 cm^{-1}. This is slightly lower than for the 20% γ-*n*-octadecyl-L-glutamate copolymer and can be attributed to the greater number of long side chains substituted off of each rigid-rod molecule. Specifically, the greater number of side chains leads to their greater degree of association even at this expanded state. As was mentioned, it is likely that the monolayer is composed of loosely packed domains.

However, as the surface pressure begins to rise, indicative of a closer packing of the monolayer at the air-water interface, the peak position soon begin to shift downward. At a surface pressure and surface area of 10 mNm^{-1} and 24 $Å^2$/chemical repeat, the CH_2 asymmetric stretching peak position shifts to 2924 cm^{-1}, a degree of conformational order equal to the most compressed state for the 20% γ-*n*-octadecyl polyglutamate sample. The side chains continue to order upon further compression of the monolayer and at an area just before the onset of the inflection point in the surface pressure/area isotherm, the peak position reaches 2922.7 cm^{-1}. At this point, the CH_2 asymmetric stretching peak position is midway between 2928 cm^{-1} and 2918 cm^{-1}, frequencies which represent correspond to an isotropic melt-like state and an all-trans chain extended conformation respectively.

The decrease in the *liquid-like* quality of the side groups provides an explanation why the monolayer-bilayer transition becomes less distinct relative to the 20% γ-*n*-octadecyl-L- glutamate sample. Whereas for the 20% γ-*n*-octadecyl-L- glutamate sample the side chains are flexible and provide a skin of *liquid-like* segments on the surface of the helices that may enhance the mobility of the rigid-rods amongst one another, the skin of segments on the surface of the helices of the 50% γ-*n*-octadecyl-L- glutamate sample become significantly less flexible and *liquid-like* as the monolayer is compressed. Related to the decrease in the flexibility of the side chains is the interaction and subsequent ordering between side chains from different individual helices adjacent to one another. Thus the transition from a monolayer to a multilayer film becomes less ordered and leads to the disappearance of a plateau region. On the other extreme, for poly(γ-methyl-L-

glutamate) where there is no such ordering of side groups between helices, the monolayer-bilayer transition is well defined.

Proceeding along the surface pressure/area isotherm, both the surface pressure and the CH_2 asymmetric stretching peak position continue to rise until at an area of ~16 $Å^2$/chemical repeat the peak frequency position begins to plateau at 2920 cm^{-1}. At this point, the long side chains form a predominantly all-trans structure and the film may be characterized as very *non-liquid-like* Comparing the CH_2 asymmetric stretching peak position for the multilayer film at the air-water interface versus that of a solid cast film, it was found that the peak positions for each of the two samples are nearly the same. The peak position for the solid cast film was found to be 2920.5 cm^{-1}. Much like for the 20% γ-*n*-octadecyl-L-glutamate sample, this again can probably be attributed to the formation of a multilayer film at the air-water interface with a structure beginning to resemble that in the bulk. A differential scanning calorimeter scan for a bulk sample of poly(γ-methyl-L-glutamate-*co*-γ-*n*-octadecyl-L-glutamate) of 50% γ-*n*-octadecyl-L-glutamate content, shown in Figure 2.30, indicates that in the bulk the long side groups do interdigitate and crystallize. The melting point of the long side groups obtained was 38.2° C. In previous thermal and x-ray studies of poly(γ-*n*-octadecyl-L-glutamate) homopolymer, the melting point of the long interdigitating side chains was found to be 62° C. In was also found for this fully side chain substituted sample that the crystallization of the side groups only occurred in roughly the last nine carbon atoms furthest from the backbone.[26] As will be more fully discussed in the next section, it should also be mentioned that above the melting point of the side chains a transition to a cholesteric liquid crystal phase occurs. Although the long side groups for the 50% γ-*n*-octadecyl-L-glutamate sample are mostly in an all-trans conformation, this however does not necessarily mean that the side groups crystallize at the air-water interface. It possible that unlike in the solid cast film, the side chains at the air-water interface though similar in conformation to the bulk state do not crystallize with one another.

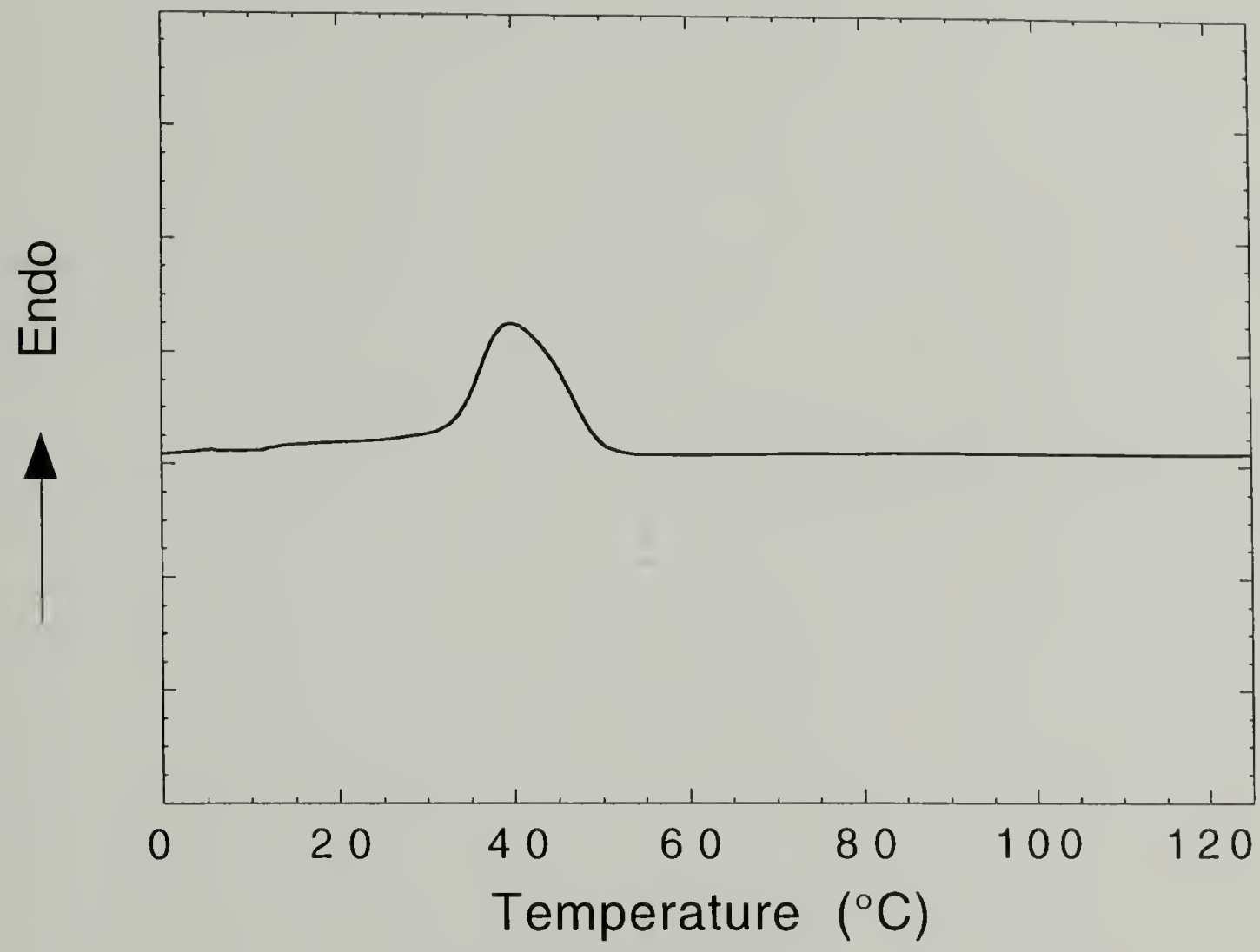

Figure 2.30 DSC thermogram of bulk poly(γ-methyl-L-glutamate-*co*-γ-*n*-octadecyl-L-glutamate) of 50% γ-*n*-octadecyl-L-glutamate composition at a scan rate of 10° C/min.

Qualitatively, it is also possible to determine the change in orientation of the *n*-alkyl side groups during compression at the air-water interface by measuring the change in relative intensity of the CH_2 asymmetric stretching mode. One can roughly estimate the transition moment direction of this vibration as perpendicular to the backbone of the linear side chains.[53-55,71] Assuming that this direction does not change significantly with side chain conformation, it is then possible by normalizing the integrated intensities of the CH_2 asymmetric stretching vibration with molecular surface area to get a measure of the change in relative orientation of the side chains with respect to the plane of the air-water interface. This is illustrated in Figure 2.31 where the s polarized infrared beam, with a polarization parallel to the plane of the interface, is shown relative to "hairy-rod" molecules at the air-water interface. In infrared spectroscopy, the absorbance for a given vibration is proportional to the squared scalar product of the incident electric vector (i.e. plane polarized radiation) and a vector representing the direction of an oscillating dipole moment.[72] Therefore, an increase in the alignment of the side groups perpendicular to the air-water interface would result in an increase in the normalized intensity of the CH_2 asymmetric stretching vibration. An increase in the alignment of the side groups parallel to the plane of the interface would result in a decrease in the normalized intensity.

Moreover, given that the hydrogen bonded backbones are more hydrophilic than the *n*-alkyl side groups, it is reasonable to assume that the general shape of a "hairy-rod" molecule at the air-water interface is such that the helical backbones are in closer contact with the water interface compared to the side groups. In this respect, the "hairy-rod" polymers can be described as having some similarities with traditional amphiphilic molecules with well defined hydrophilic heads and hydrophobic tails. This shape of the molecule and the change in orientation of the more strongly hydrophobic side groups with packing density at the air-water interface could be important in affecting transfer to solid substrates. As an example, transfer onto hydrophobic substrates may be enhanced not only when the side groups are *liquid-like* but also when the side groups have a greater

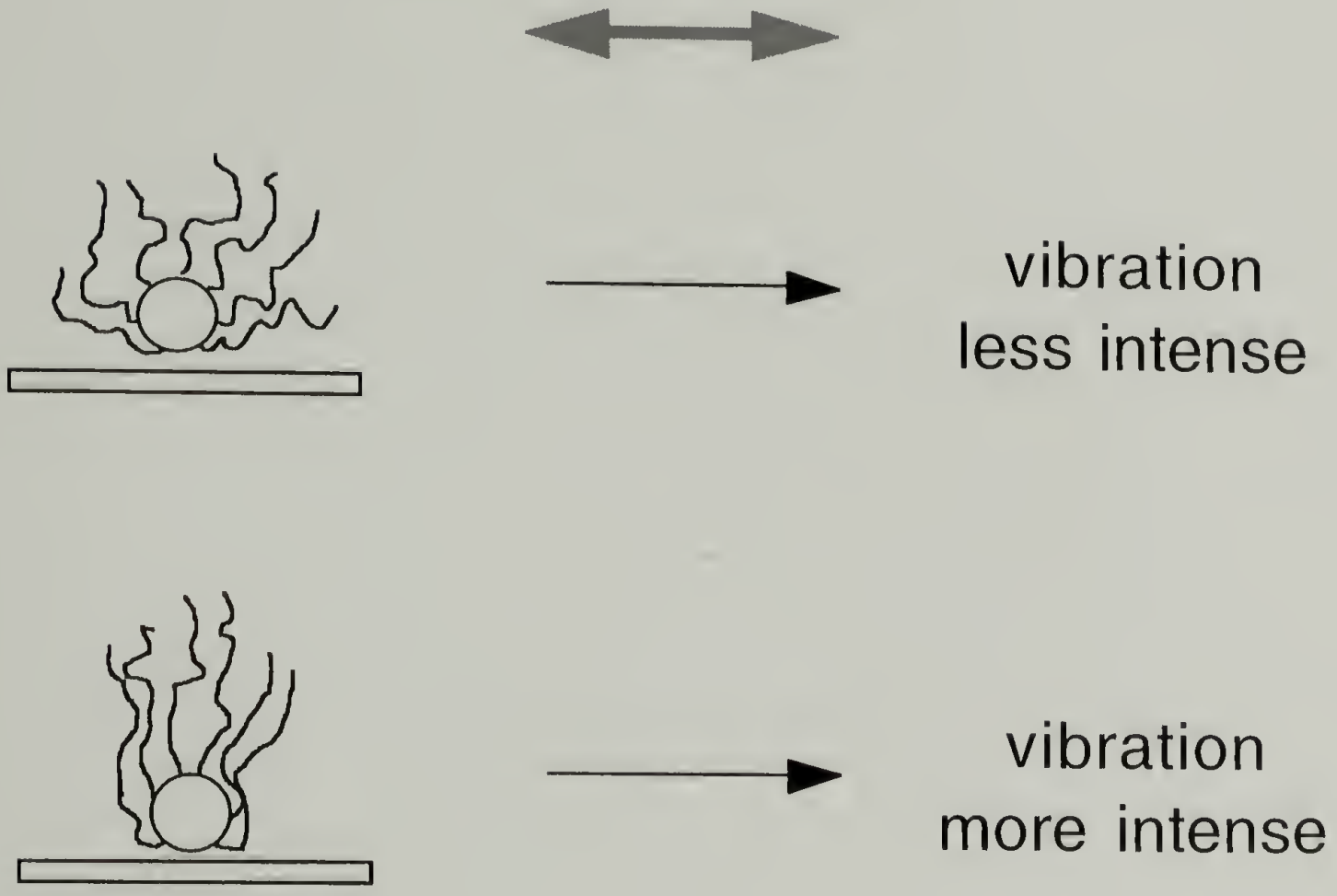

Figure 2.31 Schematic of *n*-alkyl side chains orienting with respect to the air-water interface. Approximating the CH_2 asymmetric stretching mode as perpendicular to axis of side chain, one can probe a change in orientation of these groups with s polarized infrared spectra.

orientation away from the plane of the air-water interface. Such an out-of-plane orientation would increase the interaction between a hydrophobic substrate and the hydrophobic side groups during transfer.

A plot of the normalized absorbance of the CH_2 asymmetric stretching vibration is shown with the surface pressure/area isotherm for the copolyglutamate of 20% γ-*n*-octadecyl-L-glutamate composition in Figure 2.32. Here, the orientation of the side groups appear to have two distinct changes in their relative orientation. The normalized absorbance at areas corresponding to an expanded monolayer will be taken as the reference point. The first change in the orientation occurs at a surface area coinciding with the initial formation of a condensed monolayer at ~24 $Å^2$/chemical repeat. The normalized absorbance increases from ~0.2 to ~0.25 indicating an increase in the orientation of the long side groups out of the plane of the air-water interface. In this region the lateral compressive forces at the interface can be described as forcing the side groups to stretch away from the water surface as the solid rod-like backbones pack closer. This value remains relatively constant during the formation of a condensed monolayer and through the first plateau region associated with the monolayer-bilayer transition. At the second plateau region, the second increase in the normalized absorbance occurs. Here with the formation of a sufficiently thick multilayer film, it is possible that the side chains from adjacent layers stacked parallel to the air-water interface (i.e. bilayer, trilayer etc) interdigitate and thus further stretch perpendicular to the plane of the air-water interface. As was shown previously in Figure 2.27, the conformational order of the side chains does increase very gradually during the monolayer-bilayer transition and supports the concept of chain stretching. That the two processes appear to be related is something that might be expected.

The change in the normalized CH_2 asymmetric stretching vibration for the 50% γ-*n*-octadecyl-L-glutamate composition copolyglutamate sample is shown along with the surface pressure/area isotherm in Figure 2.33. In contrast to the 20% γ-*n*-octadecyl-L-

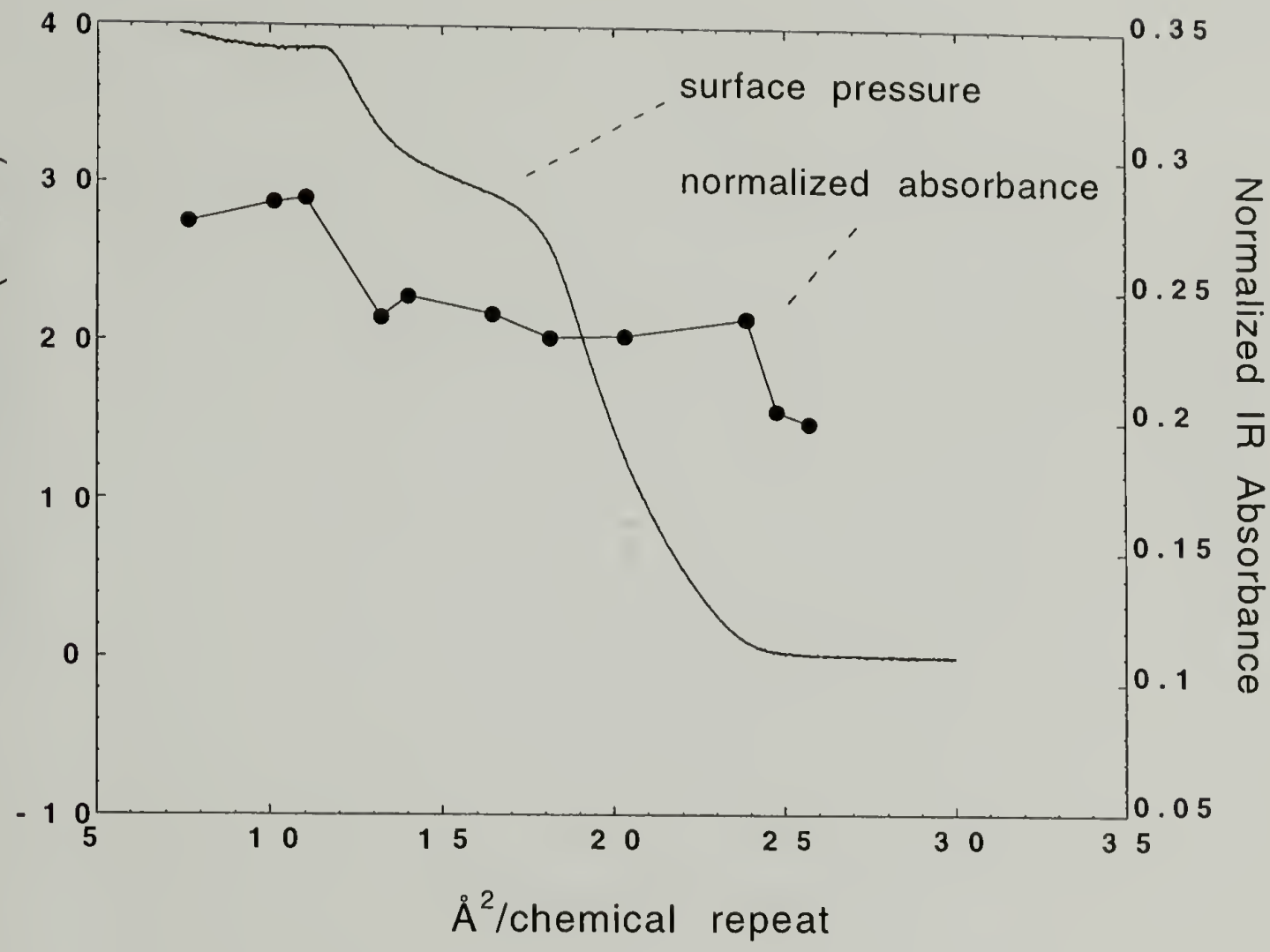

Figure 2.32 Plot of CH_2 asymmetric stretch absorbance normalized to the number of molecules per area at the air-water interface for a sample of 20% γ-*n*-octadecyl-L-glutamate composition.

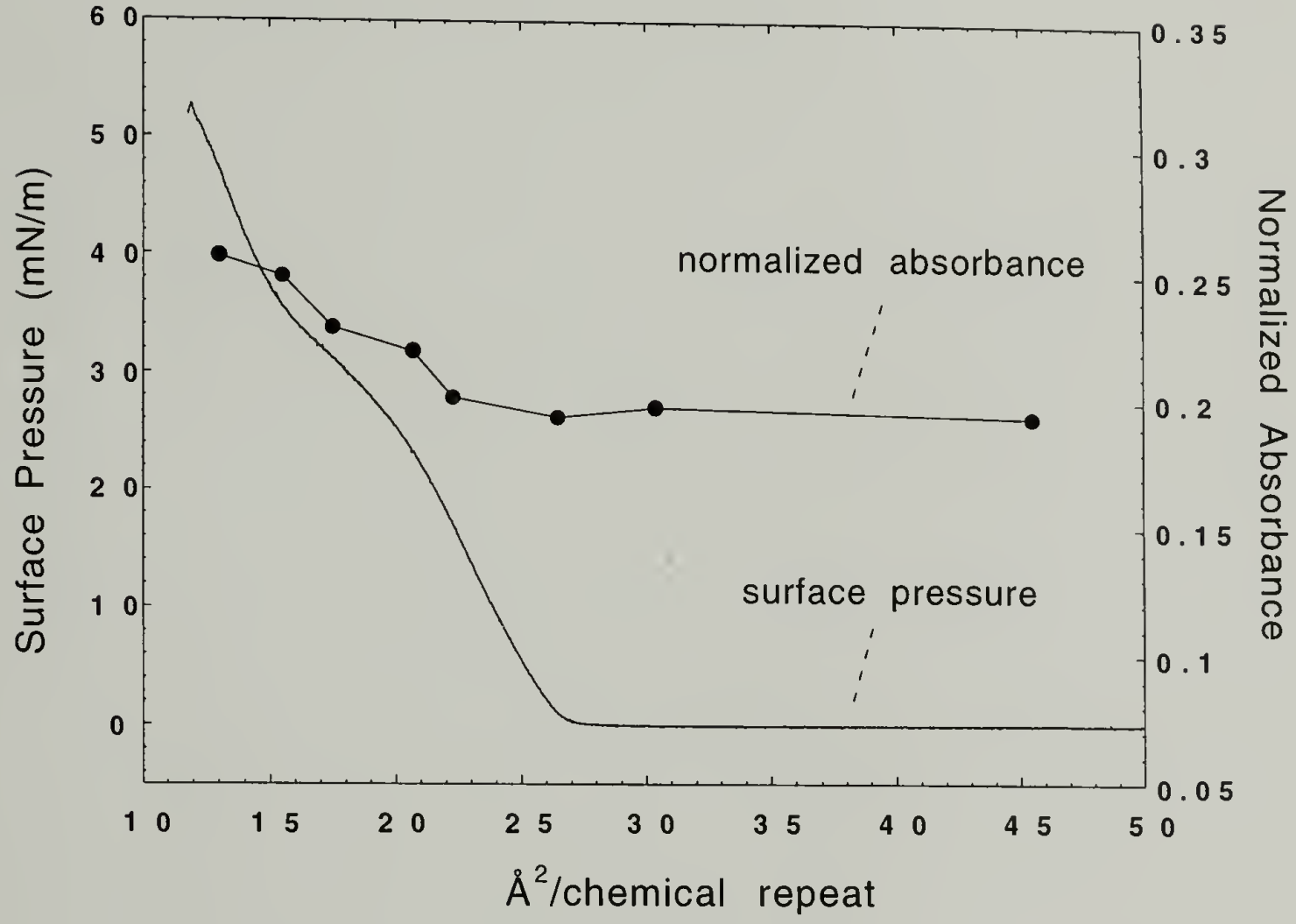

Figure 2.33 Plot of CH_2 asymmetric stretch absorbance normalized to the number of molecules per area at the air-water interface for a sample of 50% γ-*n*-octadecyl-L-glutamate composition.

glutamate sample, the change in the orientation of the *n*-alkyl side groups out of the plane of the air-water interface is gradual once the monolayer becomes compressed. The change in orientation, however, again occurs concurrently with the gradual ordering of the long side groups as the solid rigid-rod backbones pack closer. The total change is from 0.20 when the monolayer is expanded to 0.25 when the film has become a multilayer. This change in the normalized absorbance is less than it was for the 20% γ-*n*-octadecyl composition sample even though for this 50% sample a higher degree of side chain ordering was found to occur. To explain this, it may be that the side groups for the 50% γ-*n*-octadecyl composition sample are already moderately stretched away from the air-water interface even when the film is in an expanded monolayer state. In support of this, as was stated previously, the amount of conformational order present in expanded monolayers of the 50% γ-*n*-octadecyl composition sample was slightly greater than for the 20% γ-*n*-octadecyl composition sample.

2.4.2.3 Ordering of Rigid-Rod Backbones

External reflection infrared spectra in the region between 4000 cm^{-1} and 1000 cm^{-1} are shown for the three samples: poly(γ-methyl-L-glutamate), poly(γ-methyl-L-glutamate-*co*-γ-*n*-octadecyl-L-glutamate) of 20% γ-*n*-octadecyl-L-glutamate composition and the polymer of 50% γ-*n*-octadecyl-L-glutamate composition in Figure 2.34, 2.35 and 2.36 respectively. The spectra shown are representative of spectra collected along the surface pressure/area isotherms for each of the three films at the air-water interface. As was mentioned earlier, the intensities, in absorbance units, of bands arising from the films are negative. Analyzing the spectra, it is readily established that the backbones at the air-water interface are in the α-helical conformation as has often been assumed but never directly verified. This is shown by the presence and position of several well characterized infrared bands for polypeptides which are sensitive to vibrational interactions (i.e. predominantly through hydrogen bonds) between adjacent peptide groups along the

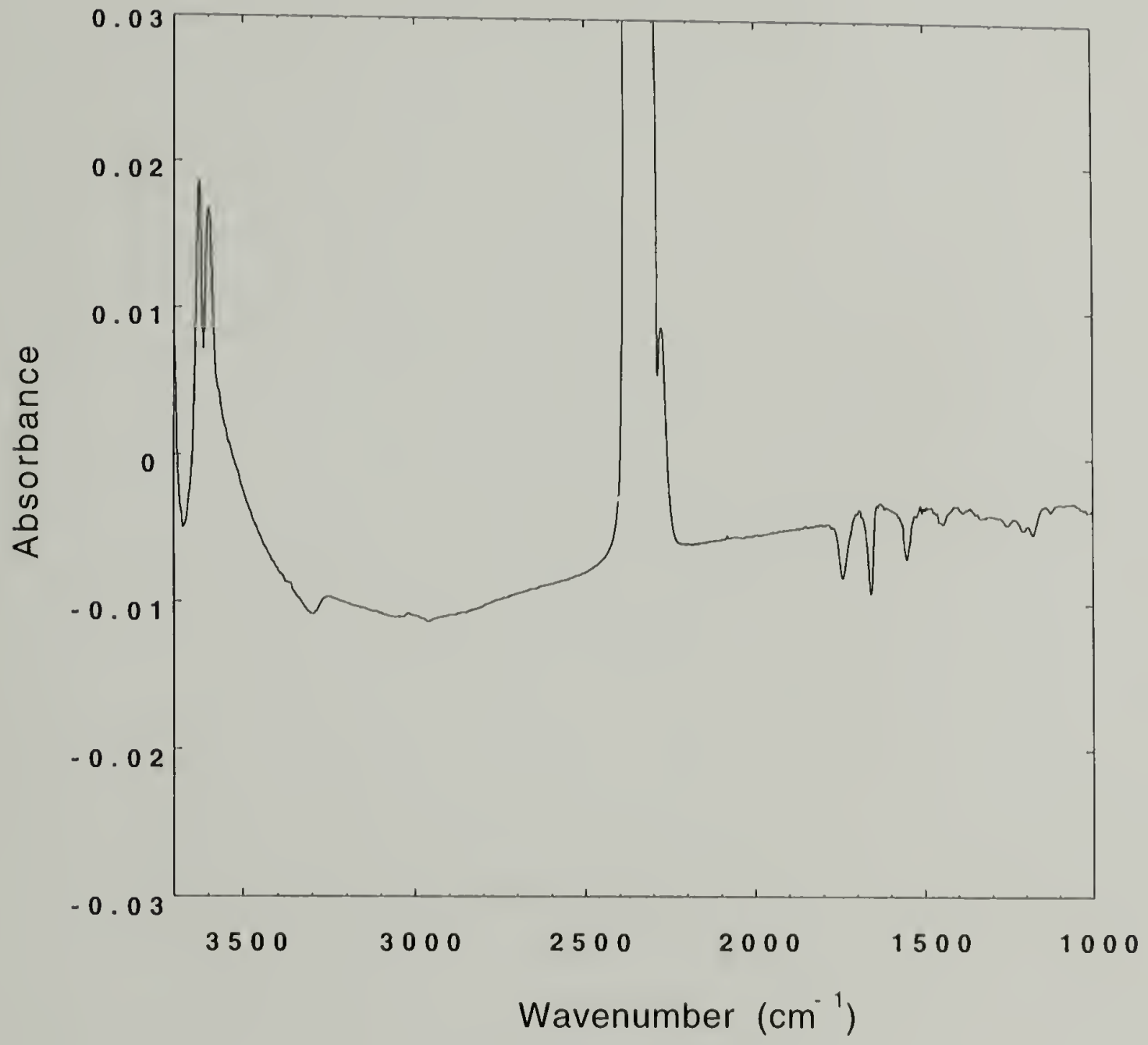

Figure 2.34 External reflection infrared spectrum of poly(γ-methyl-L-glutamate) at the air-water interface.

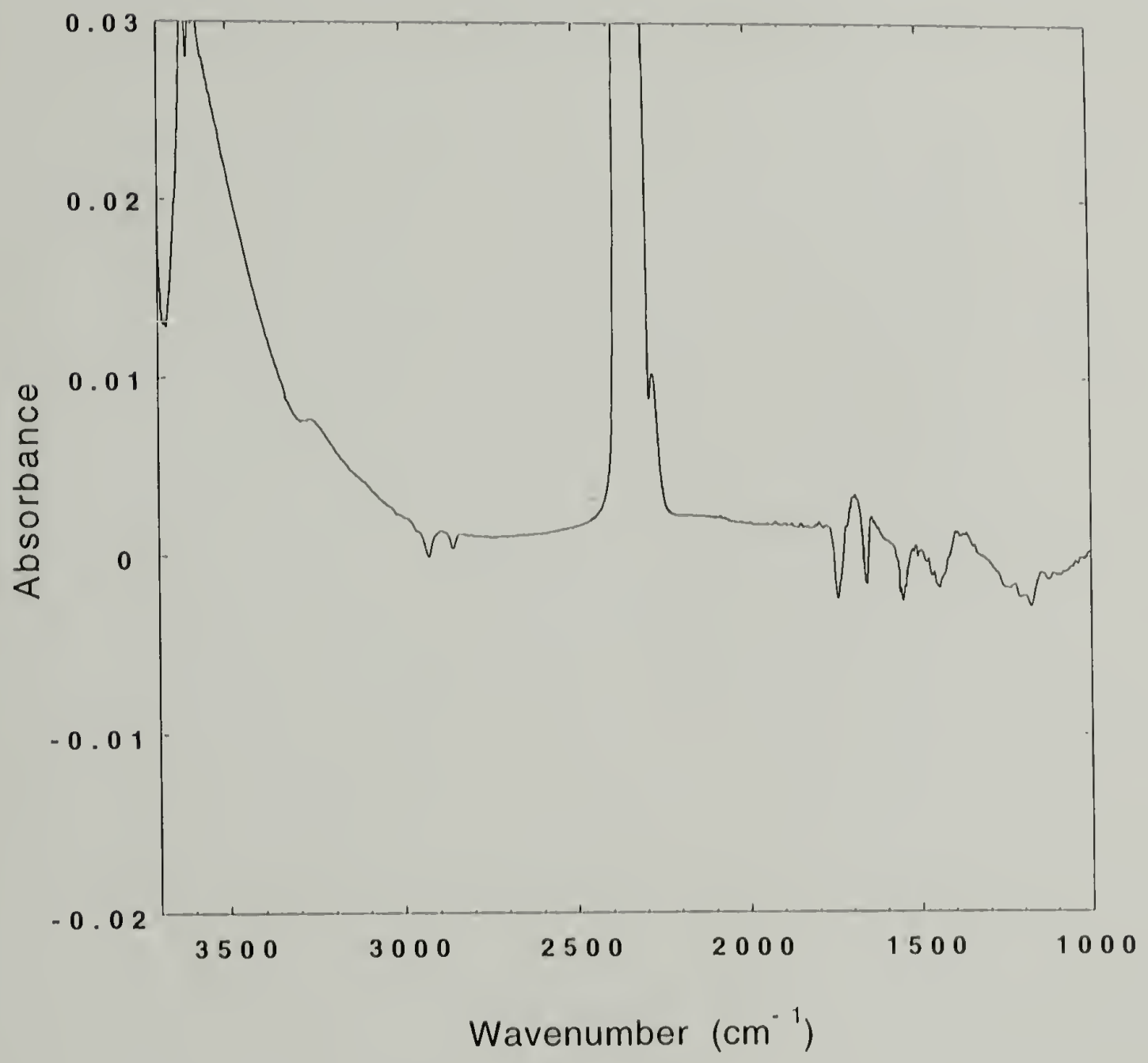

Figure 2.35 External reflection infrared spectrum of a copolyglutamate of 20% γ-*n*-octadecyl-L-glutamate composition at the air-water interface.

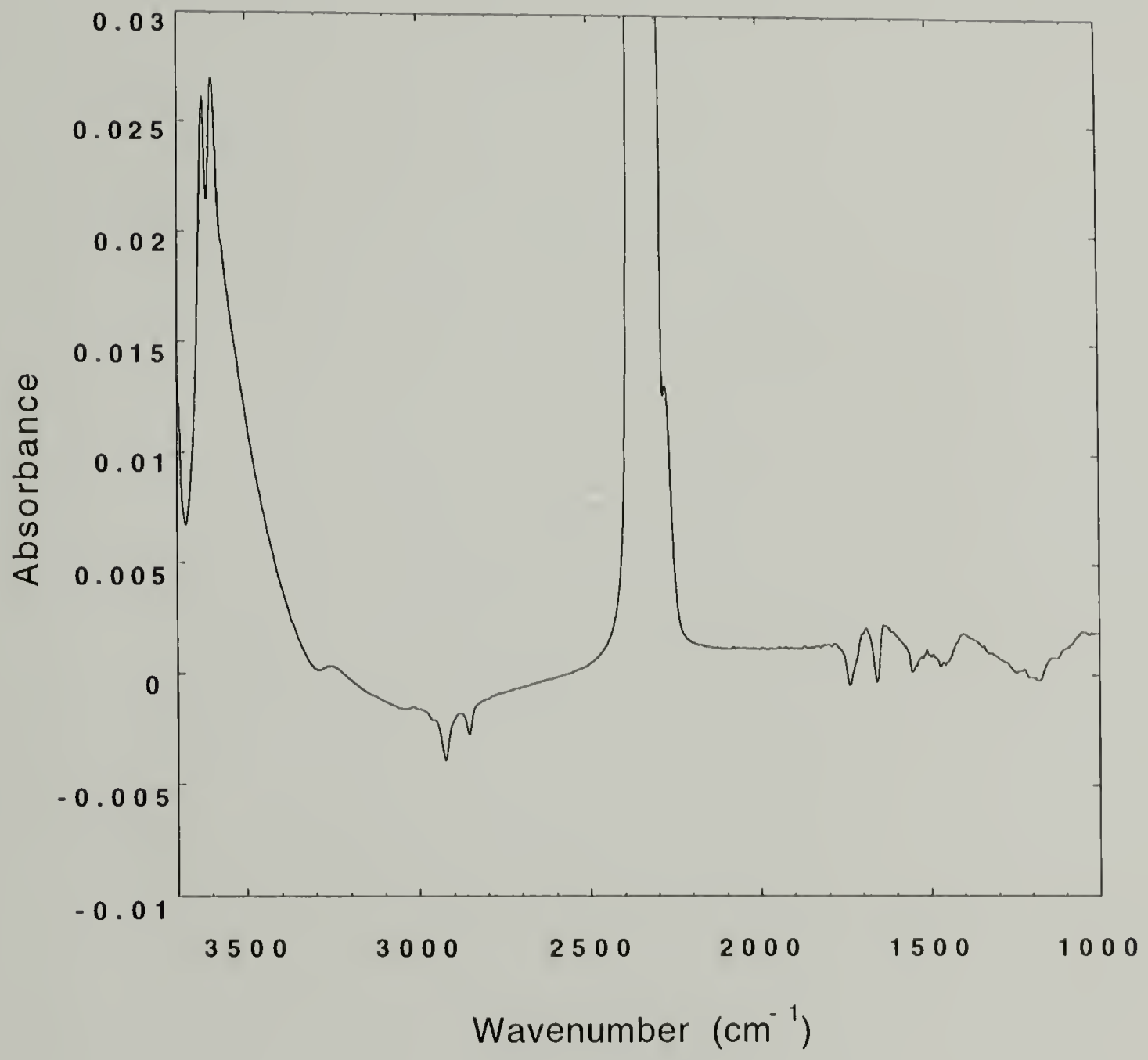

Figure 2.36 External reflection infrared spectrum of a copolyglutamate of 50% γ-*n*-octadecyl-L-glutamate composition at the air-water interface.

polymer backbone. In particular, the NH stretching band at 3290 cm^{-1}, the amide I band at 1652 cm^{-1}, and the amide II band at 1549 cm^{-1} for all three samples show that the films remain in this rigid rod-like conformation throughout the measured surface pressure/area isotherms.[73,74] Some other additional bands present in the spectra are the bands at 1736 cm^{-1}, 1450 cm^{-1} 1350 cm^{-1} and 1100 cm^{-1}.[74] The band at 1736 cm^{-1} is associated with the carbonyl C=O stretching mode arising from the ester group present in the side chains. The band at 1450 cm^{-1} is from CH_2 bending modes. Finally, the weaker bands between 1350 cm^{-1} and 1100 cm^{-1} have contributions from the amide III mode and the C-O stretching modes from the side chain ester groups, respectively. All of these bands are seen in the infrared spectra of bulk cast films of these polymers.

There are also several other features in the spectra not attributable to the polymer films themselves. The large rise in the baseline centered at ~3600 cm^{-1} is due a mismatch in the collected sample single beam spectra and the background spectra of the pure water substrate arising from the OH stretching band from water. Specifically, for an air/film/water system there is less absorption from water itself than for an air-water system. Thus the OH stretching band is positive in the ratioed spectra. Another feature associated with the water subphase at 1650 cm^{-1} was discussed previously and can also be explained in the same general manner. Lastly, the large spike at ~2350 cm^{-1} is due to the CO stretching band associated with CO_2 in the trough chamber. The presence of this band was not important for these studies, however, since it is does not overlap with bands from the polymer films themselves.

An overlay of spectra corresponding to various points along the surface pressure/area isotherm for each of the three samples is shown in Figure 2.37, 2.38 and 2.39 in the region between 2000 cm^{-1} and 1000 cm^{-1}. In the upper portion of the figures are the corresponding isotherms. On comparison, it can be clearly seen that for each sample, the intensity of the amide I band at 1652 cm^{-1} decreases relative to the amide II band at 1549 cm^{-1} and the side chain C=O stretching band at 1736 cm^{-1} during

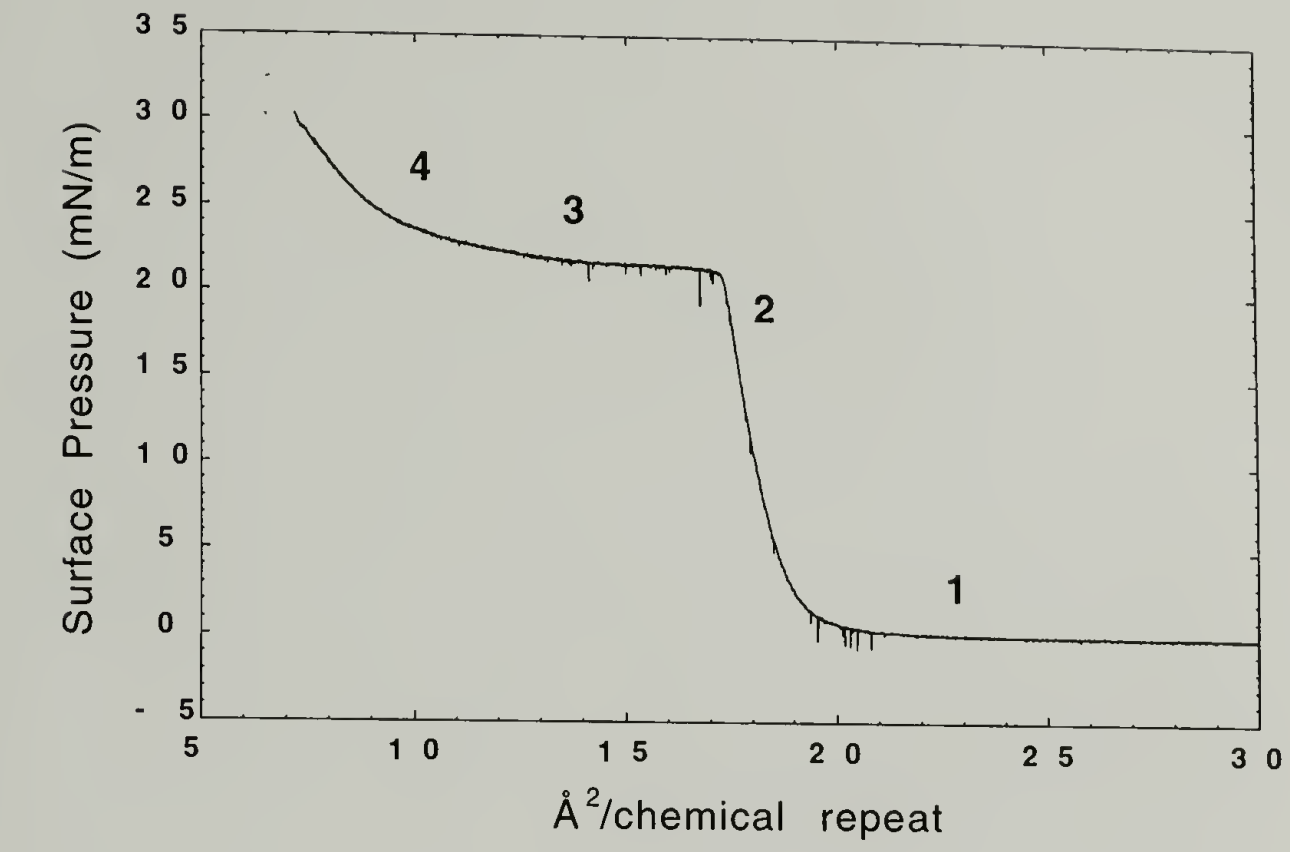

Figure 2.37 Poly(γ-methyl-L-glutamate): External reflection infrared spectra between 2000-1000 cm^{-1}.

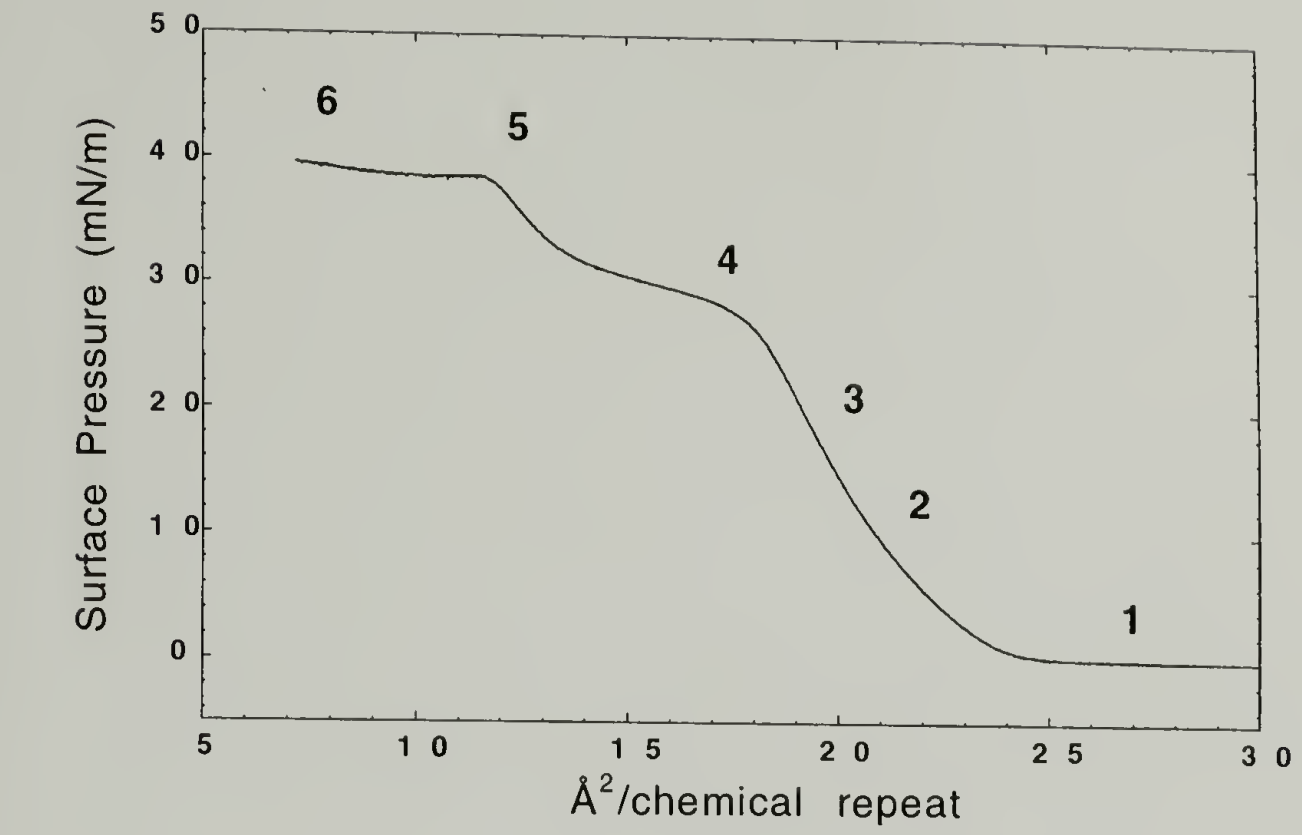

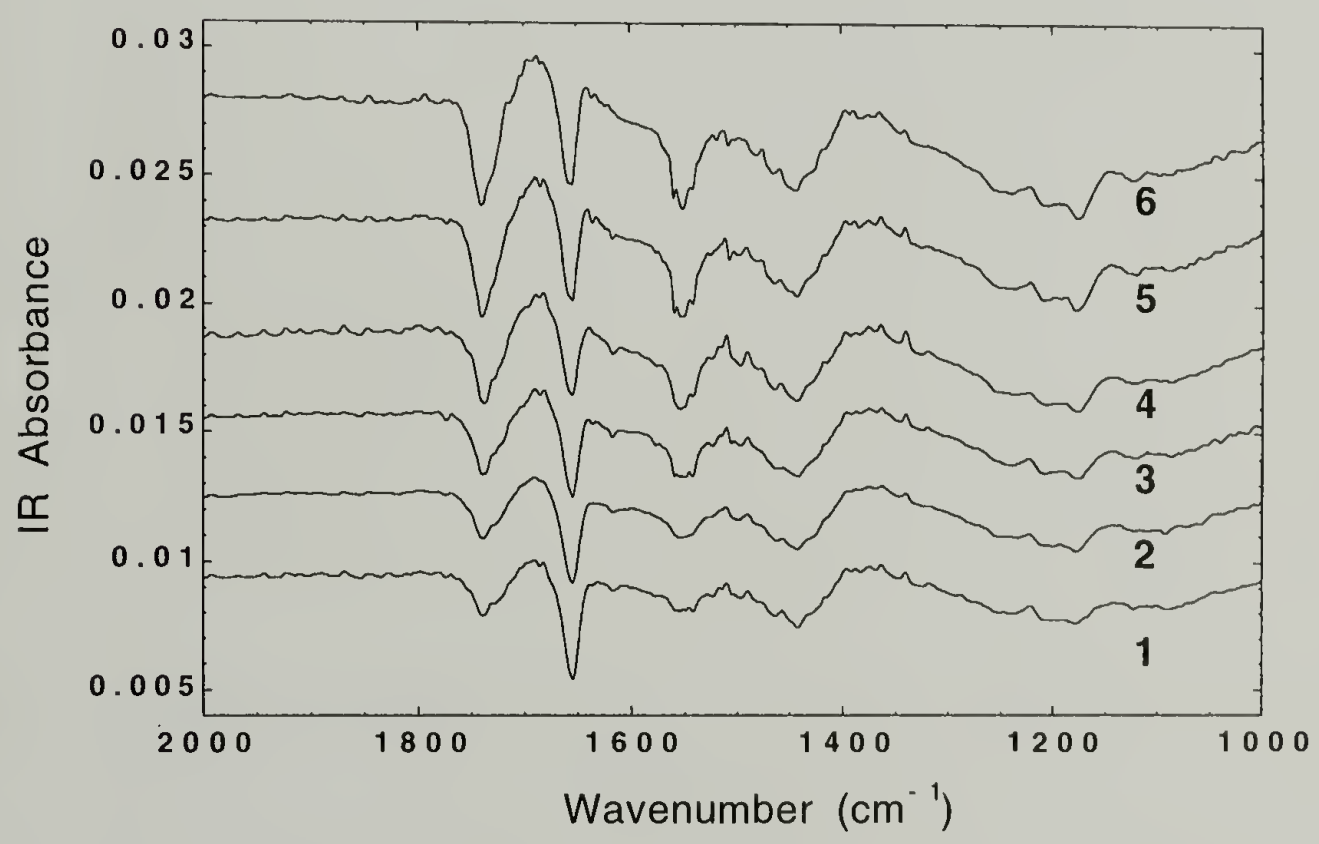

Figure 2.38 20% γ-*n*-octadecyl-L-glutamate sample: External reflection infrared spectra between 2000-1000 cm^{-1}.

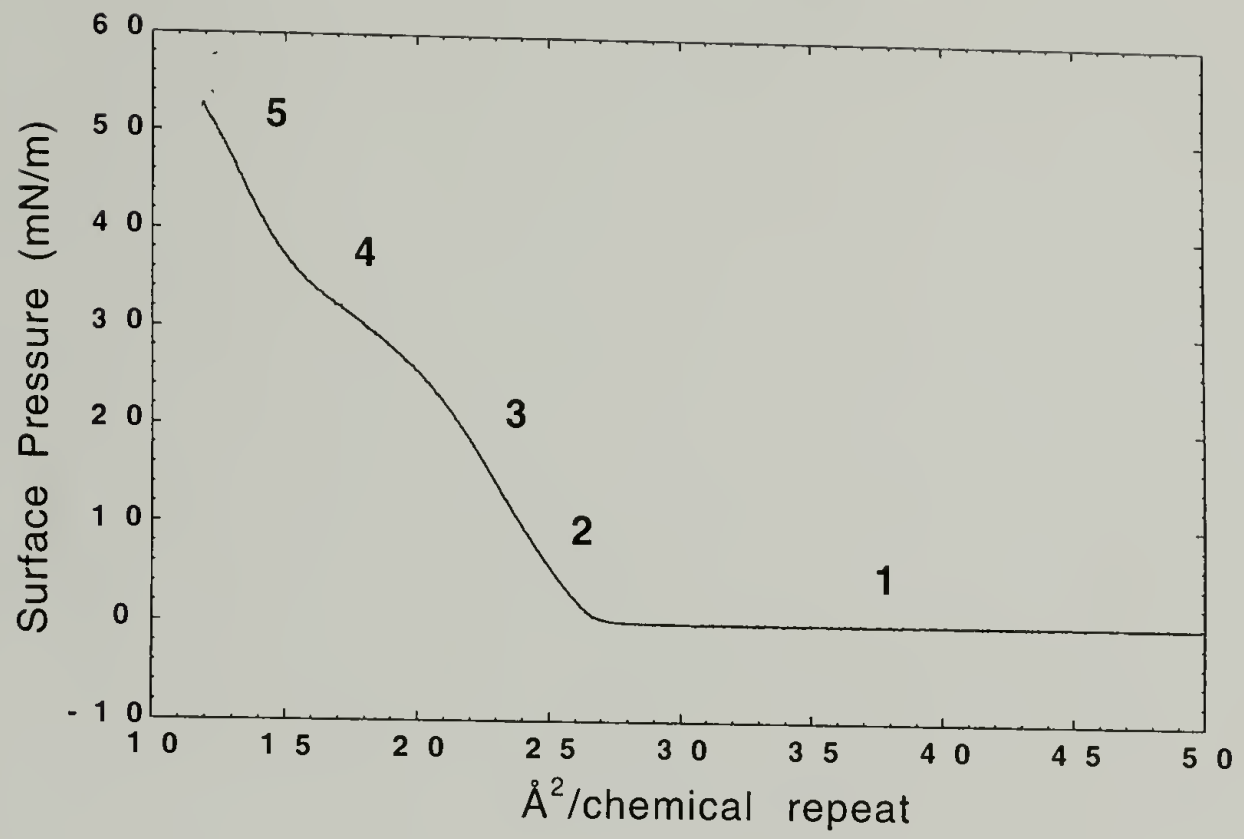

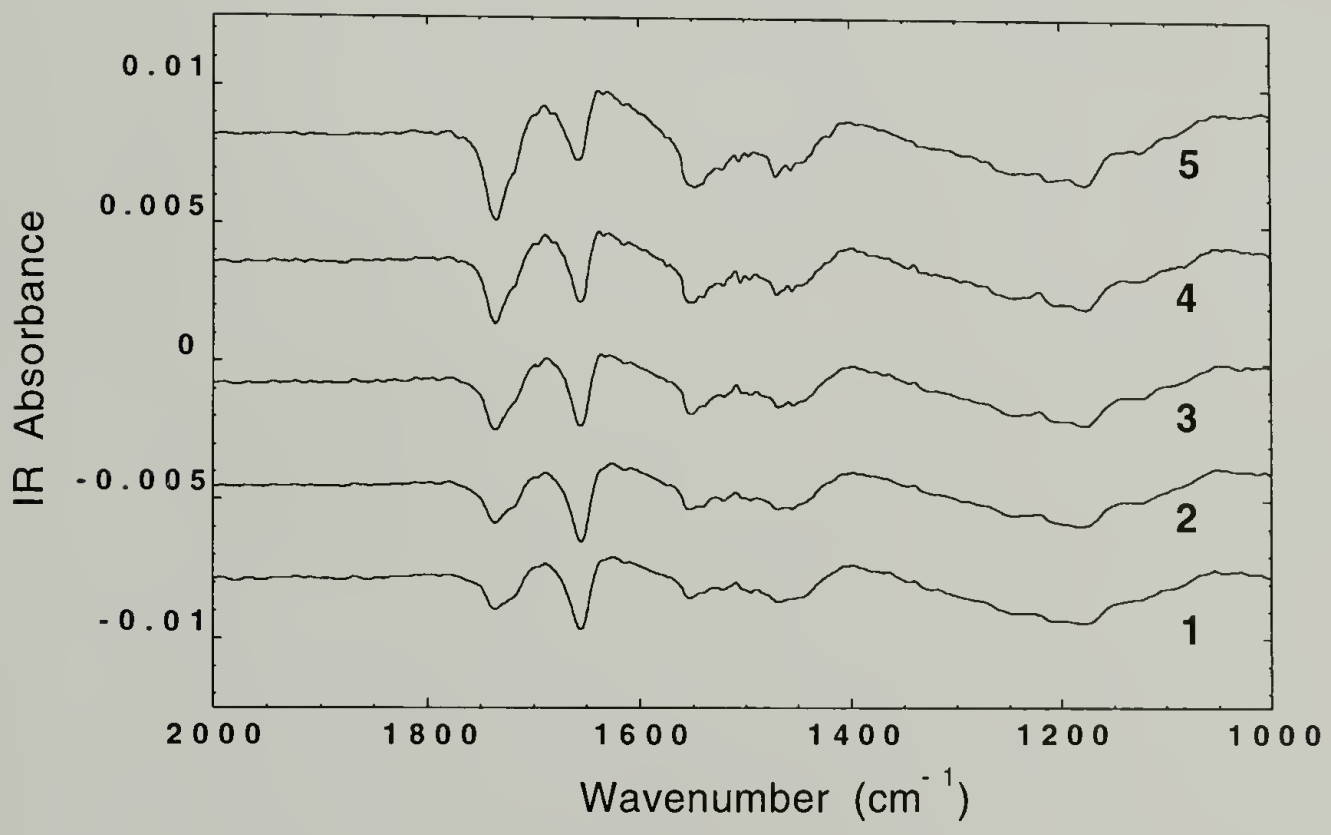

Figure 2.39 50% γ-*n*-octadecyl-L-glutamate sample: External reflection infrared spectra between 2000-1000 cm^{-1}.

compression. There are two possible explanations for this which will be discussed in the following. First, given that the molecules are known to be in the rod-like α-helical conformation, the amide I and amide II bands have well defined transition moment angles with respect to the helix axis. Specifically, the amide I and amide II transition moment directions have been determined in other studies to be inclined from the helix axis by 29-34° and 75-77°, respectively.[73,74] Generally speaking, the amide I vibration can be characterized as having a dipole moment parallel to the helix axis. The amide II vibration can be characterized as having a dipole moment perpendicular to the helix axis. This is shown schematically in Figure 2.40 where the vectors representing individual dipole moments are symmetric about the helix axis.

Recalling that all of the spectra were collected with the incident infrared beam polarized in the s direction parallel to the plane of the air-water interface and perpendicular to the compression direction, the two possible explanations for the observed change in relative intensity of the amide I and II bands are: a) as the film is compressed, the rigid-rods which initially lie flat and are isotropically oriented in the plane of the interface following spreading, gradually begin to orient out of the plane of the air-water interface, or b) as the film is compressed, the rigid-rods which initially lie flat and are isotropically oriented within the plane of the interface gradually become preferentially aligned parallel to the compression barriers within the plane of the interface. In theory, a combination of a and b is also possible. Given the long rigid-rod conformation and the somewhat hydrophilic character of the intramolecularly hydrogen bonded backbones, however, orientation of the helices out of the plane of the air-water interface is less likely. Moreover, other studies have also indicated that case b is the likelier of the two possibilities. In studies involving films of rigid-rod polypeptides transferred from the air-water surface by a horizontal touching method, it was proposed that the helices become preferentially oriented parallel with the compression barriers during compression in a Langmuir trough at the air-water interface.[75] Another study with a similar conclusion

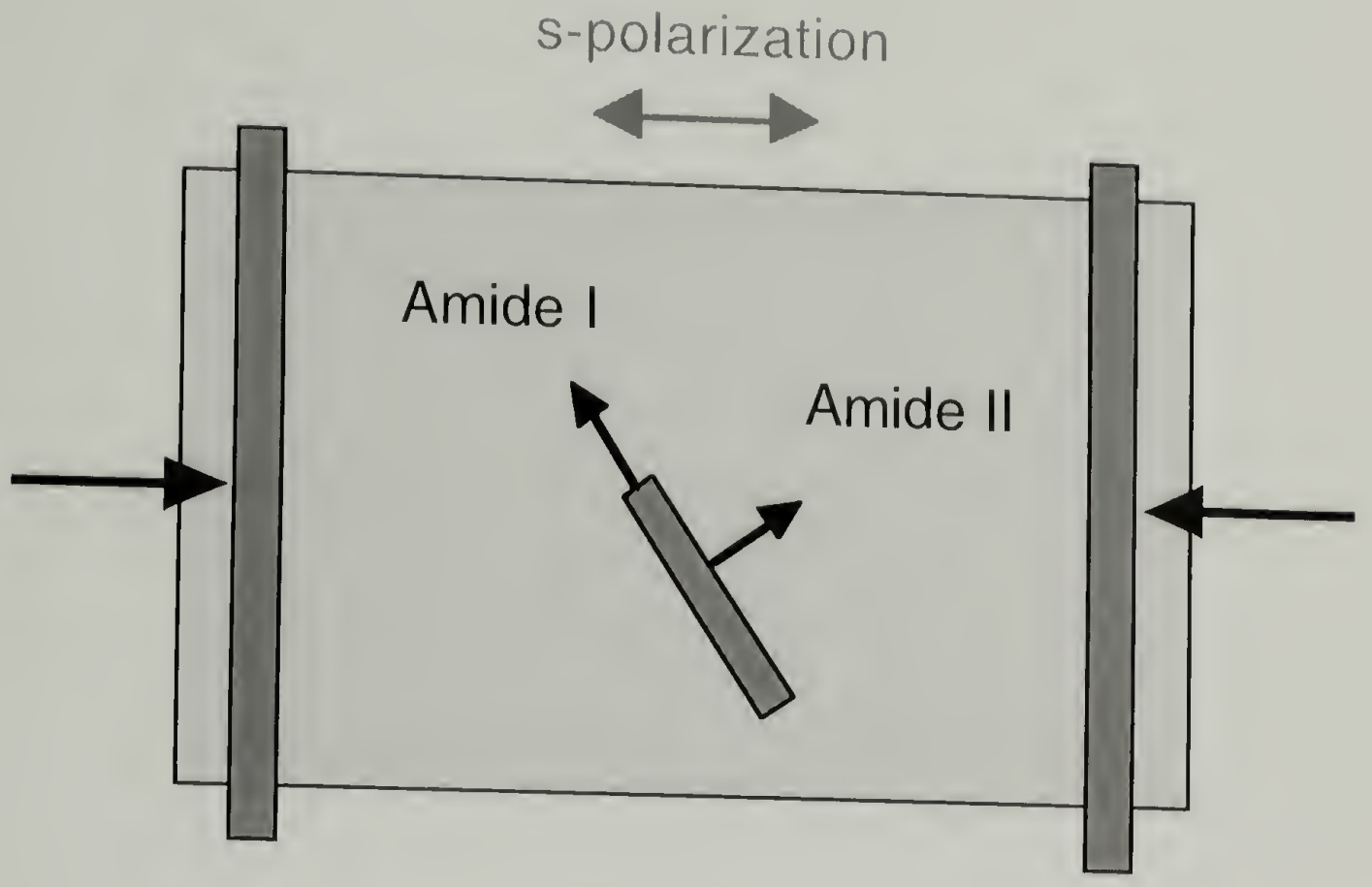

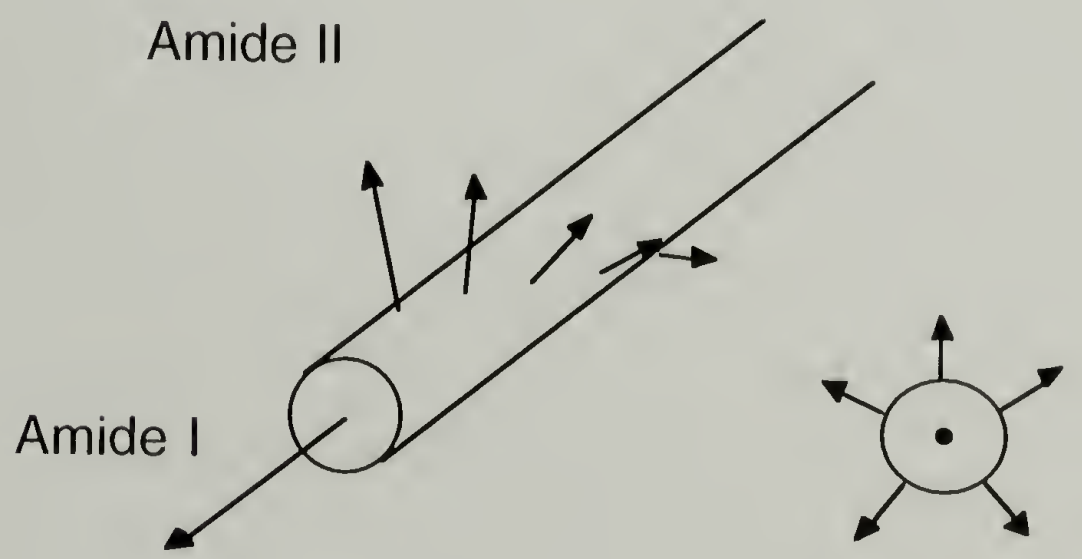

Figure 2.40 Schematic representation of dipole moment vectors for the amide I and amide II modes along the helix. Also shown is a schematic of the trough and the s-polarized infrared beam.

was one in which ripple patterns generated on the film/water surface by a vibrating probe were found to become elliptical during compression.[76] This was interpreted as being indicative of film anisotropy in the plane of the interface. Finally, in studies of Langmuir films of fully side chain substituted poly(γ-*n*-octadecyl-L-glutamate) using electrically induced capillary wave diffraction directly at the air-water interface and atomic force microscopy of these films horizontally transferred onto silicon substrates, it was also concluded that the rigid-rod polymers exhibit a preferential alignment parallel to the compression barriers during compression.[70] In none of these studies, however, was the degree of preferential in-plane alignment of the rigid-rods parallel to the barriers quantitatively determined at the air-water interface.

That the intensity of the C=O stretching band associated with the side groups also increases in intensity relative to the amide I band can perhaps in part be attributed to the stretching of the side chains away from the air-water interface during compression. This band has a dipole moment which is roughly perpendicular to the backbone of the side chain where the ester group is located.

With the change in relative intensity of the amide I and II vibrations in the measured external reflection infrared spectra, the state of orientation of the rigid-rod backbones can be quantitatively described with a set of orientation functions. First, given that the rigid-rods will be assumed to be within the plane of the air-water interface (case b), a complete description of the orientation can be made using the general equations for biaxial orientation.[77-79] The coordinate system used for describing such an orientation is shown in Figure 2.41 where z is the direction along which the helices become preferentially aligned, i.e. axis both perpendicular to the compression direction and parallel to the compression barriers, yz is the plane of the film, i.e. the air-water interface, the vectors V and P represent the axis of an individual helix and the direction of an oscillating dipole moment respectively, α represents the dipole moment angle, β is the

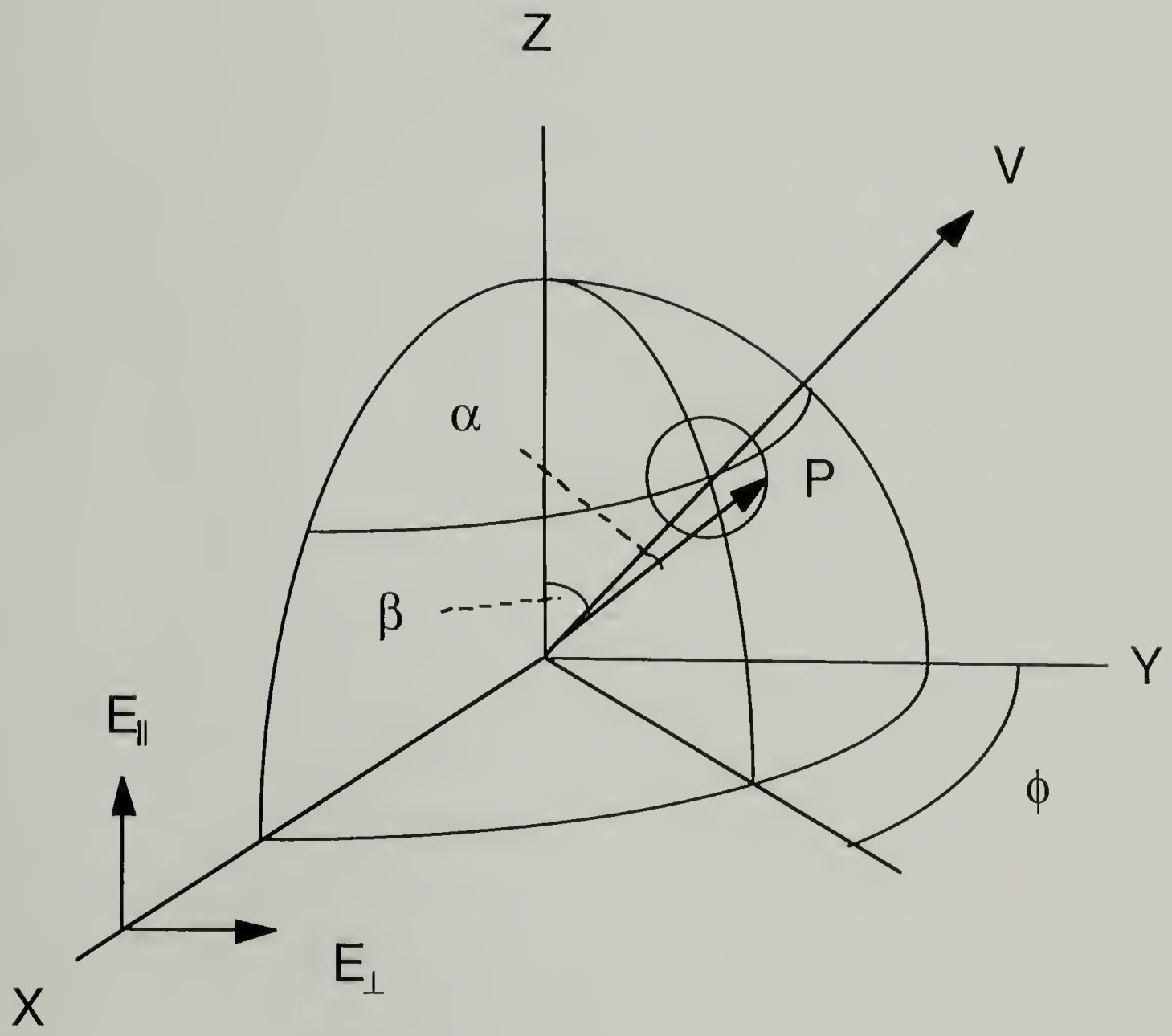

Figure 2.41 The coordinate system used for describing the orientation of the rigid helices perpendicular to the compression direction and within the plane of the interface.

angle between the helix axis and the z axis, and ϕ is the angle between the projection of V on the xy plane and the y axis.

The orientation functions are defined by the following equations:

$$f_\beta = (3\langle\cos^2\beta\rangle - 1)/2 \tag{2.13}$$

$$f_\phi = 2\langle\cos^2\phi\rangle - 1 \tag{2.14}$$

Both $\langle\cos^2\beta\rangle$ and $\langle\cos^2\phi\rangle$ are the average squared cosines of the angles that the helices make with the z axis and the yz plane respectively. f_β describes the state of orientation of the helices with respect to the compression direction and may vary from 1 to -0.5. Therefore, $f_\beta = 1$ would describe a system where the helices are perfectly aligned with the z axis, $f_\beta = -0.5$ would describe perfect alignment perpendicular to the z axis, and $f_\beta = 0$ would describe a random orientation with respect to the z axis. f_ϕ, on the other hand, characterizes the alignment of the rigid-rods with respect to the plane of the air-water interface and can vary from -1 to 1 with the latter representing perfect alignment within the plane of the air-water interface. With the long rigid-rod conformation of the polymer backbones and the results of the studies mentioned previously, it will be assumed that $f_\phi = 1$.

In traditional transmission infrared dichroism the infrared absorbances of a given band obtained with the infrared beam polarized parallel, $A_{||}$, and with the infrared beam polarized perpendicular, $A_\perp$, to a given reference direction (e.g. z axis) are used in analyzing molecular orientation. The chosen band should also have a known transition moment angle, α. $E_{||}$ and $E_\perp$, shown in Figure 2.41, represent the two plane polarized electric vectors used to obtain $A_{||}$ and $A_\perp$, respectively. The propagation direction of the radiation is along the x axis. The dichroic ratio, D, is then defined as

$$D = A_{||} / A_{\perp} \tag{2.15}$$

Given that absorption is proportional to the squared scalar product of the electric vector and P, the dichroic ratio for helices confined in the yz plane, i.e. the air-water interface, is

$$D(\alpha,\beta) = (2\cot^2\alpha\cdot\cos^2\beta + \sin^2\beta) / [\cot^2\alpha\cdot\sin^2\beta + (1 + \cos^2\beta)/2] \tag{2.16}$$

where it is assumed that the alignment can be modeled as a system where all the helices are displaced by the same angle β from the z axis.[72] f_β can then be readily determined. For such a planar alignment $\phi = 0$. An average absorbance, A_{av}, may also be defined for this type of planar alignment by the relation

$$A_{av} = (A_{||} + A_{\perp}) / 2 \tag{2.17}$$

where A_{av} is independent of the state of orientation of the helices with respect to the z axis and is proportional to the amount of absorbing species within the infrared beam.

The ratio of the intensity of the amide I vibration and the amide II vibration can then be related directly to f_β in a manner analogous to that of traditional transmission infrared dichroism. The difference, however, is that in traditional transmission infrared dichroism $A_{||}$ and $A_{\perp}$ of a single band of known transition moment angle are used in the analysis. In these experiments, the measured $A_{\perp}$, i.e. from a s polarized beam with a polarization direction which is perpendicular to the compression axis (Figure 2.42), for two different bands with different transition moment angles were used instead. Given our experimental setup, it is not possible to obtain s polarized spectra with a polarization direction parallel to the compression axis of the trough (y axis).

f_β can be determined by first considering a model planar system where the average absorbance remains constant, i.e. the amount of absorbing species in the infrared beam

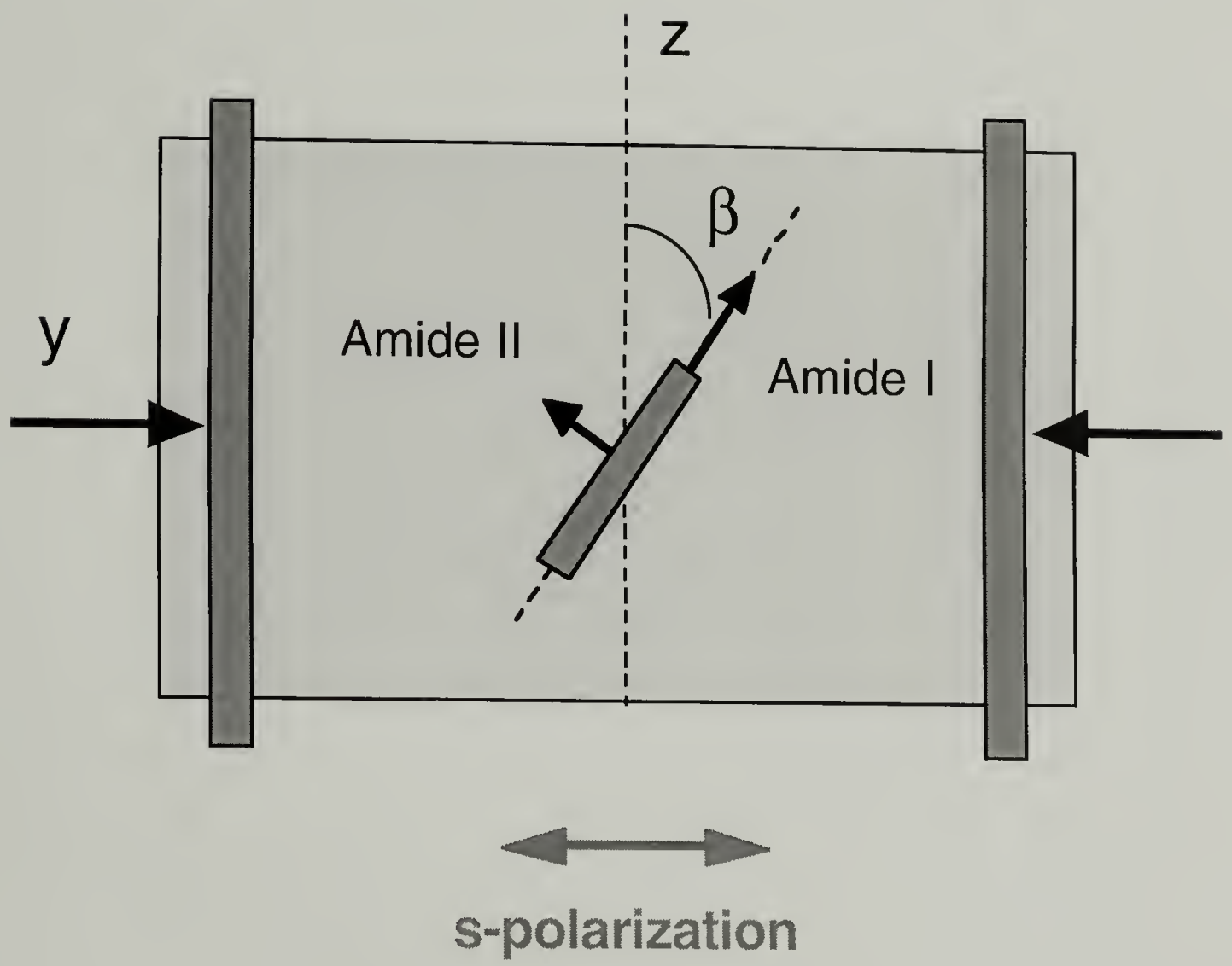

Figure 2.42 Schematic of Langmuir trough with the in-plane polarization direction of the infrared beam and the dipole moment directions for the amide I and II modes. β is the angle between the helix axis and the z-axis.

remains the same during alignment with the z axis. The following terms can subsequently be defined.

$$A_{av(I)} = (A_{||(I)f} + A_{\perp(I)f}) / 2 \tag{2.18}$$

$$A_{av(II)} = (A_{||(II)f} + A_{\perp(II)f}) / 2 \tag{2.19}$$

$$D_I = A_{||(I)f} / A_{\perp(I)f} \tag{2.20}$$

$$D_{II} = A_{||(II)f} / A_{\perp(II)f} \tag{2.21}$$

In these equations, $A_{av(I)}$ and $A_{av(II)}$ are the average absorbances for the amide I and II bands, $A_{||(I)f}$ and $A_{||(II)f}$ are the absorbances for the amide I and II bands obtained with the infrared beam polarized parallel to the z axis, $A_{\perp(I)f}$ and $A_{\perp(II)f}$ are the absorbances for the amide I and II bands obtained with the infrared beam polarized perpendicular to the z axis (i.e. along the y axis), and D_I and D_{II} are the dichroic ratios of the amide I and II bands. f_β can then be determined from the relative intensities of $A_{\perp(I)f}$ and $A_{\perp(II)f}$ if $A_{\perp(I)f}$ and $A_{\perp(II)f}$ are known for $f_\beta = 0$. Specifically, by substituting in values of β between 0° and 90° into equation 2.16, D_I and D_{II} may first be calculated as a function of β. Given the four equations, 2.18, 2.19, 2.20 and 2.21, the ratio of $A_{\perp(I)f}$ and $A_{\perp(II)f}$ may then be determined for any arbitrary value of β.

In actual compression experiments, f_β may also be determined from the measured ratio of $A_{\perp(I)f}$ and $A_{\perp(II)f}$ in this manner. This ratio is sensitive only to the orientation of the rigid-rods and not to the total number of absorbing species. The relative intensities of $A_{\perp(I)f}$ and $A_{\perp(II)f}$ when $f_\beta = 0$, $A_{\perp0(I)}$ and $A_{\perp0(II)}$ respectively, may be taken to be the intensities of the two bands in the s polarized spectra prior to compression of the film. In

this uncompressed state, the orientation of the rigid-rods is isotropic within the plane of the air-water interface. This then gives the following equations:

$$A_{\perp 0(I)} = (A_{\parallel(I)f} + A_{\perp(I)f}) / 2 \tag{2.22}$$

$$A_{\perp 0(II)} = (A_{\parallel(II)f} + A_{\perp(II)f}) / 2 \tag{2.23}$$

Again, by substituting in values of β between 0° and 90° into equation 2.16, D_I and D_{II} may be calculated as a function of β. Given the four equations, 2.20, 2.21, 2.22, and 2.23 the ratio of $A_{\perp(I)f}$ and $A_{\perp(II)f}$ may be determined for any arbitrary value of β.

The orientation function, f_β, calculated as a function of varying surface area for films of poly(γ-methyl-L-glutamate) at the air-water interface is shown in Figure 2.43. Again, positive values of f_β indicate preferential alignment of the rigid-rods perpendicular to the compression axis. The corresponding surface pressure/area isotherm is also shown.

Initially at large surface areas corresponding with an expanded monolayer, the orientation function remains constant at zero. This is as one would expect given the fact that at large surface areas the film is probably composed of individual two-dimensional nematic-like domains floating at the air-water surface.[70] Given the large area, the domains do not feel the presence of the compression barriers and the surface pressure remains at zero. Overall, the rigid-rods are isotropic within the plane of the air-water interface. However, once the film becomes a condensed monolayer corresponding with the sharp rise in the surface pressure, the orientation function increases to a value of roughly 0.25. This indicates that the rigid-rods have a small degree of orientation parallel to the compression barriers. Given the large axial ratio of the rigid-rods, such an orientation of molecules is not entirely surprising. As was mentioned previously, poly(γ-methyl-L-glutamate) exhibits lyotropic liquid crystalline behavior.[25] In some respects, the

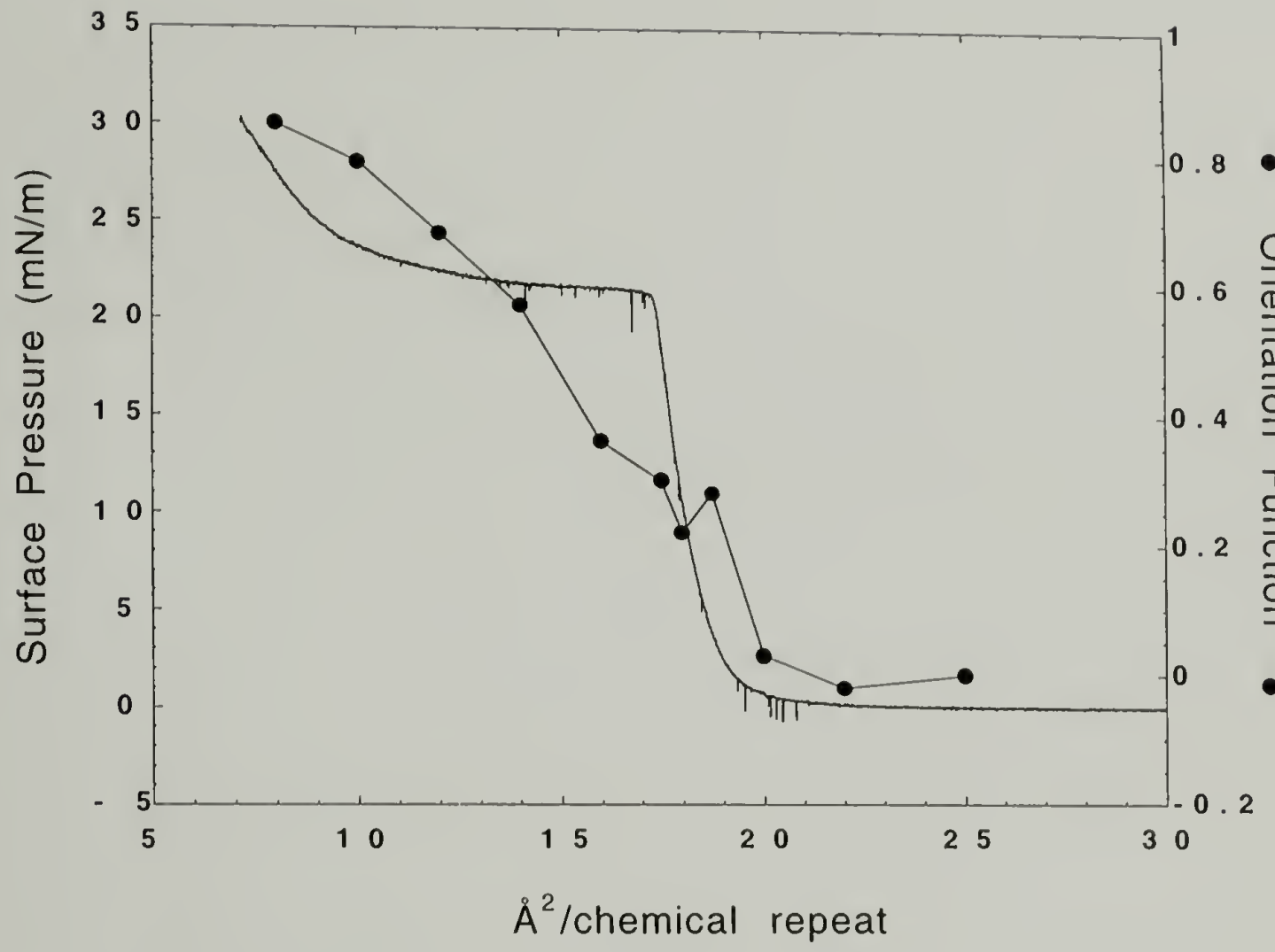

Figure 2.43 Plot of orientation function versus compression for poly(γ-methyl-L-glutamate) at the air-water interface.

water surface may be viewed as a solvent-like matrix for the rigid-rod molecules where compression of the barriers in effect increases the concentration of rigid-rods. Another factor which probably allows for the orientation of the monolayer is the stability of the film itself at the air-water interface. For molecules without such a favorable interaction with the water surface, collapse of the monolayer to a bilayer film would probably occur before molecules in the monolayer state would be given a sufficient opportunity to orient.

Upon further compression after the formation of a condensed monolayer the orientation function continues to increase. At these surface areas the film is changing from a monolayer to a multilayer. Starting at ~0.25 the orientation function rises roughly linearly reaching a final measured value of ~0.85 at a surface area of 7 $Å^2$/chemical repeat indicative of a high degree of orientation. This enhancement in the alignment of the rigid-rods during the formation of a multilayer film at the air-water interface has also been proposed by some of the previously mentioned studies on horizontally transferred films. A simple concept may explain this enhanced alignment. At a point when the monolayer is compressed to a point just prior to the monolayer-bilayer transition, the film is probably composed of domains of differing orientation. Within each domain, the rigid-rods have a relatively uniform alignment. Assuming this simple model to be true, as would be expected given the previous fluorescence microscopy measurements and the liquid crystalline behavior of poly(γ-methyl-L-glutamate), domains in which the individual helices are oriented parallel to the compression barriers would probably be more likely to initiate the formation of a bilayer than domains composed of helices oriented perpendicular. This is shown schematically in Figure 2.44. An analogy can be made to compressing a group of sticks on a flat surface in a direction perpendicular to the axis of the sticks. The formation of preferentially aligned bilayer domains, would then perhaps further dictate the alignment of other rigid-rod molecules forced from the air-water surface during compression.

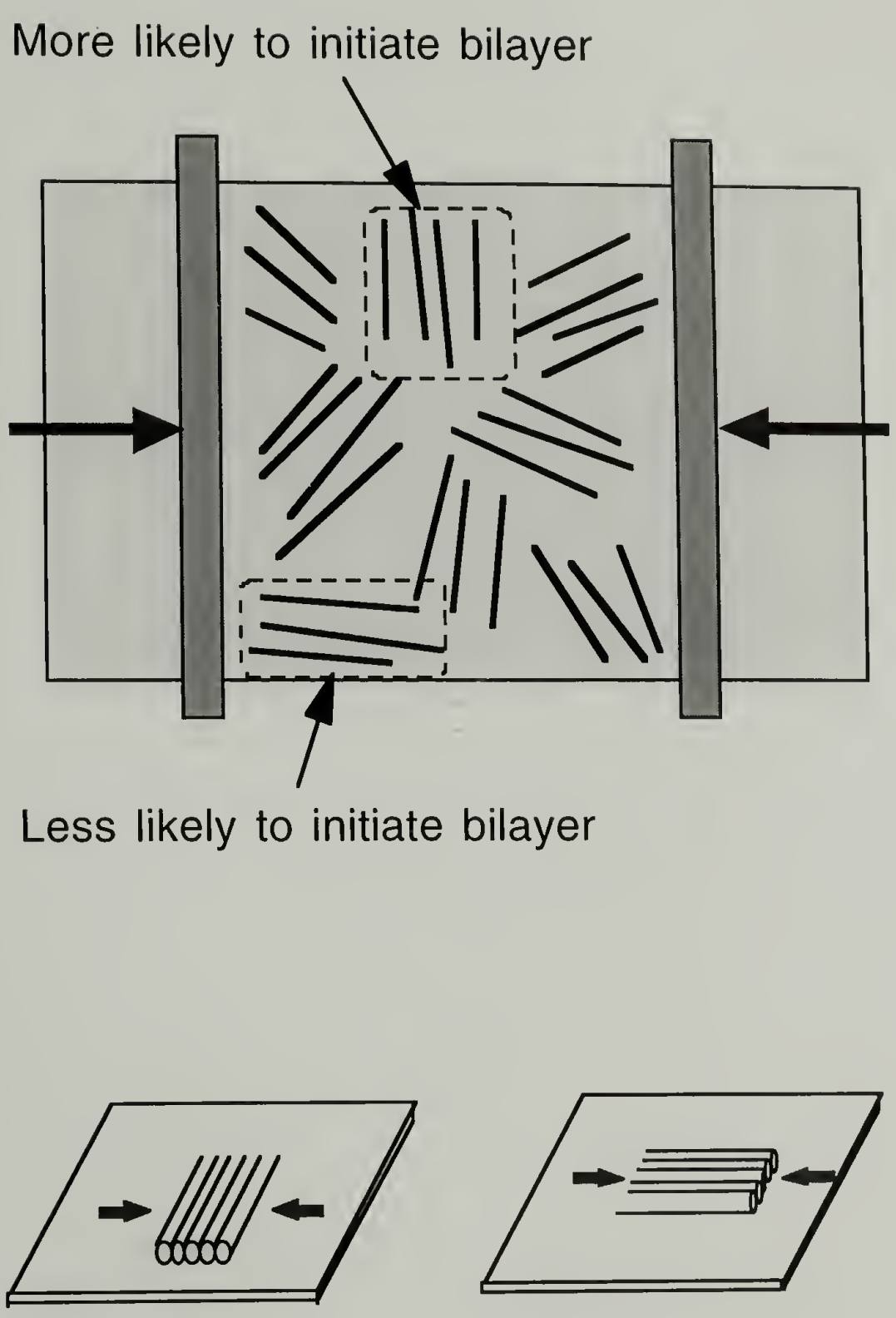

Figure 2.44 Schematic illustration of a proposed model for the formation of bilayer domains composed of helices aligned parallel to the compression barriers.

A plot of the orientation function and the CH_2 asymmetric stretching peak position for the poly(γ-methyl-L-glutamate-*co*-γ-*n*-octadecyl-L-glutamate) of 20% γ-*n*-octadecyl-L-glutamate composition is shown in Figure 2.45. As with the previous sample, the helices have no preferential orientation at areas where the monolayer film is an expanded monolayer. However, in contrast to the previous sample, the rigid-rod backbones do not initially orient upon forming a condensed monolayer. For this sample the rise in the surface pressure is less steep and it is at an area of ~19.0 $Å^2$/chemical repeat before the monolayer of rigid-rods begin orienting perpendicular to the compression direction.

This delay in the orientation can be explained by the presence of the *liquid-like* side groups. During compression of the monolayer, it is the *liquid-like* side groups of adjacent rigid-rods which first interact with one another before giving rise to what can be viewed perhaps as a *solvent-like* matrix for the rigid-rod backbones. The side groups order only slightly in this region. It is not until the monolayer is further compressed and the effective concentration of rigid-rods at the air-water interface increases that alignment of the helices first occurs. This behavior at the air-water interface may again be viewed as analogous to that of a lyotropic liquid crystal. In the previous sample without such long side groups, it is the water surface that is the solvent-like phase. Therefore, the subsequent transition from a condensed monolayer to a multilayer, shown by the steep rise in the surface pressure, is sharp. The steep rise in the surface pressure can be attributed to the impingement of the solid rigid helices. On the other hand, for the side group substituted sample it is the long *liquid-like* side groups that act as the solvent-like phase. Thus the transition from an expanded to a compressed monolayer state is more gradual upon compression.

Additionally, on comparing the degree of alignment of the rigid-rod backbones for the poly(γ-methyl-L-glutamate) sample versus the 20% γ-*n*-octadecyl content copolymer in the condensed monolayer state, it can be seen that the degree of alignment of the side chain substituted sample along the compression axis is enhanced. Before the monolayer-

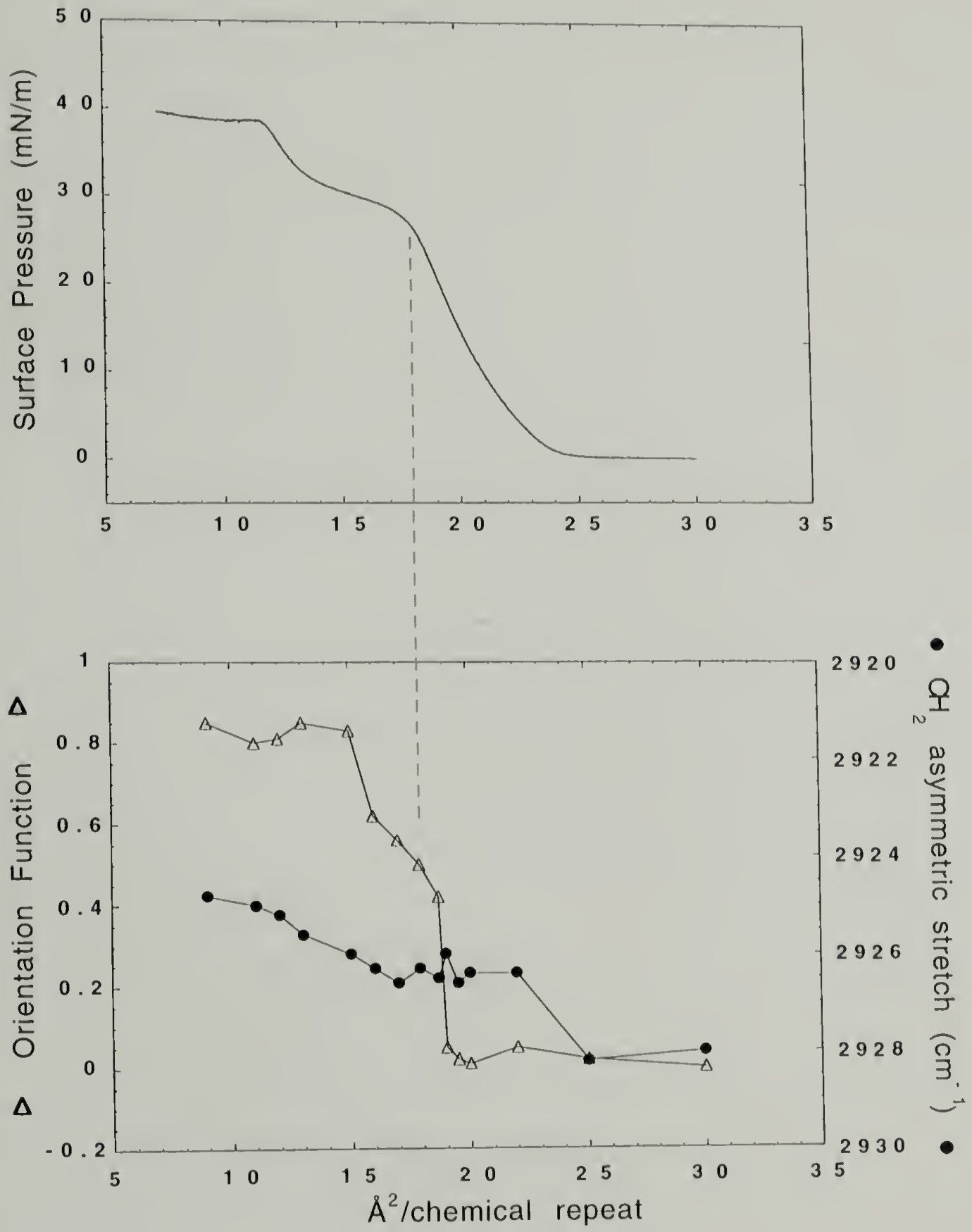

Figure 2.45 Plot of orientation function versus compression for a sample of 20% γ-*n*-octadecyl-L-glutamate composition at the air-water interface. Also shown is the variation of the CH_2 asymmetric stretching peak position.

bilayer transition, f_β reaches a value of ~0.50. This can be explained both by the enhanced stability of the monolayer prior to the monolayer-bilayer transition, indicated by the greater rise in the surface pressure before the plateau, and the *liquid-like* character of the long side groups. For the poly(γ-methyl-L-glutamate) sample, the transition from an expanded monolayer to a condensed monolayer may be too sharp to allow the helices to align further before the monolayer-bilayer transition. For the poly(γ-methyl-L-glutamate-*co*-γ-*n*-octadecyl-L-glutamate) sample of 20% γ-*n*-octadecyl-L-glutamate composition, the transition from an expanded to a condensed monolayer is less steep and abrupt. This in conjunction with the *liquid-like* skin on the surface of the helices provides the rigid-rod backbones with a greater opportunity and ability to align parallel to the compression barriers prior to the monolayer-bilayer transition. Related to the effect *liquid-like* side groups have on the ordering of these monolayer films is the fact that in the bulk, fully long side chain substituted polyglutamates have been found to form a cholesteric liquid crystal phase above the melting point of the side chains.

Upon further compression, the alignment of the rigid-rod backbones continues to increase until midway through the first plateau region. At this point the degree of alignment of the rigid-rod backbones reaches a high value of roughly $f_\beta = 0.82$ and remains relatively constant upon further compression. This degree of alignment of the multilayer film is comparable to the highest degree of alignment found for the poly(γ-methyl-L-glutamate) sample and can be explained similarly.

A plot of the alignment of the rigid-rod backbones for the "hairy-rod" polyglutamate with the highest degree of side group substitution is shown in Figure 2.46. As was discussed previously for this sample of 50% γ-*n*-octadecyl-L-glutamate composition, the *liquid-like* character of the side groups varies greatly as a function of surface area. Beginning first at expanded areas, it can be seen that the rigid-rod backbones are unoriented with $f_\beta = 0$. At surface areas corresponding to the initial formation of a condensed monolayer, however, the rigid-rod backbones begin aligning

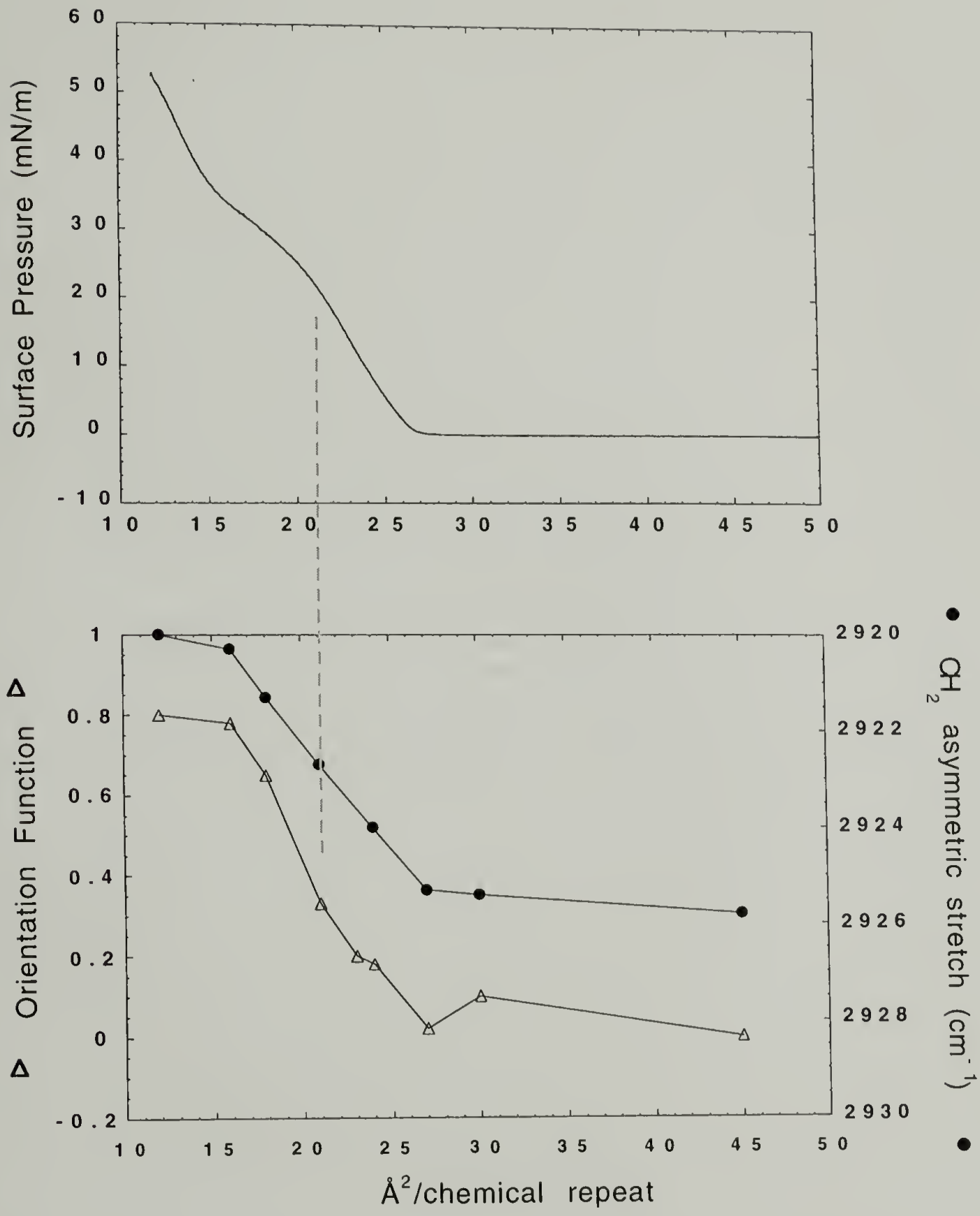

Figure 2.46 Plot of orientation function versus compression for a sample of 50% γ-*n*-octadecyl-L-glutamate composition at the air-water interface. Also shown is the variation of the CH_2 asymmetric stretching peak position.

perpendicular to the compression axis. The degree of alignment is small with f ~ 0.20. At this point the long side groups, although ordering slightly, may be characterized as *liquid-like* at the air-water interface. However, upon further compression of the monolayer just prior to the monolayer-bilayer transition indicated by the beginning of the inflection point in the isotherm, the side groups order to a state which is no longer *liquid-like*. The CH_2 asymmetric stretch peak reaches a position of 2922.7 cm^{-1}. The alignment of the rigid-rod backbones in this condensed monolayer state with $f_\beta = 0.33$ is less than it was for the condensed monolayer of the 20% γ-*n*-octadecyl-L-glutamate sample where $f_\beta = 0.50$. Thus, although the transition from an expanded to a condensed monolayer state is gradual like the 20% γ-*n*-octadecyl-L-glutamate sample, the degree of alignment of the rigid-rod backbones is decreased. This can be attributed to the gradual ordering of the long side groups during compression of the monolayer. The *liquid-like* matrix initially formed becomes less so as both the flexibility of the side groups decreases and side groups from adjacent helices begin to order with one another. Such an ordering of side groups between adjacent helices can perhaps be viewed as decreasing the overall mobility associated with individual helices at the air-water interface during compression.

Upon further compression during which a multilayer film forms, the rigid-rod backbones continue to orient in a manner much like the previous samples reaching a final orientation of $f_\beta = 0.80$. Here both the orientation of the rigid-rods and the ordering of the side groups appear to level off. As was discussed previously, at this surface area the side groups are in a predominantly all-trans conformation and are very *non-liquid-like*.

Overall, the three polyglutamates of varying long side group composition studied illustrate the effect that long side groups can play in controlling the ordering behavior of rigid-rods at an air-water interface. Moreover, the ability of the rigid-rod monolayers to order during compression may also be indicative of their transferability onto solid substrates. As was discussed previously, the Langmuir-Blodgett transfer process may introduce at flow field at the water surface. This may make the fluid dynamics of

Langmuir films an important factor in affecting their transfer onto solid substrates.[11] That the rigid-rod backbones of the copolyglutamate of 20% γ-*n*-octadecyl-L-glutamate composition reach an orientation of $f_\beta = 0.50$ during compression before the monolayer-bilayer transition is indicative of the fluid-like skin on the surfaces of individual rigid-rods and the enhanced mobility of the helices at the water surface. Given this result, it is likely that for such films, transferability onto solid substrates is enhanced. Transfer studies of a copolyglutamate of ~30% γ-*n*-octadecyl-L-glutamate composition have indeed indicated that the transferability of such a film is quite good producing films in which the rigid-rods backbones have a preferential alignment parallel to the dipping direction of the solid transfer substrate.[9-11] At this composition, the long side groups at surface areas corresponding with a condensed monolayer state are probably still *liquid-like*. The shape of the isotherm for a sample of ~30% γ-*n*-octadecyl-L-glutamate composition is similar to the isotherm for the ~20% γ-*n*-octadecyl-L-glutamate composition sample. For films with either a less fluid-like matrix for the rigid-rods or none at all (e.g. 50% γ-*n*-octadecyl-L-glutamate composition sample and poly(γ-methyl-L-glutamate)), transferability onto solid substrates and alignment of the rigid-rods parallel to the dipping direction may not be as favorable. Transfer of samples of either very high or very low γ-*n*-octadecyl-L-glutamate composition has been found to be more difficult. It should also be pointed out that with the preferential alignment of the rigid-rod backbones perpendicular to the compression axis it is possible that the transferability of such films at the air-water interface may vary depending on the orientation of the flat transfer substrate relative to the compression barriers during deposition.

2.5 Polyisocyanates

The second type of "hairy-rod" polymer studied at the air-water interface using external reflection infrared spectroscopy was the random copolyisocyanate, poly(*n*-butyl isocyanate-*co*-*n*-octadecyl isocyanate) of 40% *n*-octadecylisocyanate composition shown

in Figure 2.47. Polyisocyanates, which are not water soluble, are similar to the previous polyglutamates in that these are also polymers that are helical and stiff.[23-25,29] The stiffness of the polymer backbone is due to the partial double-bond character of the backbone amide bonds. The helical conformation of polyisocyanates can be attributed to steric hindrances which prevent the amide bonds from staying planar. In addition, these rigid helices also tend to be very long. This is caused by the fact that reversal of the helical sense (i.e. helices may be left or right handed since the molecule is not chiral) requires that at least one monomer unit obtain a reversal conformation. However, because of the much higher energy associated with reversal conformations versus the helical conformation, reversal of the helical sense for molecules is not common. Subsequently, poly(*n*-alkyl isocyanates) have been found to form both lyotropic and thermotropic liquid crystal phases.[23,24]

2.5.1 Materials

The synthesis of the polymer and the catalyst were made by Georg Maxein of the Johannes Gutenberg University of Mainz.

The catalyst cyclopentadienyl-dimethylamido-titanium-dichloride ($CpTiCl_2N(CH_3)_2$) was made in the following manner.[80] First, in a synproportionation reaction tetanocen dichloride (Cp_2TiCl_2) and titanium tetrachloride ($TiCl_4$) were converted into 2 equivalents of cyclopentadienyl titanium trichloride ($CpTiCl_3$). This was then later reacted with (N,N-dimethyl-trimethylsilyl)-amine $(CH_3)_3SiN(CH_3)_2$ at room temperature to yield the final desired product.

The general procedure for the random copolymerization of *n*-butyl isocyanate (Aldrich) and *n*-octadecyl isocyanate (95%) (Pfaltz & Bauer, United States) was carried out in the following manner.[81] In a dry box, a volumetric "stock" solution of the catalyst, typically 0.01 mmol per 50 µl toluene was prepared. All monomers were stirred for about 24 hours over calcium hydride and vacuum distilled prior to their usage. To the

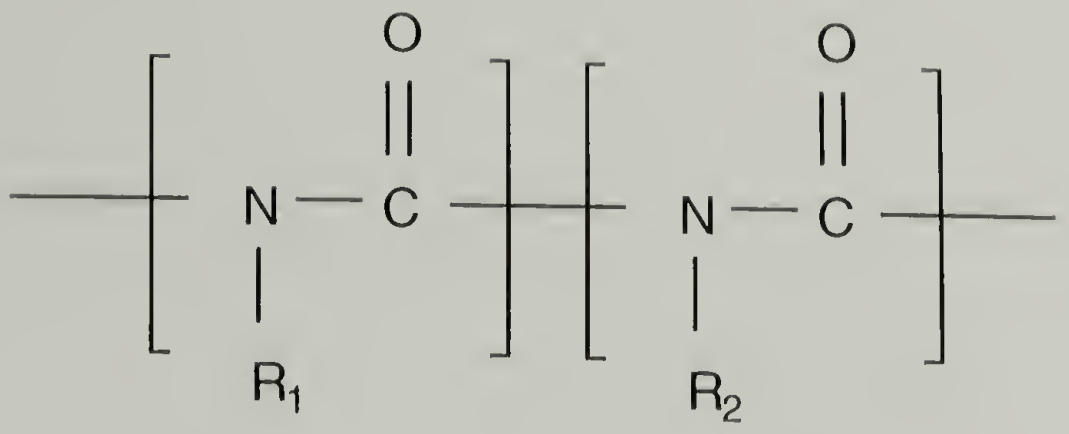

R_1 linear C_4H_9

R_2 linear $C_{18}H_{37}$

Figure 2.47 Chemical structure of poly(*n*-butyl isocyanate-*co*-*n*-octadecyl isocyanate).

degassed monomer feed in a 4 ml serew cap vial together with a magnetic stir bar, a measured amount of the stock solution, depending on the monomer to initiator ratio, was added via syringe. The vial was closed and stirred in the drybox for 2-4 days, depending on the planned moleeular weight, at room temperature.

All workup steps were then performed in the dark or under filtered light (yellow). After the polymerization was eomplete, the solid orange mass was dissolved in 15 ml of a 5% solution of methanol in chloroform. This solution was then poured into 200 ml of cold methanol after whieh a white solid preeipitated. The polymer was isolated by filtration and washed with eold methanol. After reprecipitation from chloroform in methanol, the volatile materials were plaeed under vaeuum. The total range of yields was between 80-90%. M_n and M_w were then determined by gel permeation ehromatography to be 1.515×10^4 g/mol and 1.577×10^4 g/mol, respectively, with $M_n/M_w = 1.041$.

Attempts were also made to polymerize random eopolymers of methylisocyanate and *n*-oetadeeylisoeyanate. This, however, was met with limited suecess due to the large diserepaney in the reaetivities of the two monomers whieh made producing random eopolymers diffieult. Additionally, it was also found that these polymers were difficult to solubilize in solvents suitable for spreading at an air-water interfaee.

2.5.2 Results and Diseussion

The surfaee pressure area isotherm of the "hairy-rod" polyisoeyanate is shown in Figure 2.48. In general, the shape of the eurve is similar to the isotherm of poly(γ-methyl-L-glutamate) and ean be interpreted in a like manner. The rise in the surfaee pressure beginning at ~24 $Å^2$/ehemieal repeat corresponds with the formation of a eondensed monolayer. This is then followed by a plateau region during whieh heliees from the monolayer are forced from the air-water surfaee to form a second layer, speeifieally a bilayer. The plateau region in the surface pressure/area isotherm is relatively flat and therefore implies that this transition is one whieh is well ordered. Finally, the

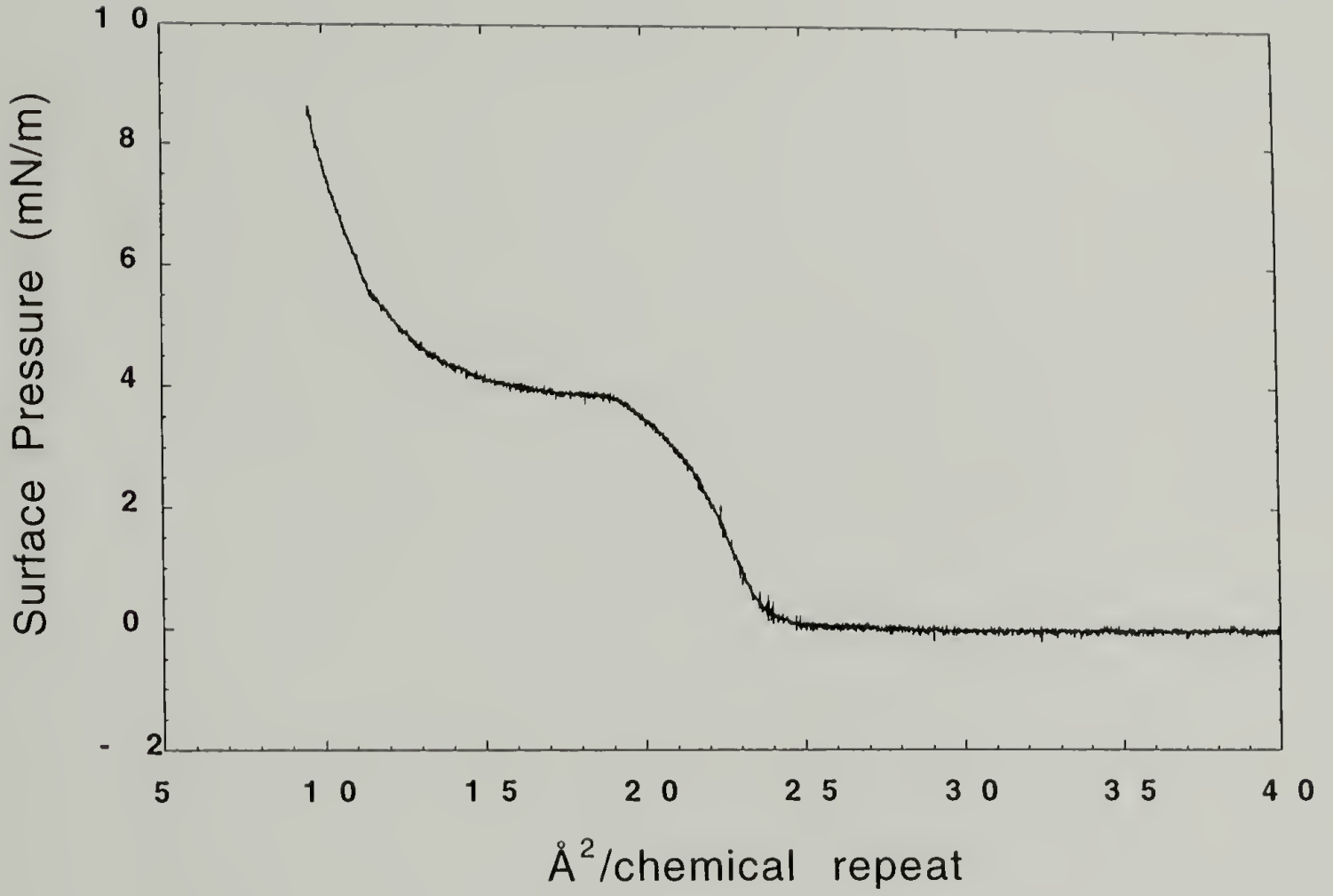

Figure 2.48 Surface pressure/area isotherm for the "hairy-rod" polyisocyanate.

surface pressure begins to rise steeply again at an area of ~13.5 Å^2/chemical repeat. As was for the the poly(γ-methyl-L-glutamate) film, the onset of this rise occurs at a surface area close to half that at which the first rise occurs.

However, the largest and most obvious difference in the isotherm of this "hairy-rod" polyisocyanate versus the polyglutamates is the much smaller rise in the surface pressure prior to the monolayer-bilayer transition. As was discussed previously, the height of this rise is indicative of the stability of the monolayer at the air-water interface. Whereas the rise for the polyisocyanate is ~4 mNm^{-1}, the rise for the poly(γ-methyl-L-glutamate) is ~22 mNm^{-1}. *N*-alkyl side chain substitution between 20-50% side chain composition further increases the stability of "hairy-rod" polyglutamates. The large difference in the stability the polyisocyanate versus the polyglutamates can be explained by the more strongly hydrophobic character of the polyisocyanate. The backbones of the polyglutamates with their more strongly hydrophilic amide backbone groups and the ester groups in the side chains provide these rigid-rods with a greater affinity for the air-water surface. The polyisocyanate studied here has a sufficient affinity for the air-water interface to allow the molecules to form a monolayer at the air-water interface. However, the affinity is much less than it is for the polyglutamate. Since the helical backbone of the polyisocyanate is more hydrophilic than the *n*-alkyl side groups, attempts were made to expose more of the helix to the air-water surface by synthesizing a random copolymer of poly(methyl isocyanate-*co*-*n*-octadecyl isocyanate). It was felt that the decreased density of *n*-alkyl side groups for such a sample would allow the long side groups to better orient away from the interface. Such an orientation of the side groups would further enhance the interaction of the polymer backbone with the air-water surface. These attempts, however, were largely unsuccessful as was discussed previously.

A plot of the full range external reflection infrared spectrum of the poly(*n*-butyl isocyanate-*co*-*n*-octadecyl isocyanate) of 40% *n*-octadecylisocyanate composition film at an air-water interface is shown in Figure 2.49. Examining the spectrum, bands

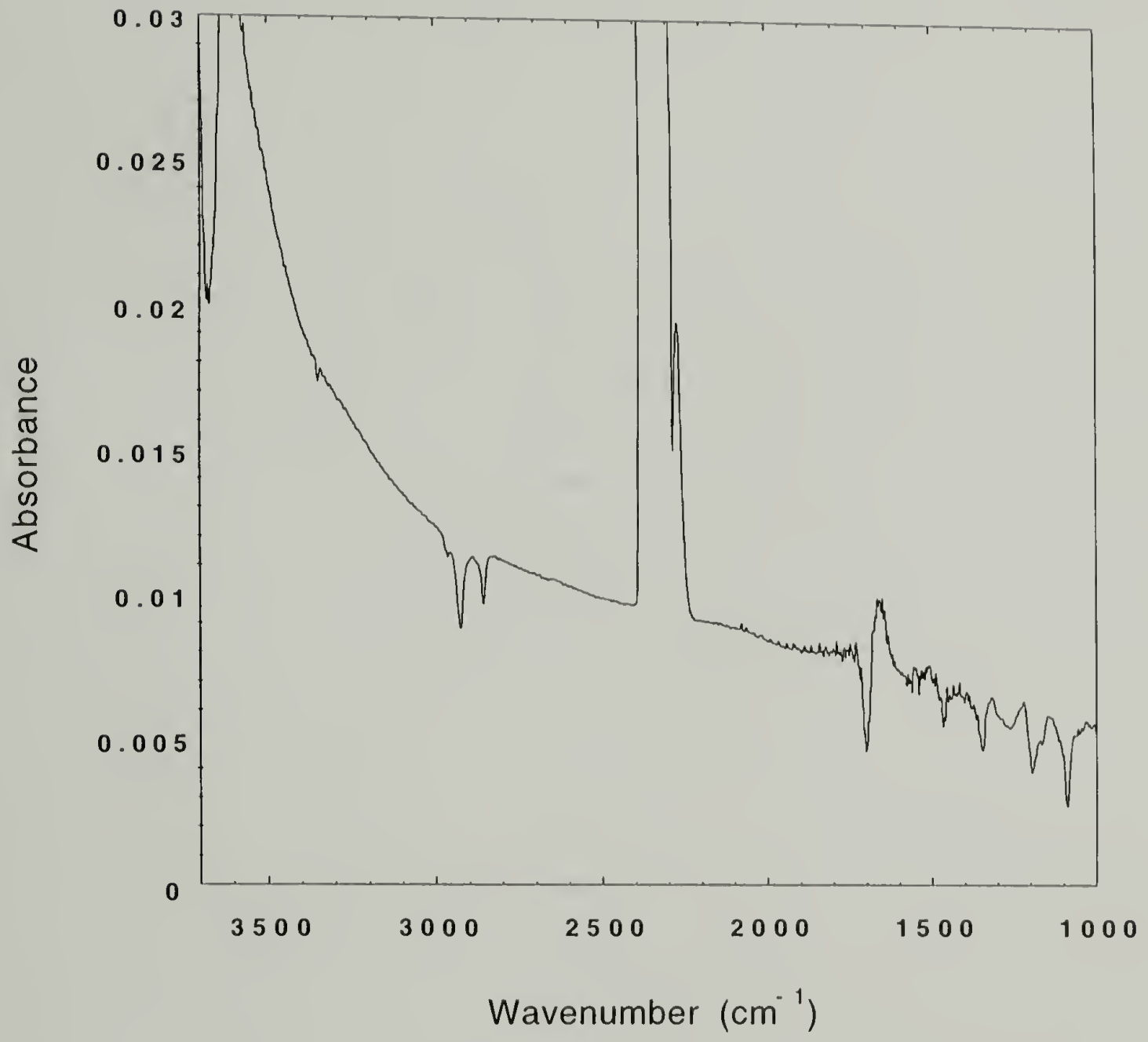

Figure 2.49 Full range spectrum of the "hairy-rod" polyisocyanate at the air-water interface.

associated with the CH_2 stretching mode can be clearly observed in the 2900 cm^{-1} region. The band at 1695 cm^{-1} associated with the C=O stretching mode is also readily identifiable. As the film was compressed, none of the bands below 1700 cm^{-1} were observed to change in either relative intensity or position. This indicates that in contrast to the polyglutamates, there may not be any type of preferential alignment of the rigid-rod backbones during compression at the air-water interface.

This was not the case with the CH_2 asymmetric stretching band associated with the *n*-alkyl side chains. The CH_2 asymmetric stretching band is shown as a function of compression in Figure 2.50. Here it can be clearly observed that the position of the CH_2 asymmetric stretching band shifts, in a manner similar to the 50% γ-*n*-octadecyl-L-glutamate sample, to lower position as the film is compressed. The total shift is large and can be characterized as one where the side chains vary from being *liquid-like* to *non-liquid-like*. A plot of the CH_2 asymmetric stretching peak position is shown in Figure 2.51. Initially, at large surface areas where the monolayer is expanded, the side chains can be characterized as *liquid-like* with a peak position of ~2925.1 cm^{-1}. However, unlike the 50% γ-*n*-octadecyl-L-glutamate sample, the *liquid-like* character of the side chains remains upon the formation of a condensed monolayer. This behavior is illustrative of the difference in the stability of the polyisocyanate monolayer versus polyglutamate monolayers. Given that the polyisocyanate is highly side chain substituted with 20% of the backbone atoms having a *n*-octadecyl group, this "hairy-rod" polymer can be likened to the polyglutamate of 50% γ-*n*-octadecyl-L-glutamate composition (i.e. 16.7% of the polyglutamate backbone atoms have a *n*-octadecyl side group) in terms of overall *n*-alkyl side chain content. For the polyglutamate, the stability of the film at the air-water interface allows the monolayer to be compressed sufficiently such that the long side chains from adjacent helices intermingle and order. In contrast, for the polyisocyanate film, the monolayer collapses to a bilayer before the long side chains of adjacent helices in the monolayer state can be compressed close enough to order.

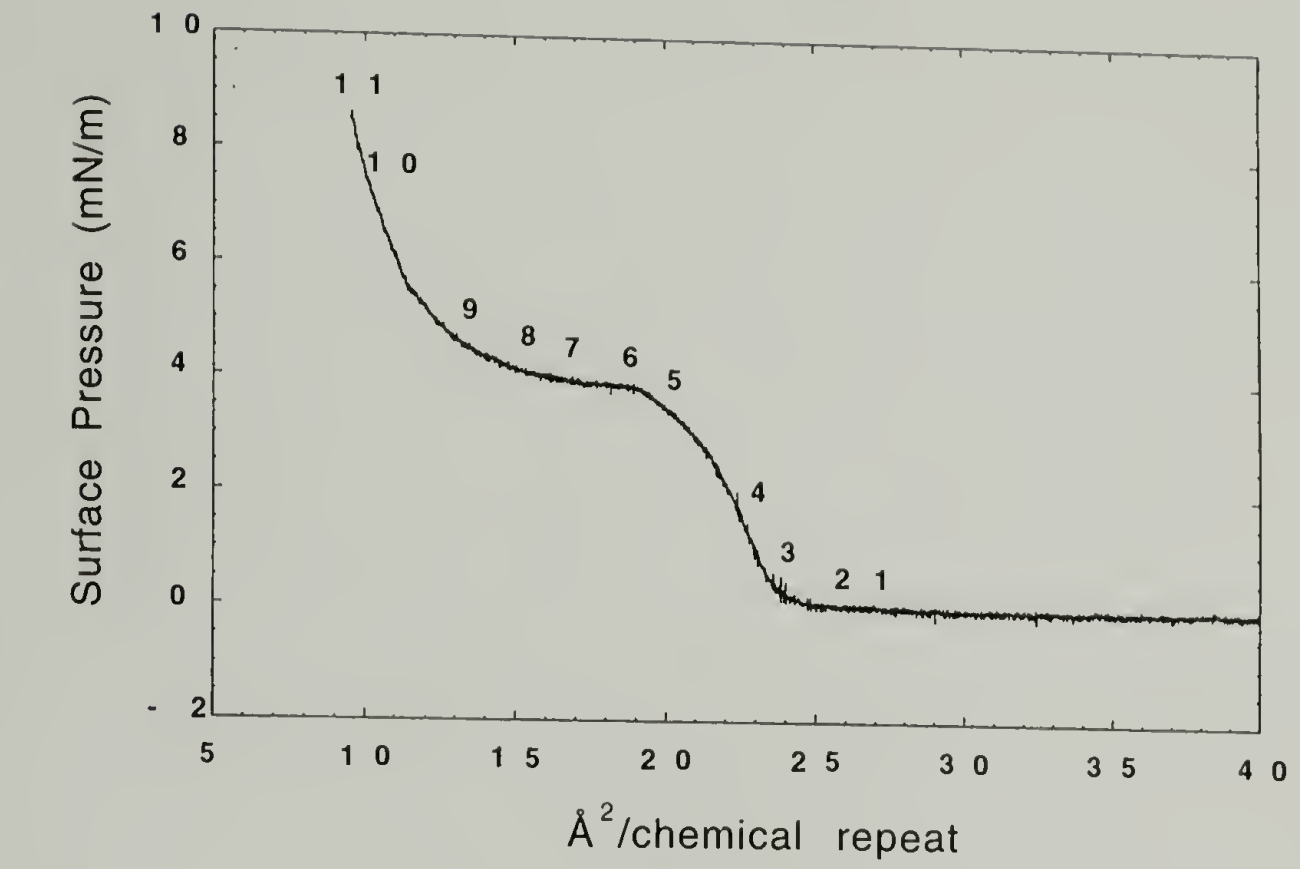

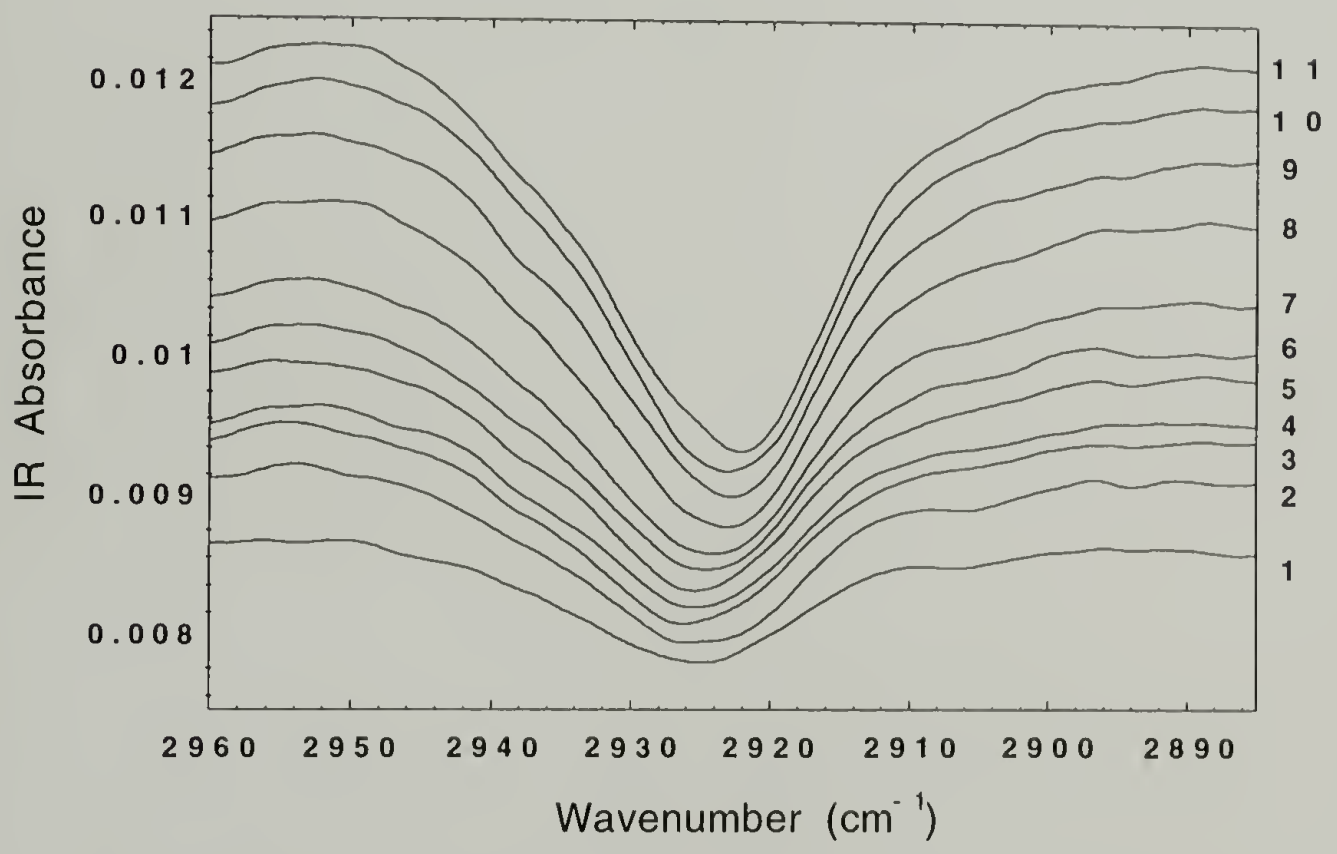

Figure 2.50 Overlay of CH_2 asymmetric stretching band with compression at the air-water interface for the "hairy-rod" polyisocyanate.

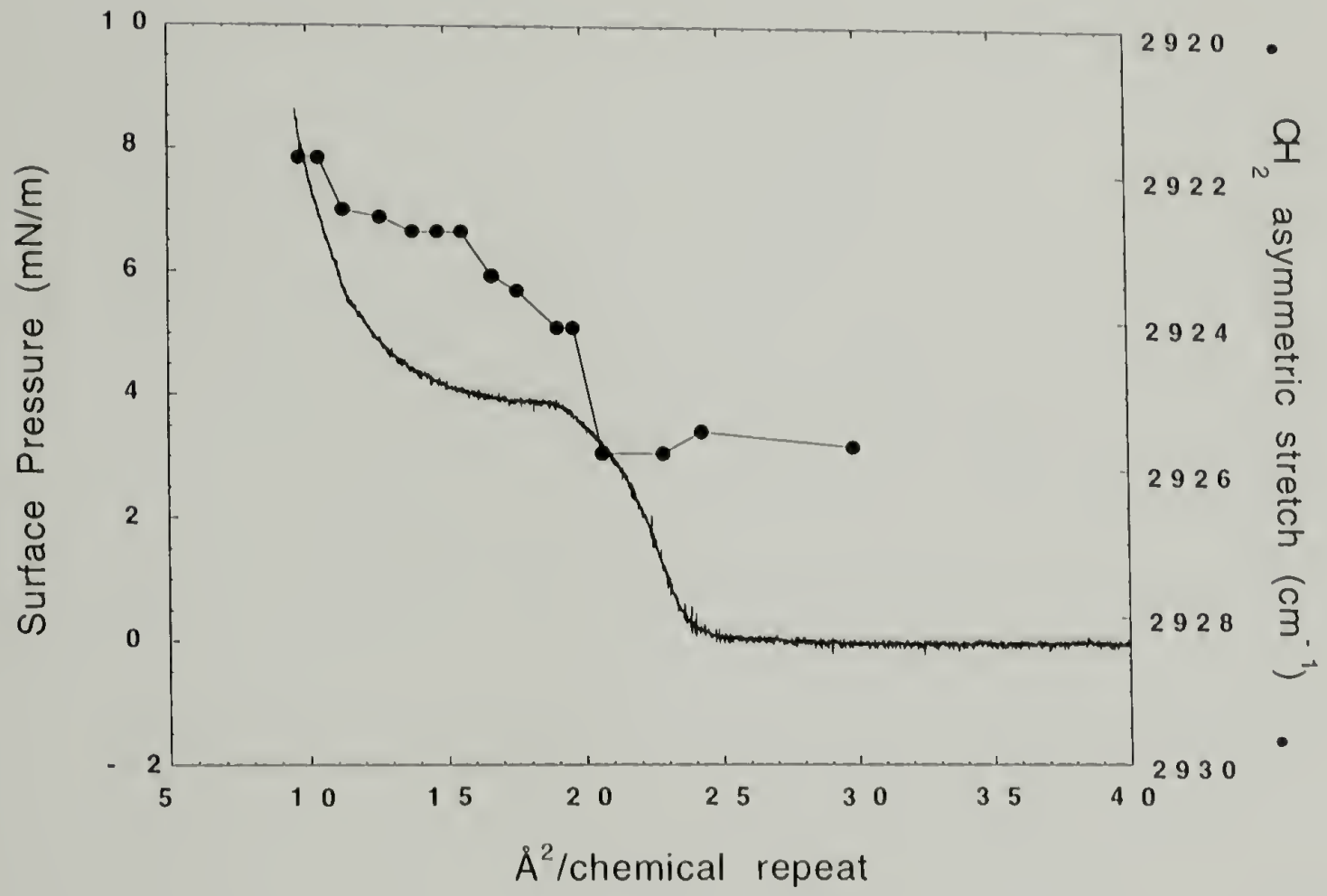

Figure 2.51 Plot of CH_2 asymmetric stretch peak position versus compression at the air-water interface.

Upon the formation of a bilayer and subsequently a structure more closely resembling one in the bulk, the side chains finally do begin ordering. This ordering of the long side groups continues throughout the plateau region and the final rise in the surface pressure. At a surface area of 10 $Å^2$/chemical repeat the CH_2 asymmetric stretching peak position reaches a value of 2921.8 cm^{-1}. This is close to the CH_2 asymmetric stretching peak position measured for a bulk film cast by standard transmission infrared spectroscopy. The peak position for such a film was 2921.3 cm^{-1}.

The instability of polyisocyanate monolayers has subsequently presented difficulties in the transfer of these films onto solid substrates. Specifically, in studies on polyisocyanates with azo-dye and *n*-alkyl side groups, it was found that although the polymers form monolayers at an air-water interface, they are not stable enough to be deposited by the Langmuir-Blodgett technique.[29] The surface pressure/area isotherms of these molecules were similar in shape to the *n*-alkyl side group polyisocyanates studied here. In particular, the rises in the surface pressure prior to the monolayer-bilayer transition for these molecules were small, typically on the order of 5 mNm^{-1}. In a different study on a series of polyisocyanides, also rigid helical polymers with similarly hydrophobic backbones, however, it was found that with the addition of hydrophilic ester groups in the side chains, film stability increased making the monolayers transferable.[30] The addition of hydrophilic groups could therefore increase the applicability of "hairy-rod" polyisocyanates.

2.6 Conclusions

Overall, it was observed by external refection infrared spectroscopy that the structure of "hairy-rod" polymer films at the air-water interface varies depending on the state of the long side groups attached to the rigid backbone. Specifically, for the series of copolyglutamates studied, it was found that the *liquid-like* character of long *n*-octadecyl side groups at an air-water interface affects the ordering and subsequent alignment of the

rigid-rod backbones. It is also very likely that this *liquid-like* character of the side groups at the air-water interface plays an important role in determining the transferability of these "hairy-rod" films. Both main chain spectra as well as side chain spectra were readily obtained and analyzed along the surface pressure/area isotherm in these studies.

On comparing the results of "hairy-rod" polyglutamates with a "hairy-rod" polyisocyanate, it was also demonstrated that the overall stability of a monolayer at an air-water interface also effects the structure of the monolayer as well as the onset of the monolayer-bilayer transition. The stability of the monolayers also affects transferability.

References

(1) Ulman, A. *An Introduction to Ultrathin Organic Films*; Academic Press: Boston, 1991.

(2) Roberts, G. *Langmuir-Blodgett Films*; Plenum Press: New York, 1990.

(3) Hupfer, B.; Ringsdorf, H. *Polymeric Monolayers and Liposomes as Models for Biomembranes and Cells; ACS Symp. Ser.; No. 175*; American Chemical Society: Washington, DC, 1981.

(4) Gregoriadis, G.; Allison, A. C. *Liposomes in Biological Systems*; Wiley: New York, 1980.

(5) Swalen, J. D. *J. Mol. Electron.* **1986**, *2*, 155.

(6) Menzel, H.; Weichart, B.; Schmidt, A.; Paul, S.; Knoll, W.; Stumpe, J.; Fischer, T. *Langmuir* **1994**, *10*, 1926.

(7) Menzel, H.; McBride, J. S.; Weichart, B.; Ruther, M. *Thin Solid Films* **1996**, *284-285*, 640.

(8) Hickel, W.; Duda, G.; Jurich, M.; Krohl, T.; Rochford, K.; Stegeman, G. I.; Swalen, J. D.; Wegner, G.; Knoll, W. *Langmuir* **1990**, *6*, 1403.

(9) Wegner, G. *Ber. Bunsenges. Phys. Chem.* **1991**, *95*, 1326.

(10) Wegner, G. *Thin Solid Films* **1992**, *216*, 105.

(11) Schwiegk, S.; Vahlenkamp, T.; Xu, Y.; Wegner, G. *Macromolecules* **1992**, *25*, 2513.

(12) Mathauer, K.; Mathy, A.; Bubeck, C.; Wegner, G. *Thin Solid Films* **1992**, *210/211*, 449.

(13) Mathy, A.; Mathauer, K.; Wegner, G.; Bubeck, C. *Thin Solid Films* **1992**, *215*, 98.

(14) Mumby, S. J. *Macromolecules* **1986**, *19*, 1054.

(15) Tieke, B. *Adv. Polym. Sci.* **1985**, *71*, 79.

(16) Vierheller, T. R.; Foster, M. D.; Schmidt, A.; Mathauer, K.; Knoll, W.; Wegner, G.; Satija, S.; Majkrzak, C. F. *Macromolecules* **1994**, *27*, 6893.

(17) Tsukruk, V. V.; Foster, M. D.; Reneker, D. H.; Schmidt, A.; Wu, H.; Knoll, W. *Macromolecules* **1994**, *27*, 1274.

(18) Tsukruk, V. V.; Foster, M. D.; Reneker, D. H.; Schmidt, A.; Knoll, W. *Langmuir* **1993**, *9*, 3538.

(19) Stumpe, J.; Fischer, T.; Menzel, H. *Macromolecules* **1996**, *29*, 2831.

(20) Schmidt, A.; Mathauer, K.; Reiter, G.; Foster, M. D.; Stamm, M.; Wegner, G.; Knoll, W. *Langmuir* **1994**, *10*, 3820.

(21) Menzel, H.; Hallensleben, M. L.; Schmidt, A.; Knoll, W.; Fischer, T.; Stumpe, J. *Macromolecules* **1993**, *26*, 3644.

(22) Menzel, H.; Weichart, B.; Hallensleben, M. L. *Thin Solid Films* **1993**, *223*, 181.

(23) Aharoni, S. *Macromolecules* **1979**, *12*, 94.

(24) Aharoni, S. M. *Macromolecules* **1981**, *14*, 222.

(25) Daly, W. H.; Poche, D.; Negulescu, I. I. *Prog. Polym. Sci.* **1994**, *19*, 79.

(26) Watanabe, J.; Ono, H.; Uematsu, I.; Abe, A. *Macromolecules* **1985**, *18*, 2141.

(27) Watanabe, J.; Takashina, Y. *Macromolecules* **1991**, *24*, 3423.

(28) Lee, S.; Dutcher, J. R.; Stegeman, G. I.; Duda, G.; Wegner, G.; Knoll, W. *Phys. Rev. Lett.* **1993**, *70*, 2427.

(29) Muller, M.; Zentel, R. *Makromol. Chem.* **1992**, *194*, 101.

(30) Teerenstra, M. N.; Hagting, J. G.; Oostergetel, G. T.; Schouten, A. J.; Devillers, M. A. C.; Nolte, R. J. M. *Thin Solid Films* **1994**, *248*, 110.

(31) Dulong, L.; Gittinger, A.; Roth, S.; Wagner, T. *Makromol. Chem.* **1993**, *194*, 493.

(32) Ferencz, A.; Ries, R.; Wegner, G. *Angew. Chem. Int. Ed. Engl.* **1993**, *32*, 1184.

(33) Vahlenkamp, T.; Wegner, G. *Macromol. Chem. Phys.* **1994**, *195*, 1933.

(34) Buchel, M.; Sekkat, Z.; Paul, S.; Weichart, B.; Menzel, H.; Knoll, W. *Langmuir* **1995**, *11*, 4460.

(35) Duda, G.; Schouten, A. J.; Arndt, T.; Lieser, G.; Schmidt, G. F.; Bubeck, C.; Wegner, G. *Thin Solid Films* **1988**, *159*, 221.

(36) Duda, G.; Wegner, G. *Makromol. Chem., Rapid Commun.* **1988**, *9*, 495.

(37) Menzel, H.; Weichart, B.; Hallensleben, M. L. *Polym. Bull.* **1992**, *27*, 637.

(38) Yase, K.; Schwiegk, S.; Lieser, G.; Wegner, G. *Thin Solid Films* **1992**, *213*, 130.

(39) Menzel, H.; Hallensleben, M. L. *Polym. Bull.* **1991**, *27*, 89.

(40) Boury, F.; Gulik, A.; Dedieu, J. C.; Proust, J. E. *Langmuir* **1994**, *10*, 1654.

(41) Fisher, A.; Sackmann, E. *J. Colloid Interface Sci.* **1986**, *112*, 1.

(42) Neuman, R. D.; Fereshtehkhou, S. *J. Colloid Interface Sci.* **1988**, *125*, 34.

(43) Takeda, F.; Matsumoto, M.; Takenaka, T.; Fujiyoshi, Y. *J. Colloid Interface Sci.* **1981**, *84*, 220.

(44) Takenaka, T.; Harada, K.; Matsumoto, M. *J. Colloid Interface Sci.* **1980**, *73*, 569.

(45) Schwartz, D. K.; Schlossman, M. L.; Pershan, P. S. *J. Chem. Phys.* **1992**, *96*, 2356.

(46) Weissbuch, I.; Leveiller, F.; Jacquemain, D.; Kjaer, K.; Als-Nielsen, J.; Leiserowitz, L. *J. Phys. Chem.* **1993**, *97*, 12858.

(47) Weis, R. M. *Chem. Phys. Lipids* **1991**, *57*, 227.

(48) Allara, D. L.; Nuzzo, R. G. *Langmuir* **1985**, *1*, 45.

(49) Allara, D. L.; Nuzzo, R. G. *Langmuir* **1985**, *1*, 52.

(50) Li, M.; Rice, S. A. *J. Chem. Phys.* **1996**, *104*, 6860.

(51) Dluhy, R. A.; Wright, N. A.; Griffiths, P. R. *Appl. Spectros.* **1988**, *42*, 138.

(52) Dluhy, R. A.; Mitchell, M. L.; Pettenski, T.; Beers, J. *J. Appl. Spectrosc.* **1988**, *42*, 1289.

(53) Buontempo, J. T.; Rice, S. A. *J. Chem. Phys.* **1993**, *98*, 5835.

(54) Buontempo, J. T.; Rice, S. A. *J. Chem. Phys.* **1993**, *98*, 5825.

(55) Buontempo, J. T.; Rice, S. A.; Karaborni, S.; Siepmann, J. I. *Langmuir* **1993**, *9*, 1604.

(56) Gericke, A.; Simon-Kutscher, J.; Huehnerfuss, H. *Langmuir* **1993**, *9*, 2119.

(57) Gericke, A.; Michailov, A. V.; Huhnerfuss, H. *Vib. Spectros.* **1993**, *4*, 335.

(58) Ren, Y. Thesis, University of Massachusetts, 1995.

(59) Ren, Y.; Meuse, C. W.; Hsu, S. L. *J. Phys. Chem.* **1994**, *98*, 8424.

(60) Flournoy, P. A.; Schaffers, W. J. *Spectrochim. Acta* **1966**, *22*, 5.

(61) Born, M.; Wolf, E. *Principles of Optics*; Permagon Press: London, 1959.

(62) Hansen, W. N. *J. Opt. Soc. Am.* **1968**, *58*, 380.

(63) Yokomori, Y.; Uematsu, Y.; Uematsu, I. *Rep. Prog. Polym. Phys. Jpn.* **1972**, *15*, 633.

(64) Malcolm, B. R. *Nature (London)* **1962**, *195*, 901.

(65) Malcolm, B. R. *Polymer* **1966**, *7*, 595.

(66) Malcolm, B. R. *Proc. Roy. Soc. (London)* **1968**, *A305*, 363.

(67) Malcolm, B. R. *J. Colloid Interface Sci.* **1985**, *104*, 520.

(68) Lavigne, P.; Tancrede, P.; Lamarche, F.; Max, J. *Langmuir* **1992**, *8*, 1988.

(69) Lavigne, P.; Tancrede, P.; Lamarche, F.; Grandbois, M.; Salesse, C. *Thin Solid Films* **1994**, *242*, 229.

(70) Sohn, D.; Yu, H.; Nakamatsu, J.; Russo, P. S.; Daly, W. H. *J. Polym. Sci., Polym. Phys. Ed.* **1996**, *34*, 3025.

(71) Snyder, R. G.; Strauss, H. L.; Elliger, C. A. *J. Phys. Chem.* **1982**, *86*, 5145.

(72) Fraser, R. D. B. *J. Chem. Phys.* **1953**, *21*, 1511.

(73) Miyazawa, T.; Blout, E. R. *J. Am. Chem. Soc.* **1961**, *83*, 712.

(74) Tsuboi, M. *J. Polym. Sci.* **1962**, *59*, 139.

(75) Jones, R.; Tredgold, R. H. *J. Phys. D: Appl. Phys.* **1988**, *21*, 449.

(76) Tredgold, R. H.; Jones, R. *Langmuir* **1989**, *5*, 531.

(77) Stein, R. S. *J. Polym. Sci.* **1958**, *XXXI*, 327.

(78) Stein, R. S. *J. Polym. Sci.* **1958**, *XXXI*, 335.

(79) Stein, R. S. *J. Polym. Sci.* **1961**, *L*, 339.

(80) Patten, T. E.; Novak, B. M. *J. Am. Chem. Soc.* **1996**, *118*, 1906.

(81) Patten, T. E.; Novak, B. M. *Macromolecules* **1993**, *26*, 436.

CHAPTER 3

OBSERVATION OF A LONGITUDINAL ACOUSTIC MODE IN POLY(β-HYDROXYBUTYRATE)

3.1 Introduction

In the previous studies on "hairy-rod" polymers at an air-water interface, vibrational spectroscopy was used as a direct probe of the short range conformational order of long *n*-alkyl side groups. The subsequent characterization of the *liquid-like* quality of these side groups was than related to the ordering behavior of the rigid-rod main chains. In general, it was found that the *liquid-like* quality of the side groups, or in other words their short range conformational order, was important in controlling the overall ordering of monolayers of these "hairy-rod" polymers. In this chapter, however, it will be shown that vibrational spectroscopy is also a technique that can probe long range conformational order.

Since they were first discovered in 1949,[1] longitudinal acoustic modes (LAM) have been well established for a number of semicrystalline polymers. Polymers found to exhibit this mode include poly(tetrafluoroethylene),[2] isotactic polypropylene,[3,4] polyoxymethylene,[3] and poly(ethylene oxide)[5,6] as well as some linear aliphatic polyesters.[7-9] For polyethylene and *n*-alkanes, in particular, the frequency ν_m of this Raman mode has been found experimentally to be well described by the relation

$$\nu_m = (m/2cL)(E/\rho)^{1/2} \qquad (3.1)$$

where m is the integer order of the mode, c is the speed of light, L is the length of the vibrating chain or chain segment, E is the elastic modulus of a single chain, and ρ is the single chain density.[1,10,11] Only modes of odd m are Raman active. This vibration has

often been described as an accordion-like motion where for the simplest case of a planar zig-zag structure of m = 1, there is a node of zero atomic displacement in the center of the vibrating chain. This is shown schematically in Figure 3.1. As opposed to the CH_2 stretching mode discussed in the infrared spectra of "hairy-rod" films at an air-water interface in Chapter 2, longitudinal acoustic modes comprise the entire length of the vibrating ordered chain segment and as such are sensitive to the length of the vibrating chain segment. The CH_2 stretching mode is a much more localized vibration.

The chain length versus frequency dependence given by the above relation provides the potential for a unique morphological tool by which it may be possible to probe conformationally ordered chain segment lengths. For semicrystalline polymers exhibiting chain folded lamella, longitudinal acoustic modes are a means of measuring the crystalline fold segment length distribution and subsequently the crystalline core thickness. This is different than the information provided by small angle x-ray scattering. With x-ray, scattering is based on the long range periodicity between crystalline lamella. X-ray long spacings are therefore a measure of this periodicity and do not provide direct information on neither the crystalline fold segment length distribution nor the crystalline core thickness for semicrystalline polymers. Attempts to make such determinations with x-ray are model dependent. In addition, since x-ray is dependent on the periodicity between lamella, x-ray is unsuitable for determining ordered chain segment lengths for systems which do not exhibit such a periodicity. One such example is with ultraoriented polymers, polyethylene in particular, where oftentimes lamella unfold upon forming a structure composed of long ordered chain segments.[12] In contrast, with longitudinal acoustic modes, being sensitive explicitly to individual ordered chain segments, such measurements are possible. For these reasons, this Raman technique has been of interest for studying diverse areas in polymer morphology such as the melting of lamellae, interlamellar interactions, polymorphism, drawing behavior, conformational defects, chain branching and chain refolding/annealing behavior.

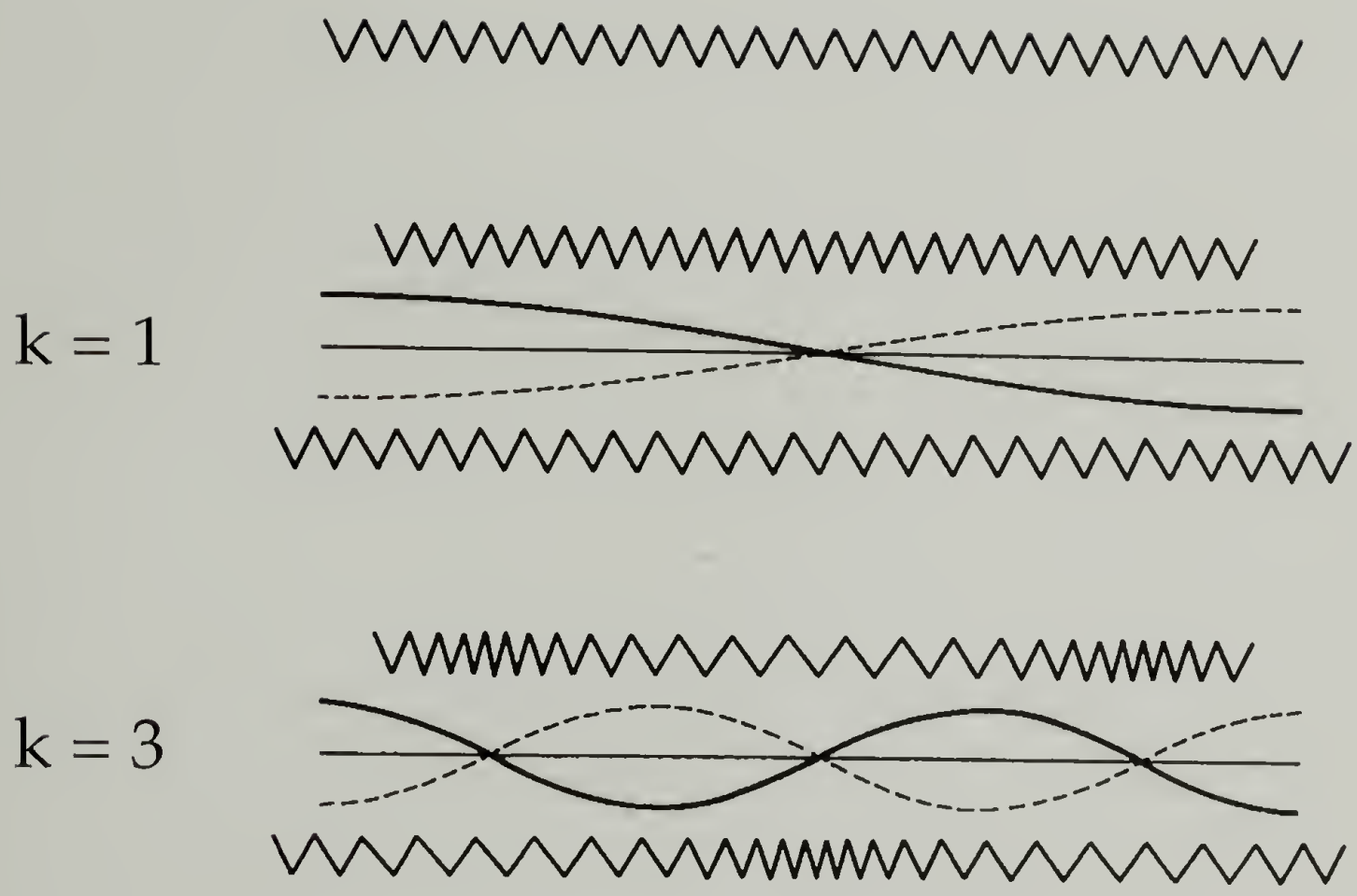

Figure 3.1 Schematic of atomic displacements for a longitudinal acoustic mode in a chain segment with an all-trans structure. At top is the structure of a non-vibrating segment. k =1 corresponds with a LAM-1 vibration with a node in the center of the segment of zero atomic displacement. k = 3 corresponds with a LAM-3 vibration where there are three such nodes.

We report here the observation of a LAM in a thermoplastic biodegradable polyester, poly(β-hydroxybutyrate) (PHB).[13] Its chemical structure is shown in Figure 3.2. First isolated in 1925, PHB is an optically active polymer produced by a bacterial fermentation process.[14] The polymer is produced as an energy reserve material by a variety of bacteria.[15] It is presently made commercially by Imperial Chemical Industries (ICI) under the trade name Biopol. As previously reported, PHB, due to its exceptional purity and chemical regularity, is a model material for fundamental studies of polymer crystallization and nucleation.[16] Morphological aspects can be complex, however. Studies have suggested the presence of a strain induced β-form of PHB in which the chains are in a highly extended state.[17,18] It has been reported that at the spread at the air-water interface, PHB changes with increasing surface pressure from an expanded monolayer form to a crystalline monolayer and subsequently to a crystalline bilayer in the helical form.[19] Others suggest that the chains crystallize in the β-form at the air-water interface.[20] The observation of a LAM in PHB provides an additional morphological tool by which these aspects of polymer structure may be further studied.

The identification of a LAM in PHB is also intriguing from a spectroscopic point of view. In order to develop LAMs as a more widely used method for characterizing polymer morphology, numerous attempts have been made to observe LAM-like vibrations in other non-polyethylene like polymers. In studies along these lines, simple linear aliphatic chains were modified by the placement of well-spaced ester groups along the polymer backbone. A LAM-like vibration was observed.[7-9] Attempts, however, with structures deviating significantly from that of polyethylene have not resulted in much success. Polymers such as well-defined model polypeptides are notable failures.[21-23] Successful observation of LAMs has mainly been confined to polymers possessing fairly simple chain conformations and chemical units. PHB differs, in its chemistry and in its equilibrium conformation, significantly from other polymers in which a LAM has previously been observed. Thus, in addition to its use as a morphological tool, a LAM in

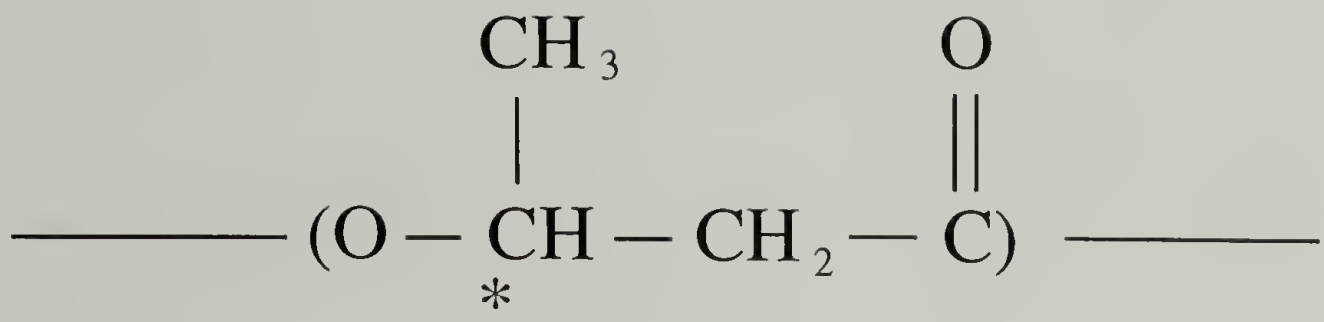

Figure 3.2 Chemical structure of poly(β-hydroxybutyrate).

PHB provides an opportunity to study the origin of a LAM in a structurally more complicated polymer than those in which a LAM has been reported in earlier studies. As such, it should assist in the isolation of the factors that dominate the appearance or nonappearance of a LAM in specific polymer chains, leading to a better understanding of LAMs in non-polyethylene-like structures.

3.2 Experimental

Poly(β-hydroxybutyrate) of M_n = 133 000 and propylene carbonate were obtained from Aldrich Co. Single crystals of poly(β-hydroxybutyrate) or PHB were grown over a range of crystallization temperatures from dilute (0.04% (w/v)) propylene carbonate solution by using a self-seeding technique.[24] Samples were first dissolved at 155 °C and quenched to 45 °C where they were kept for 24 hours. Crystal seeds were then obtained by heating the solution slowly (~20 °C/hour) until the solution cleared. With the seeded solution, highly crystalline samples were grown at specific crystallization temperatures for ~48 hours. The solutions were then filtered, forming oriented single crystal mats. The mats were subsequently rinsed with hot propylene carbonate to remove any residual non-crystallized material. This was followed by a final rinsing with methanol to ensure the removal of all propylene carbonate.

Raman spectra were obtained with a Jobin-Yvon U-1000 laser-Raman spectrometer excited using the 5145 Å line of a Spectra Physics 165-08 Ar ion laser. Bandpass was maintained at 2 cm^{-1} at 5000 Å. Laser power at the sample was maintained at 75 mW. Due to residual fluorescence in some samples, a higher laser power may have altered the as-prepared samples and was not used for this reason. The scattered intensity at each frequency was collected for 13-17 seconds to accumulate sufficient counts to provide an acceptable signal to noise ratio. The scattered intensity collected at the peak for a given LAM spectra was roughly 1000 counts per second. Rayleigh scattering near the excitation frequency was removed using a fitting routine in the data analysis package LAB

CALC provided by Galactic Industries Corp. The spectra were also corrected for temperature and frequency effects.[25,26]

Small-angle x-ray diffraction of the long spacings of the single crystal mats were obtained with a Rigaku Denki instrument with a camera distance of 230 mm and pin hole collimation. The crystal mats were oriented in the plane of the x-ray beam. The long spacings were measured without further correction.

3.3 Results and Discussion: LAM in Poly(β-hydroxybutyrate)

Indicating sample uniformity, second order reflections in the x-ray patterns corresponding to lamella long spacings were detected for all single crystal mats. A typical small-angle x-ray scattering pattern is shown in Figure 3.3. X-ray studies of PHB indicate that PHB packs in an orthorhombic unit cell in a left-handed 2_1 helix with a fiber repeat of 5.96 Å.[18] Previous small- and wide-angle x-ray studies on PHB single crystals indicate the presence of little or no chain tilt; the chains are essentially perpendicular to the lamellar surface thus making any correction for chain inclination unnecessary.[16] The long spacings measured are listed in Table 3.1.

The low frequency Raman spectra of the PHB single crystals crystallized at temperatures ranging from 25 to 87° C are shown in Figure 3.4. The as-obtained spectra show a low-frequency band present at 15 cm^{-1} for all samples. The band moves to lower frequencies as the crystallization temperature is increased. This corresponds with longer lamella fold lengths, as indicated by the small-angle x-ray measurements. When the Raman data are corrected by subtraction of the Rayleigh background and then for the effect of temperature, the band near 15 cm^{-1} has a half-width that is about 5 cm^{-1} or less. The frequency and for the most part the half-width of the band both decrease with increasing crystallization temperature, as summarized in Table 3.1. A second band is apparent near 9 cm^{-1} in some samples. Given the relative intensity of the two low-frequency Raman bands and the fact that only one lamella fold length distribution is

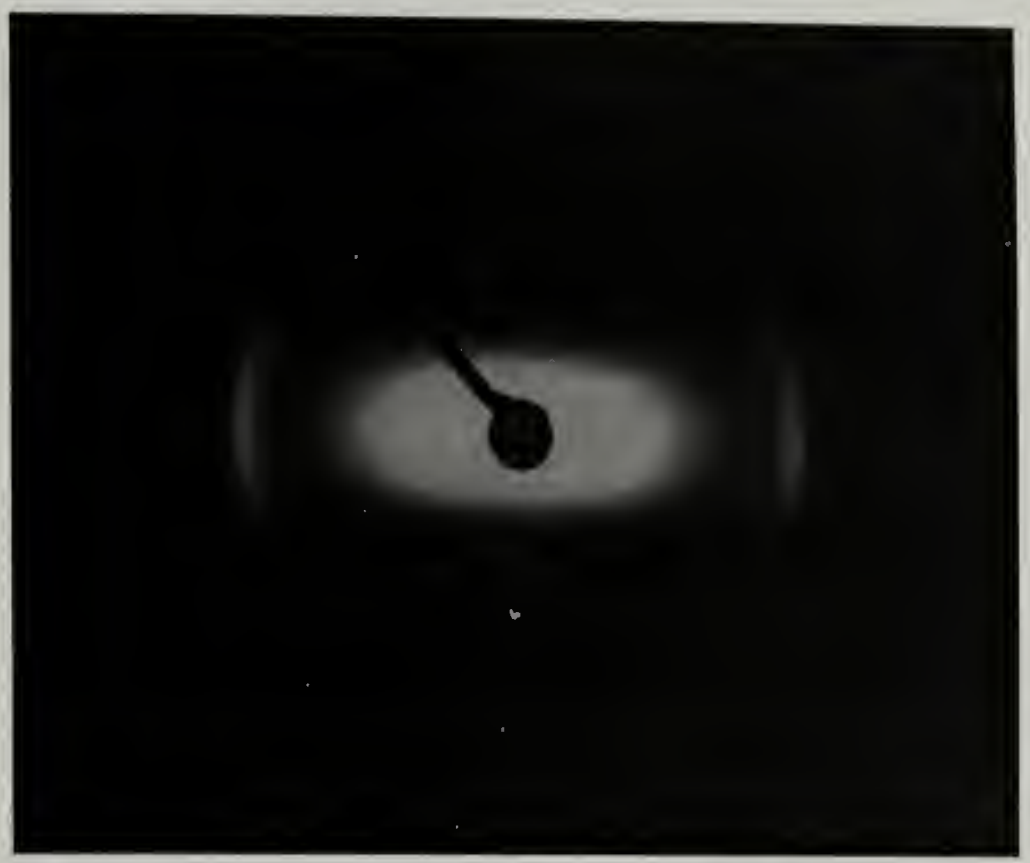

Figure 3.3 Small-angle x-ray scattering pattern of poly(β-hydroxybutyrate) single crystal mat. The x-ray beam is incident in the plane of the mat.

Table 3.1 Table listing peak position of LAM vibration for PHB single crystal mats from the as-obtained spectra without corrections, the spectra corrected for the Rayleigh background, and the spectra corrected for both the Rayleigh background and temperature/frequency effects. $\Delta\nu_{1/2}$ is the half width of the band from the latter spectra. The long spacing was obtained from small-angle x-ray measurements.

Crystallization Temperature	Uncorrected Peak Position	Background Subtracted ν	Temperature/ν Corrected ν	$\Delta\nu_{1/2}$	Long Spacing
25 °C	17.0 cm^{-1}	18.8 cm^{-1}	19.5 cm^{-1}	5.26 cm^{-1}	41.9 Å
45	16.8	17.8	18.4	5.5	43.4
60	14.6	16.2	16.6	4.5	49.4
70	14.1	14.6	14.9	3.5	53.1
75	12.9	13.8	14.12	3.7	59.2
87	------	11.3	11.89	3.6	62.3

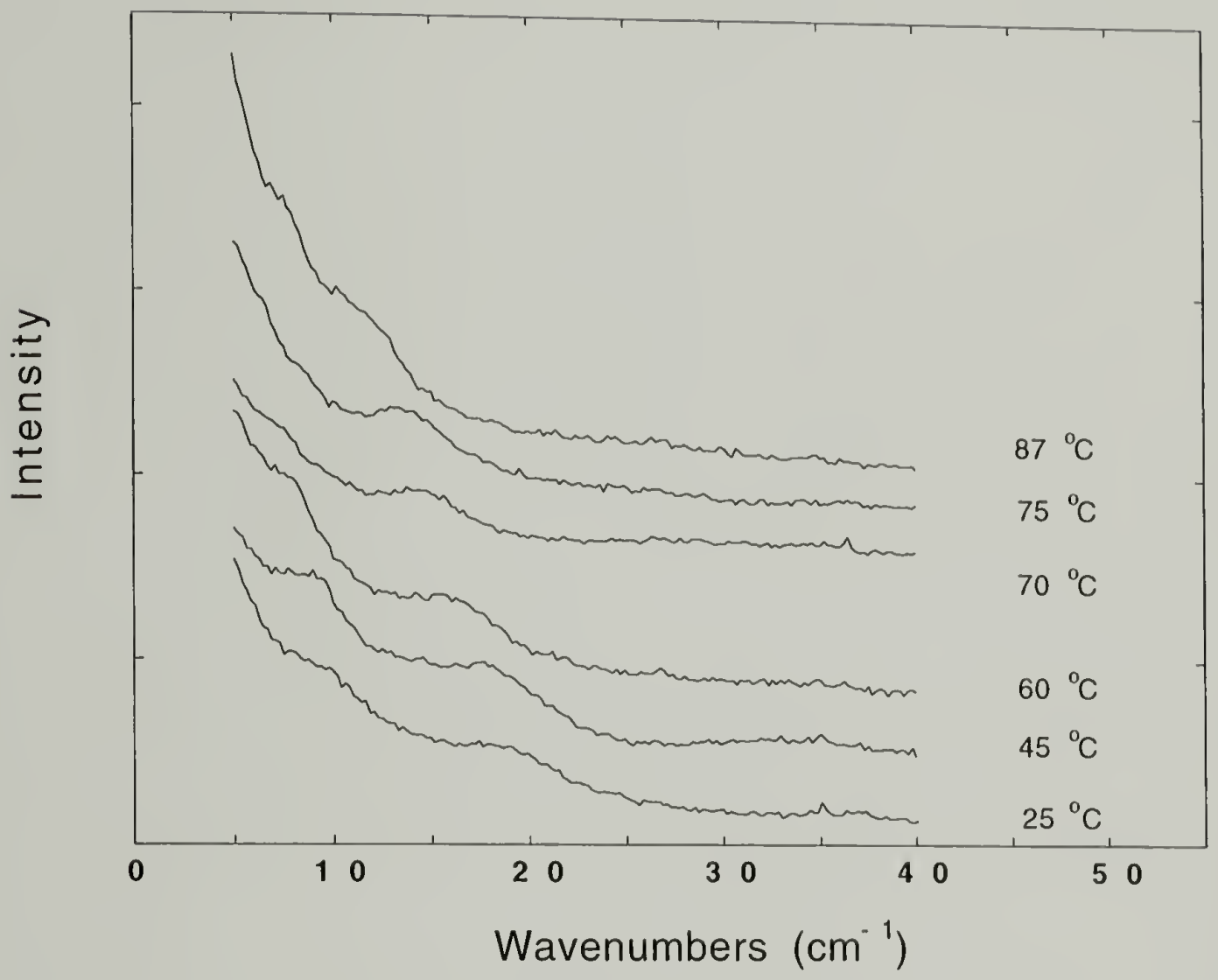

Figure 3.4 As obtained low frequency Raman spectra of PHB single crystal mats crystallized at temperatures ranging from 25°C to 87°C.

indicated by the small-angle x-ray measurements, it is unlikely that the second band is caused be a second distinct lamella fold length distribution. However, due to substantial overlap with the Rayleigh line, it was not possible to isolate this low-frequency band during subtraction of the background.

The strongest evidence that the band near 15 cm^{-1} is due to a LAM associated with the crystalline lamellae it the linear dependence of the band frequency on the reciprocal lamellar thickness, as given by equation 3.1. A plot of the peak frequency of the band near 15 cm^{-1} from the temperature and frequency corrected spectrum against the inverse long spacing measured by SAXS is shown in Figure 3.5. In this plot, the data are fitted by least squares to a straight line which essentially intercepts the origin. Failure of such a line to pass through the origin has been interpreted in other LAM studies as indicating the following: (1) presence of an amorphous or loosely folded layer of material at the lamellar surface thus affecting the measured x-ray long spacing,[8,11] or (2) anharmonic effects resulting from the significant chain-end amplitude associated with the LAM-1 vibration.[27] LAMs originates from the ordered chain segments in the crystalline core and may be perturbed by the presence of an amorphous layer. That the line does essentially pass through zero for PHB may indicate that the long spacings measured by x-ray correspond closely with the thickness of the crystalline lamella core. This is consistent with earlier observations by Barham et al. in which they suggested that given the thickness and observed values of crystallinity for PHB single crystals, the fold structure cannot consist of much looseness.[16] The range of lamellar thicknesses indicated in Table 3.1 allow only 6-11 repeat units/fold stem in PHB single crystals.

Additionally, the intensity of the vibration centered around 15 cm^{-1} is high as is characteristic of LAM bands. The peak height of the low-frequency vibration found in the PHB samples is roughly twice that for the CH_2 bending motion in the 1400 cm^{-1} region. The ν vs 1/L dependence and the relative intensity of the low-frequency mode found in these samples together provide strong evidence that the observed mode is a LAM. In

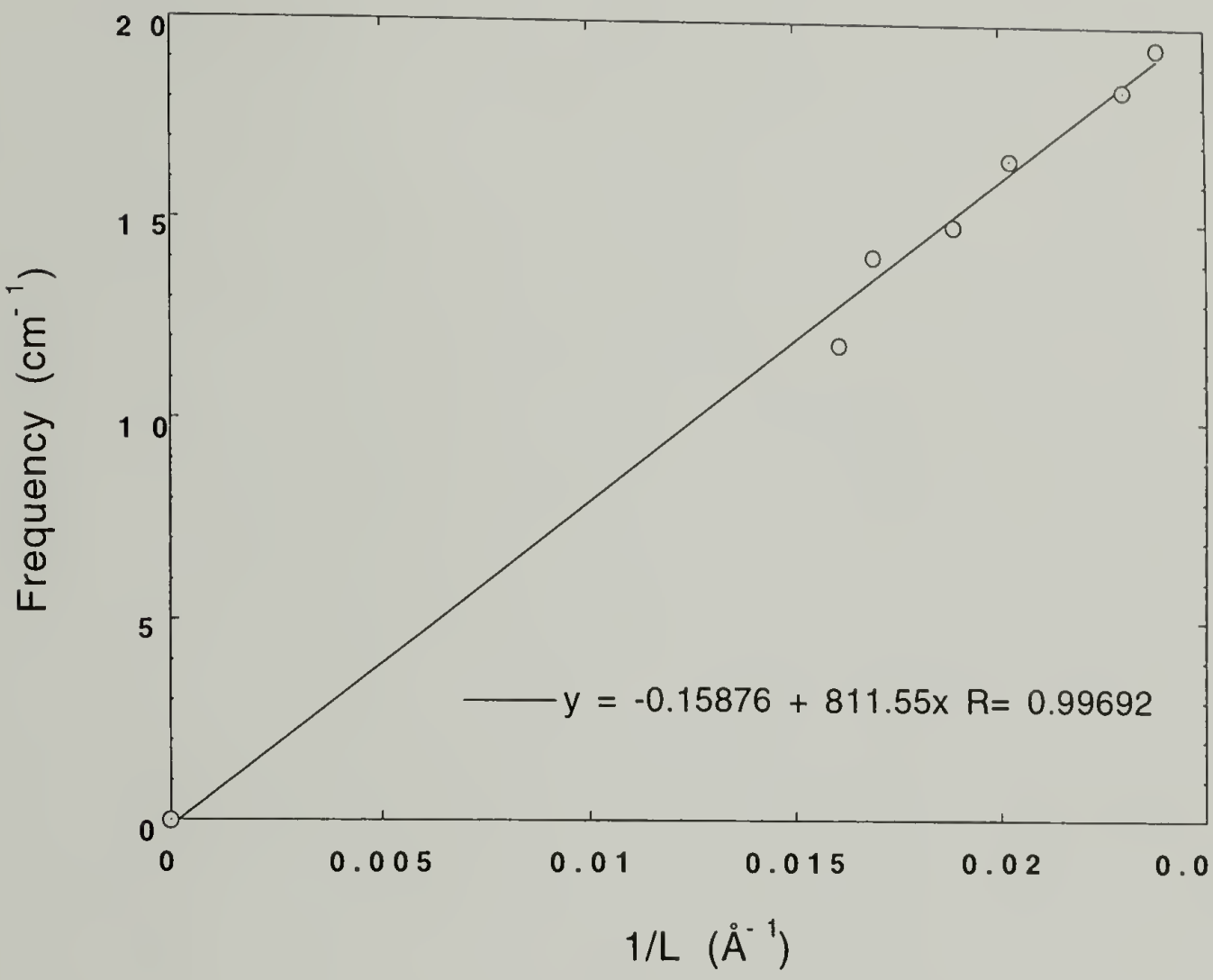

Figure 3.5 Plot of temperature/frequency corrected Raman frequency centered around 15 cm^{-1} versus L^{-1} where L is the measured small-angle x-ray long spacing.

earlier studies dealing with polyethylene-like chains, the strong intensity has been attributed to the large change in the polarizability associated with the long-chain motion of this mode and the Boltzman factor associated with low frequency vibrations.[10,28,29] The change in the polarizability of this mode for PHB has yet to be determined and may in fact be quite small. Therefore, the strong intensity observed may simply be due to frequency/temperature effects.[28]

Using the relation given in equation 3.1, the single chain elastic modulus within a crystalline lamella for PHB was calculated from the slope of the line fitted to the plot of ν vs 1/L in Figure 3.5. Given the crystal density of PHB to be 1.25 g/cm^3,[18] the single chain elastic modulus was calculated to be 29.6 GPa, a value consistent with that expected for a helix. For example, for isotactic polypropylene the measured value and value calculated by using torsional force constants from a valence force field are 41 and 33 GPa, respectively.[4,30]

LAM in the simplest case for all-trans *n*-alkanes is a symmetric accordion-like longitudinal vibration.[1,10,31] Success in finding LAM in polymers with non-polyethylene-like structures has been very scarce. This can be understood from the fact that force as well as mass perturbations along the chain may lead to coupling of transverse and longitudinal motions. This effect has been shown for a series of linear aliphatic polyesters, mentioned previously, in which well-spaced ester groups act as unbalanced mass units which lead to the presence of several LAM-like modes, each with differing amounts of transverse and longitudinal character.[9] This may provide an explanation for the presence of the second unassigned low-frequency band centered around 9 cm^{-1} found for PHB. With increased structural complexity, these effects may become more significant, leading eventually to the total disruption of any longitudinal acoustic mode. The effect of "perturbing" influences within chains, such as methyl side-group placement

on *n*-alkanes,[32] double bond placement in *trans*-alkenes[33] and hydrogen bonds,[34] has been studied and shown to affect this mode to varying degrees in both intensity and frequency.

Interestingly, however, PHB, even with a large number of such perturbing groups comprising a mix of both closely spaced methyl units and ester groups as well as possibly an intermolecular effect between ester groups, clearly exhibits a LAM. Furthermore, in contrast to the series of linear aliphatic polyesters mentioned previously, PHB, which forms a 2_1 helix in the crystalline state, is conformationally more complex.[18] The ester groups for the linear aliphatic polyesters were sufficiently well-spaced such that in the crystalline state the chains essentially formed a planar zigzag.[9] Previous normal coordinate analysis of crystalline poly(ethylene oxide) has shown that, as opposed to all-trans polyethylene chains, LAMs in helical chains have a significant interchain effect due to the large radial component present in the atomic displacement of LAM for such polymers.[6] Compared with polymers such as isotactic polypropylene, poly(oxymethylene), poly(ethylene oxide), and poly(tetrafluoroethylene) in which LAMs have been observed, PHB is clearly the most unlike polyethylene. Nevertheless, the LAM observed in PHB follows a $\nu \propto 1/L$ dependence quite closely, as evidenced by the straight line fit to the Raman and x-ray data in Figure 3.5.

3.4 Annealing of Poly(β-hydroxybutyrate) Single Crystals

Previous x-ray studies on the annealing behavior of PHB single crystals have indicated that chain refolding is characterized as a function of increasing annealing temperature by a step doubling of the initial fold spacing followed by a hyperbolic increase in the fold period.[35] This is shown in Figure 3.6. In an attempt to study this further, the Raman-active longitudinal acoustic mode established for PHB in the previous

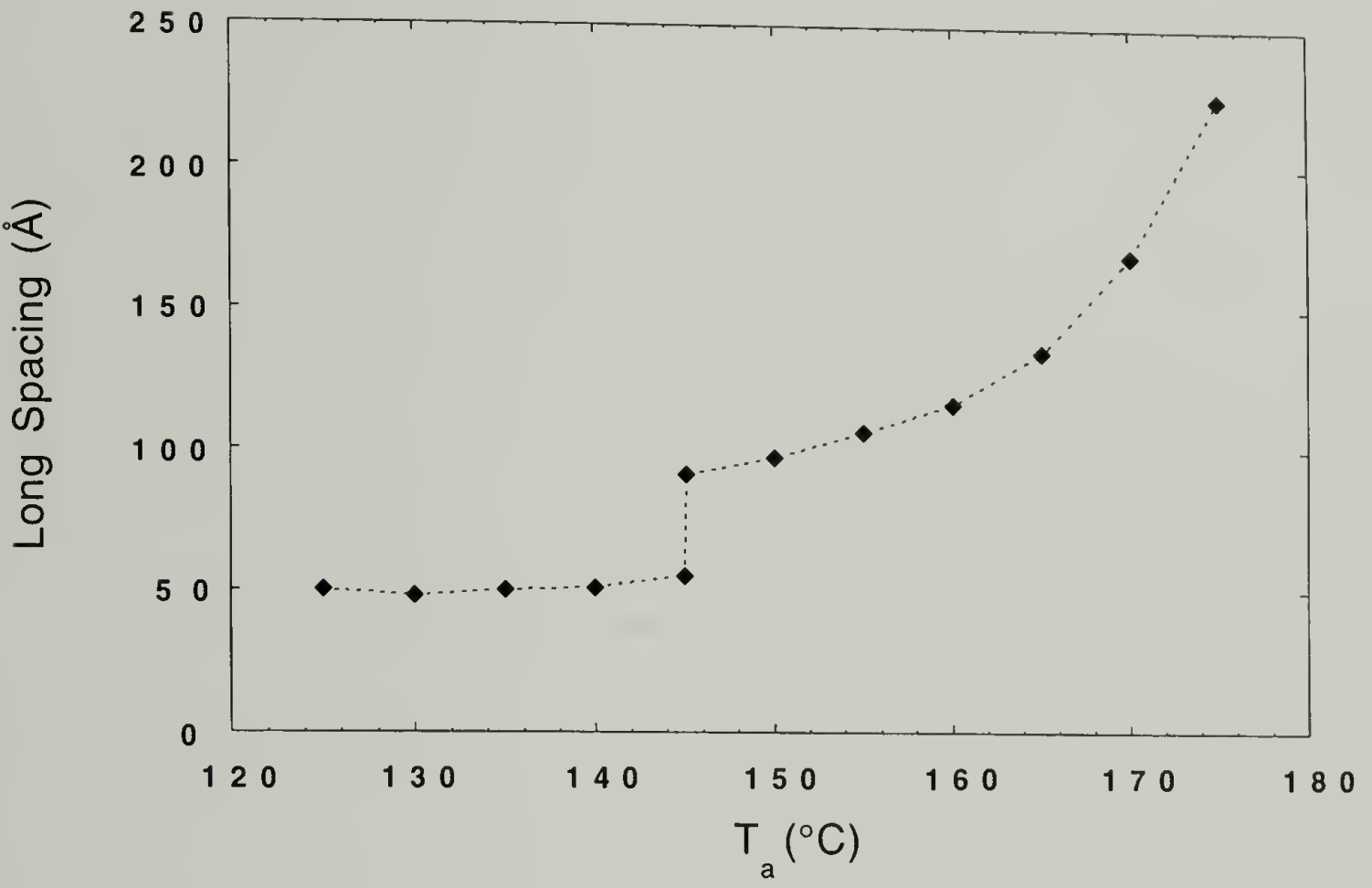

Figure 3.6 Plot of x-ray long spacings of poly(β-hydroxybutyrate) single crystal mats against annealing temperature, T_a.[35]

section was used to follow the annealing behavior of PHB single crystal mats. The single crystal mats studied were solution crystallized at a crystallization temperature of 60° C and had unannealed long spacings of 49.4 Å.

The spectra for four of these annealed mats is shown in Figure 3.7. In the first three spectra, the LAM mode is centered at roughly 17 cm^{-1}. A second unassigned band at ~8 cm^{-1}, discussed previously, is also present. The four spectra correspond with the following: (1) unannealed, (2) annealed at 122° C for 21 hours, (3) annealed at 140° C for 5 hours, and (4) annealed at 155° C for 6 hours. The melting temperature of PHB is ~180° C. From the first two spectra, it can be seen that at an annealing temperature of 122° C, the folding of the single crystal mat remains unchanged. Upon increasing the annealing temperature to 140° C the LAM band also remains largely the same. There may be a slight indication of a broadening of the band to lower frequency, but given the Rayleigh background this is difficult to analyze. Finally, at an annealing temperature of 155° C, the LAM band does shift to lower frequency. In this spectra, the band is probably the small hump imposed on the Rayleigh background at roughly 8 cm^{-1}. Again, a quantitative analysis of the band is difficult due to the Rayleigh background. The corresponding small-angle x-ray pattern, however, does indicate that the lamella fold period doubles and is shown in Figure 3.8. It should be noted that as opposed to the x-ray scattering pattern of the as-crystallized mat, the pattern does not exhibit a second order reflection. The reflection corresponding to the long spacing is also less sharp. This implies that there is a decrease in the overall uniformity of the lamella following doubling.

A number of other polymers have also been found to exhibit discrete quantized increases in the fold period on annealing.[36-38] In most cases, these polymers have strong intermolecular interactions between the individual fold stems. One such example is with some polyamides where it has been found that the fold length increases by factors of two.[36,38] This has been attributed to the interaction of amide groups from adjacent individual fold stems. In contrast, for polyethylene the lamella thickness increases

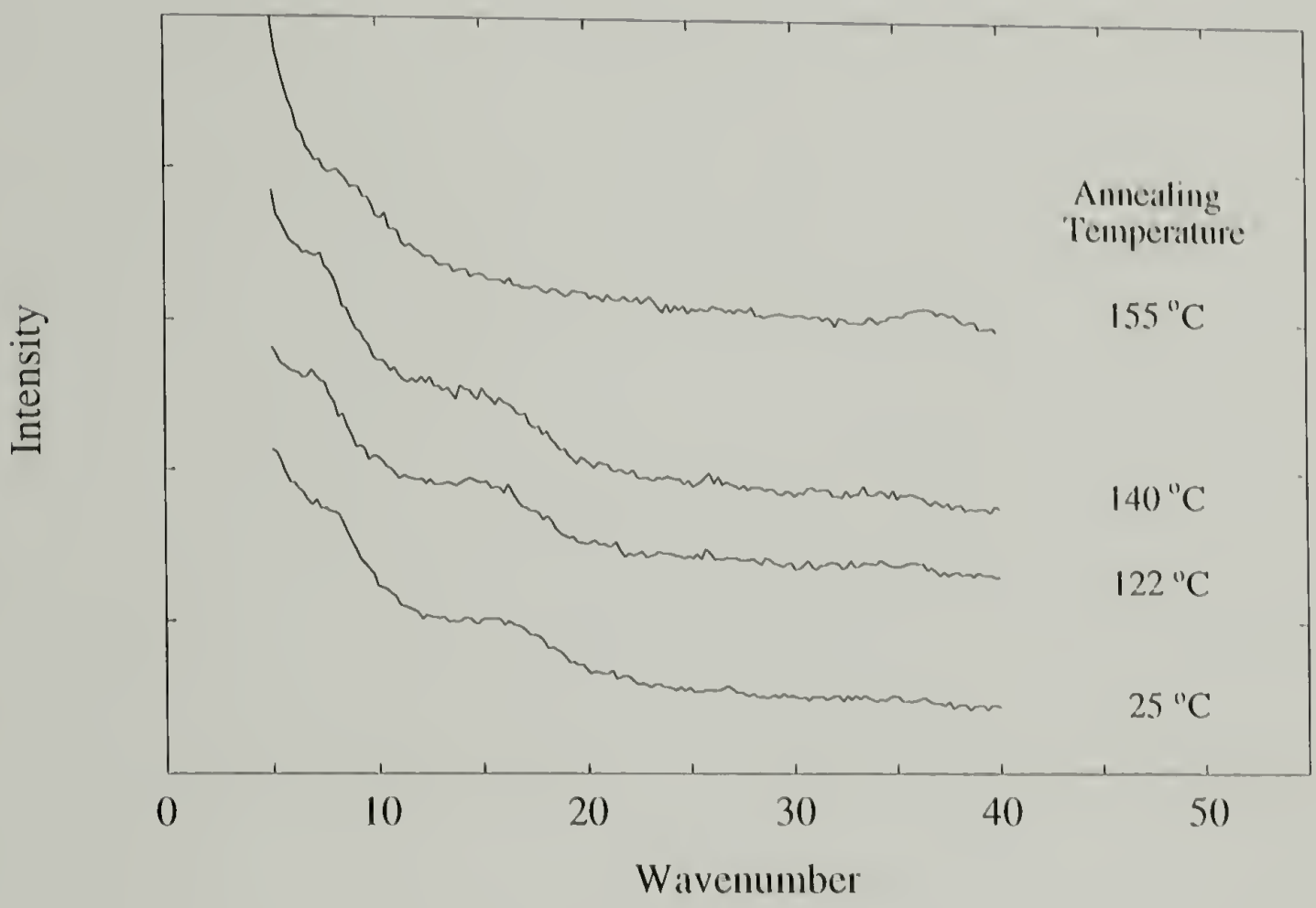

Figure 3.7 Raman spectra of PHB single crystal mat (crystallization temperature = 60° C) annealed at various temperatures. Annealing times were in the range of several hours.

Figure 3.8 Small-angle x-ray scattering pattern of poly(β-hydroxybutyrate) single crystal mat after annealing at 155° C. The x-ray beam is incident in the plane of the mat.

continuously on annealing.[39] The annealing behavior of PHB, with both a discontinuous doubling and a region of continuous thickening, can be regarded as having a combination of both behaviors.

A simple model for chain refolding suggested by Keller can perhaps be used to explain PHB's observed annealing behavior.[37,38] A schematic representation of the model is shown in Figure 3.9. Part a, shows the initial unannealed state of a single lamella. In this idealized two-dimensional model, it is assumed that chain refolding occurs by the consumption of individual folds (fold 2) by neighbor folds (folds 1 and 3). This is shown in part b where for the sake of simplicity fold 2 is consumed equally by both fold 1 and 3 and can be visualized by making 2 recede. At this point the gap formed between 1 and 3 gives rise to a "fold" dislocation (part c) and in effect corresponds to an edge dislocation in a two-dimensional lattice. On continued refolding, the "fold" dislocation climbs until it leaves the space between 1 and 3 (part d). Part e then represents the stage where both the dislocation energy is regained and a single fold has doubled in length.

Using this model, it is the energy associated with the formation of such a "fold" dislocation which determines whether or not a given sample will refold in a continuous manner or in discrete steps. As an example, for a system in which the energy for the formation of a dislocation is large relative to the climb, intermediate stages between the initial formation of a dislocation and the doubled state would quickly pass through. In this case, a fold doubling would be observed. For a case where the energy associated with the formation of a dislocation is comparable to that required for the climb, intermediate stages would be observed during chain annealing. The initial doubling of the fold length for PHB may be explained in this manner. The intermolecular interaction between ester groups from adjacent fold stems may make intermediate fold stages rare relative to the doubled fold length state.

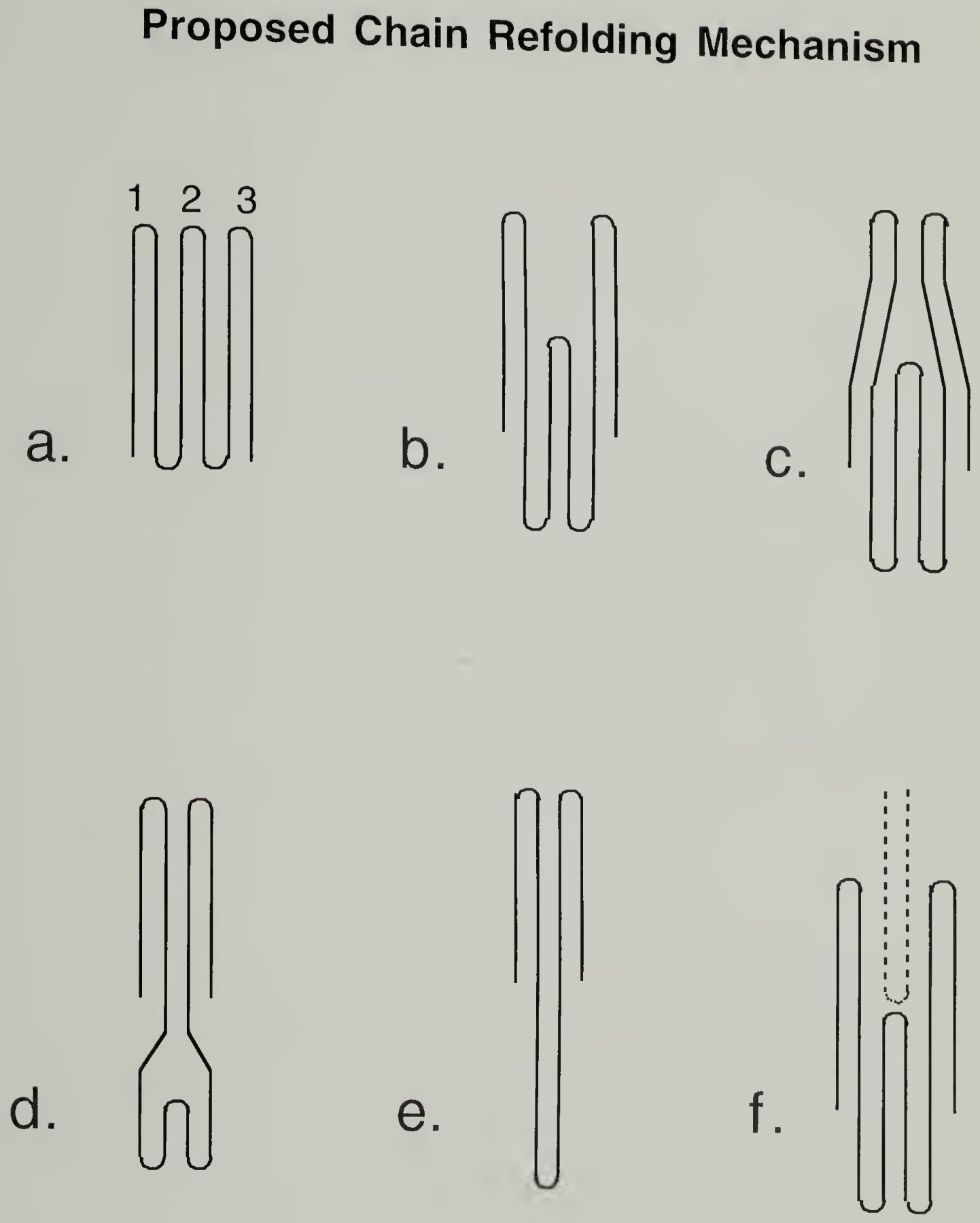

Figure 3.9 Schematic representation of various stages of the fold length increasing to a doubled fold length.

The continuous increase of the fold length observed for PHB after the initial doubling may also be explained by this model. Following the doubling of the fold length, it is possible that folds from adjacent lamella may interpenetrate (part f). Interpenetration of the lamella would then allow the folds to increase continuously without the formation of "fold" dislocations.

3.5 Conclusions

In summary, a longitudinal acoustic mode is observed for the first time in the biodegradable polymer, poly(β-hydroxybutyrate). A clear inverse relationship between the long period measured by small-angle x-ray scattering and the band frequency was found. This observation is especially interesting for poly(β-hydroxybutyrate) since its chemical structure is significantly different from all other polymers known to have longitudinal acoustic modes. Using this band, the annealing behavior of poly(β-hydroxybutyrate) single crystals was also examined.

References

(1) Mizushima, S. I.; Shimanouchi, T. *J. Am. Chem. Soc.* **1949**, *71*, 1320.

(2) Rabolt, J. F.; Fanconi, B. *Polymer* **1977**, *14*, 491.

(3) Rabolt, J. F.; Fanconi, B. *J. Polym. Sci. Polym. Lett. Ed.* **1977**, *15*, 121.

(4) Hsu, S. L.; Krimm, S.; Krause, S.; Yeh, G. S. Y. *J. Polym. Sci. Polym. Lett. Ed.* **1976**, *14*, 195.

(5) Hartley, A.; Leung, Y. K.; Booth, C.; Shepherd, I. W. *Polymer* **1976**, *17*, 354.

(6) Song, K.; Krimm, S. *J. Polym. Sci. Polym. Phys. Ed.* **1990**, *28*, 63.

(7) Folkes, M. J.; Keller, A.; Stejny, J. *Colloid Polym. Sci.* **1975**, *253*, 354.

(8) Wang, Y. K.; Shu, P. H. C.; Stein, R. S.; Hsu, S. L. *J. Polym. Sci. Polym. Phys. Ed.* **1980**, *18*, 2287.

(9) Chang, C.; Wang, Y. K.; Waldman, D. A.; Hsu, S. L. *J. Polym. Sci. Polym. Phys. Ed.* **1984**, *22*, 2185.

(10) Schaufele, R. F. *J. Chem. Phys.* **1967**, *47*, 3605.

(11) Peticolas, W. L.; Hibler, G. W.; Lippert, J. L.; Peterlin, A.; Olf, H. *Appl. Phys. Lett.* **1971**, *18*, 87.

(12) Porter, R. S.; Wang, L. *J. Macromol. Sci.-Rev.* **1995**, *C35(1)*, 63.

(13) Chien, B. T.; Hsu, S. L.; Stidham, H. D. *Macromolecules* **1996**, *29*, 4247.

(14) Lemoigne, M. *Ann. Inst. Past.* **1925**, *39*, 144.

(15) Merrick, J. *Photosynth. Bact.* **1978**, *199*, 219.

(16) Barham, P. J.; Keller, A.; Otun, E. L.; Holmes, P. A. *J. Mater. Sci.* **1984**, *19*, 2781.

(17) Orts, W. J.; Marchessault, R. H.; Bluhm, T. L.; Hamer, G. K. *Macromolecules* **1990**, *23*, 5368.

(18) Yokouchi, M.; Chatani, Y.; Tadokoro, H.; Teranishi, K.; Tani, H. *Polymer* **1973**, *14*, 267.

(19) Lambeek, G.; Vorenkamp, E. J.; Schouten, A. J. *Macromolecules* **1995**, *28*, 2023.

(20) Nobes, G. A. R.; Holden, D. A.; Marchessault, R. H. *Polymer* **1994**, *35*, 435.

(21) Fanconi, B. *Biopolymers* **1973**, *12*, 2759.

(22) Renugopalakrishnan, V.; Collette, T. W.; Carreira, L. A.; Bhatnagar, R. S. *Macromolecules* **1985**, *18*, 1786.

(23) Painter, P. C.; Mosher, L. E.; Rhoads, C. *Biopolymers* **1982**, *21*, 1469.

(24) Blundell, D. J.; Keller, A.; Kovacs, A. J. *J. Polym. Sci., Part B* **1966**, *4*, 481.

(25) Snyder, R. G.; Krause, S. J.; Scherer, J. R. *J. Polym. Sci. Polym. Phys. Ed.* **1978**, *16*, 1593.

(26) Woodward, L. A.; Long, D. A. *Trans. Faraday Soc.* **1949**, *45*, 1131.

(27) Snyder, R. G.; Strauss, H. L.; Alamo, R.; Mandelkern, L. *J. Chem. Phys.* **1994**, *100*, 5422.

(28) Wilson, E. B.; Decius, J. C.; Cross, P. C. *Molecular Vibrations*; McGraw-Hill: New York, 1955.

(29) Strobl, G. R.; Eckel, R. *Colloid Polym. Sci.* **1980**, *258*, 570.

(30) Sakurada, I.; Ito, T.; Nakamae, K. In *U.S.-Japan Seminar in Polymer Physics (J. Polym. Sci. C, 15)*; R. S. Stein and S. Onogi, Ed.; Interscience: New York, 1966; pp 75.

(31) Shimanouchi, T.; Tasumi, M. *Indian J. Pure Appl. Phys.* **1971**, *9*, 953.

(32) Fanconi, B.; Crissman, J. *J. Polym. Phys. Ed.* **1975**, *13*, 421.

(33) Rabolt, J. F.; Twieg, R. *J. Chem. Phys.* **1982**, *76*, 1646.

(34) Rabolt, J. *J. Polym. Sci. Polym. Phys. Ed.* **1979**, *17*, 1457.

(35) Mitomo, H.; Barham, P. J.; Keller, A. *Sen-i Gakkaishi* **1986**, *42*, T-589.

(36) Burmester, A. F.; Dreyfuss, P.; Geil, P.; Keller, A. *J. Polym. Sci. Polym. Phys. Ed.* **1972**, *10*, 769.

(37) Dreyfuss, P.; Keller, A. *J. Polym. Sci. Part C* **1970**, *8*, 253.

(38) Dreyfuss, P.; Keller, A. *J. Macromol. Sci.* **1970**, *B4*, 811.

(39) Keller, A.; Priest, D. J. *J. Polym. Sci. Part C* **1970**, *8*, 13.

BIBLIOGRAPHY

1. Aharoni, S. M. *Macromolecules* **1981**, *14*, 222.

2. Aharoni, S. *Macromolecules* **1979**, *12*, 94.

3. Allara, D. L.; Nuzzo, R. G. *Langmuir* **1985**, *1*, 45.

4. Allara, D. L.; Nuzzo, R. G. *Langmuir* **1985**, *1*, 52.

5. Barham, P. J.; Keller, A.; Otun, E. L.; Holmes, P. A. *J. Mater. Sci.* **1984**, *19*, 2781.

6. Blundell, D. J.; Keller, A.; Kovacs, A. J. *J. Polym. Sci., Part B* **1966**, *4*, 481.

7. Born, M.; Wolf, E. *Principles of Optics*; Permagon Press: London, 1959.

8. Boury, F.; Gulik, A.; Dedieu, J. C.; Proust, J. E. *Langmuir* **1994**, *10*, 1654.

9. Bower, D. I.; Maddams, W. F. *The Vibrational Spectroscopy of Polymers*; 10. Cambridge Univeristy Press: Great Britain, 1989.

10. Buchel, M.; Sekkat, Z.; Paul, S.; Weichart, B.; Menzel, H.; Knoll, W. *Langmuir* **1995**, *11*, 4460.

11. Buontempo, J. T.; Rice, S. A. *J. Chem. Phys.* **1993**, *98*, 5825.

12. Buontempo, J. T.; Rice, S. A. *J. Chem. Phys.* **1993**, *98*, 5835.

13. Buontempo, J. T.; Rice, S. A.; Karaborni, S.; Siepmann, J. I. *Langmuir* **1993**, *9*, 1604.

14. Burmester, A. F.; Dreyfuss, P.; Geil, P.; Keller, A. *J. Polym. Sci. Polym. Phys. Ed.* **1972**, *10*, 769.

15. Chang, C.; Wang, Y. K.; Waldman, D. A.; Hsu, S. L. *J. Polym. Sci. Polym. Phys. Ed.* **1984**, *22*, 2185.

16. Chien, B. T.; Hsu, S. L.; Stidham, H. D. *Macromolecules* **1996**, *29*, 4247.

17. Daly, W. H.; Poche, D.; Negulescu, I. I. *Prog. Polym. Sci.* **1994**, *19*, 79.

18. Dluhy, R. A.; Mitchell, M. L.; Pettenski, T.; Beers, J. *J. Appl. Spectrosc.* **1988**, *42*, 1289.

19. Dluhy, R. A.; Wright, N. A.; Griffiths, P. R. *Appl. Spectros.* **1988**, *42*, 138.

20. Dreyfuss, P.; Keller, A. *J. Polym. Sci. Part C* **1970**, *8*, 253.

21. Duda, G.; Schouten, A. J.; Arndt, T.; Lieser, G.; Schmidt, G. F.; Bubeck, C.; Wegner, G. *Thin Solid Films* **1988**, *159*, 221.

22. Duda, G.; Wegner, G. *Makromol. Chem., Rapid Commun.* **1988**, *9*, 495.

23. Dulong, L.; Gittinger, A.; Roth, S.; Wagner, T. *Makromol. Chem.* **1993**, *194*, 493.

24. Fanconi, B. *Biopolymers* **1973**, *12*, 2759.

25. Fanconi, B.; Crissman, J. *J. Polym. Phys. Ed.* **1975**, *13*, 421.

26. Ferencz, A.; Ries, R.; Wegner, G. *Angew. Chem. Int. Ed. Engl.* **1993**, *32*, 1184.

27. Fisher, A.; Sackmann, E. *J. Colloid Interface Sci.* **1986**, *112*, 1.

28. Flournoy, P. A.; Schaffers, W. J. *Spectrochim. Acta* **1966**, *22*, 5.

29. Folkes, M. J.; Keller, A.; Stejny, J. *Colloid Polym. Sci.* **1975**, *253*, 354.

30. Fraser, R. D. B. *J. Chem. Phys.* **1953**, *21*, 1511.

31. Frech, R.; Manning, J.; Teeters, D.; Black, B. E. *Polymer* **1988**, *60*, 1785.

32. Gericke, A.; Michailov, A. V.; Huhnerfuss, H. *Vib. Spectros.* **1993**, *4*, 335.

33. Gericke, A.; Simon-Kutscher, J.; Huehnerfuss, H. *Langmuir* **1993**, *9*, 2119.

34. Gregoriadis, G.; Allison, A. C. *Liposomes in Biological Systems*; Wiley: New York, 1980.

35. Hansen, W. N. *J. Opt. Soc. Am.* **1968**, *58*, 380.

36. Hartley, A.; Leung, Y. K.; Booth, C.; Shepherd, I. W. *Polymer* **1976**, *17*, 354.

37. Henderson, J. A.; Richards, R. W.; Penfold, J.; Thomas, R. K.; Lu, J. R. *Macromolecules* **1993**, *26*, 4591.

38. Hickel, W.; Duda, G.; Jurich, M.; Krohl, T.; Rochford, K.; Stegeman, G. I.; Swalen, J. D.; Wegner, G.; Knoll, W. *Langmuir* **1990**, *6*, 1403.

39. Hsu, S. L.; Krimm, S.; Krause, S.; Yeh, G. S. Y. *J. Polym. Sci. Polym. Lett. Ed.* **1976**, *14*, 195.

40. Hupfer, B.; Ringsdorf, H. *Polymeric Monolayers and Liposomes as Models for Biomembranes and Cells; ACS Symp. Ser.; No. 175*; American Chemical Society: Washington, DC, 1981.

41. Jones, R.; Tredgold, R. H. *J. Phys. D: Appl. Phys.* **1988**, *21*, 449.

42. Keller, A.; Priest, D. J. *J. Polym. Sci. Part C* **1970**, *8*, 13.

43. Lambeek, G.; Vorenkamp, E. J.; Schouten, A. J. *Macromolecules* **1995**, *28*, 2023.

44. Lavigne, P.; Tancrede, P.; Lamarche, F.; Grandbois, M.; Salesse, C. *Thin Solid Films* **1994**, *242*, 229.

45. Lavigne, P.; Tancrede, P.; Lamarche, F.; Max, J. *Langmuir* **1992**, *8*, 1988.

46. Lee, S.; Dutcher, J. R.; Stegeman, G. I.; Duda, G.; Wegner, G.; Knoll, W. *Phys. Rev. Lett.* **1993**, *70*, 2427.

47. Lemoigne, M. *Ann. Inst. Past.* **1925**, *39*, 144.

48. Li, M.; Rice, S. A. *J. Chem. Phys.* **1996**, *104*, 6860.

49. Malcolm, B. R. *J. Colloid Interface Sci.* **1985**, *104*, 520.

50. Malcolm, B. R. *Nature (London)* **1962**, *195*, 901.

51. Malcolm, B. R. *Polymer* **1966**, *7*, 595.

52. Malcolm, B. R. *Proc. Roy. Soc. (London)* **1968**, *A305*, 363.

53. Mathauer, K.; Mathy, A.; Bubeck, C.; Wegner, G. *Thin Solid Films* **1992**, *210/211*, 449.

54. Mathy, A.; Mathauer, K.; Wegner, G.; Bubeck, C. *Thin Solid Films* **1992**, *215*, 98.

55. Menzel, H.; Hallensleben, M. L. *Polym. Bull.* **1991**, *27*, 89.

56. Menzel, H.; Hallensleben, M. L.; Schmidt, A.; Knoll, W.; Fischer, T.; Stumpe, J. *Macromolecules* **1993**, *26*, 3644.

57. Menzel, H.; McBride, J. S.; Weichart, B.; Ruther, M. *Thin Solid Films* **1996**, *284-285*, 640.

58. Menzel, H.; Weichart, B.; Hallensleben, M. L. *Polym. Bull.* **1992**, *27*, 637.

59. Menzel, H.; Weichart, B.; Hallensleben, M. L. *Thin Solid Films* **1993**, *223*, 181.

60. Menzel, H.; Weichart, B.; Schmidt, A.; Paul, S.; Knoll, W.; Stumpe, J.; Fischer, T. *Langmuir* **1994**, *10*, 1926.

61. Merrick, J. *Photosynth. Bact.* **1978**, *199*, 219.

62. Mitomo, H.; Barham, P. J.; Keller, A. *Sen-i Gakkaishi* **1986**, *42*, T-589.

63. Miyazawa, T.; Blout, E. R. *J. Am. Chem. Soc.* **1961**, *83*, 712.

64. Mizushima, S. I.; Shimanouchi, T. *J. Am. Chem. Soc.* **1949**, *71*, 1320.

65. Muller, M.; Zentel, R. *Makromol. Chem.* **1992**, *194*, 101.

66. Mumby, S. J. *Macromolecules* **1986**, *19*, 1054.

67. Neuman, R. D.; Fereshtehkhou, S. *J. Colloid Interface Sci.* **1988**, *125*, 34.

68. Nobes, G. A. R.; Holden, D. A.; Marchessault, R. H. *Polymer* **1994**, *35*, 435.

69. Orts, W. J.; Marchessault, R. H.; Bluhm, T. L.; Hamer, G. K. *Macromolecules* **1990**, *23*, 5368.

70. Painter, P. C.; Mosher, L. E.; Rhoads, C. *Biopolymers* **1982**, *21*, 1469.

71. Patten, T. E.; Novak, B. M. *J. Am. Chem. Soc.* **1996**, *118*, 1906.

72. Patten, T. E.; Novak, B. M. *Macromolecules* **1993**, *26*, 436.

73. Peticolas, W. L.; Hibler, G. W.; Lippert, J. L.; Peterlin, A.; Olf, H. *Appl. Phys. Lett.* **1971**, *18*, 87.

74. Porter, R. S.; Wang, L. *J. Macromol. Sci.-Rev.* **1995**, *C35(1)*, 63.

75. Rabolt, J. F.; Fanconi, B. *J. Polym. Sci. Polym. Lett. Ed.* **1977**, *15*, 121.

76. Rabolt, J. F.; Fanconi, B. *Polymer* **1977**, *14*, 491.

77. Rabolt, J. F.; Twieg, R. *J. Chem. Phys.* **1982**, *76*, 1646.

78. Rabolt, J. *J. Polym. Sci. Polym. Phys. Ed.* **1979**, *17*, 1457.

79. Ren, Y. Thesis, University of Massachusetts, 1995.

80. Ren, Y.; Meuse, C. W.; Hsu, S. L. *J. Phys. Chem.* **1994**, *98*, 8424.

81. Ren, Y.; Shoichet, M. S.; McCarthy, T. J.; Stidham, H. D.; Hsu, S. L. *Macromolecules* **1995**, *28*, 358.

82. Renugopalakrishnan, V.; Collette, T. W.; Carreira, L. A.; Bhatnagar, R. S. *Macromolecules* **1985**, *18*, 1786.

83. Roberts, G. *Langmuir-Blodgett Films*; Plenum Press: New York, 1990.

84. Sakurada, I.; Ito, T.; Nakamae, K. In *U.S.-Japan Seminar in Polymer Physics (J. Polym. Sci. C, 15)*; R. S. Stein and S. Onogi, Ed.; Interscience: New York, 1966; pp 75.

85. Schantz, S.; Torell, L. M.; Stevens, J. R. *J. Appl. Phys.* **1988**, *64*, 2038.

86. Schaufele, R. F. *J. Chem. Phys.* **1967**, *47*, 3605.

87. Schaufele, R. F.; Shimanouchi, T. *J. Chem. Phys.* **1967**, *47*, 3605.

88. Schmidt, A.; Mathauer, K.; Reiter, G.; Foster, M. D.; Stamm, M.; Wegner, G.; Knoll, W. *Langmuir* **1994**, *10*, 3820.

89. Schwartz, D. K.; Schlossman, M. L.; Pershan, P. S. *J. Chem. Phys.* **1992**, *96*, 2356.

90. Schwiegk, S.; Vahlenkamp, T.; Xu, Y.; Wegner, G. *Macromolecules* **1992**, *25*, 2513.

91. Shimanouchi, T.; Tasumi, M. *Indian J. Pure Appl. Phys.* **1971**, *9*, 953.

92. Snyder, R. G.; Krause, S. J.; Scherer, J. R. *J. Polym. Sci. Polym. Phys. Ed.* **1978**, *16*, 1593.

93. Snyder, R. G.; Strauss, H. L.; Alamo, R.; Mandelkern, L. *J. Chem. Phys.* **1994**, *100*, 5422.

94. Snyder, R. G.; Strauss, H. L.; Elliger, C. A. *J. Phys. Chem.* **1982**, *86*, 5145.

95. Sohn, D.; Yu, H.; Nakamatsu, J.; Russo, P. S.; Daly, W. H. *J. Polym. Sci., Polym. Phys. Ed.* **1996**, *34*, 3025.

96. Song, K.; Krimm, S. *J. Polym. Sci. Polym. Phys. Ed.* **1990**, *28*, 63.

97. Stein, R. S. *J. Polym. Sci.* **1958**, *XXXI*, 327.

98. Stein, R. S. *J. Polym. Sci.* **1958**, *XXXI*, 335.

99. Stein, R. S. *J. Polym. Sci.* **1961**, *L*, 339.

100. Strobl, G. R.; Eckel, R. *Colloid Polym. Sci.* **1980**, *258*, 570.

101. Stumpe, J.; Fischer, T.; Menzel, H. *Macromolecules* **1996**, *29*, 2831.

102. Swalen, J. D. *J. Mol. Electron.* **1986**, *2*, 155.

103. Takeda, F.; Matsumoto, M.; Takenaka, T.; Fujiyoshi, Y. *J. Colloid Interface Sci.* **1981**, *84*, 220.

104. Takenaka, T.; Harada, K.; Matsumoto, M. *J. Colloid Interface Sci.* **1980**, *73*, 569.

105. Teerenstra, M. N.; Hagting, J. G.; Oostergetel, G. T.; Schouten, A. J.; Devillers, M. A. C.; Nolte, R. J. M. *Thin Solid Films* **1994**, *248*, 110.

106. Tieke, B. *Adv. Polym. Sci.* **1985**, *71*, 79.

107. Tredgold, R. H.; Jones, R. *Langmuir* **1989**, *5*, 531.

108. Tsuboi, M. *J. Polym. Sci.* **1962**, *59*, 139.

109. Tsukruk, V. V.; Foster, M. D.; Reneker, D. H.; Schmidt, A.; Knoll, W. *Langmuir* **1993**, *9*, 3538.

110. Tsukruk, V. V.; Foster, M. D.; Reneker, D. H.; Schmidt, A.; Wu, H.; Knoll, W. *Macromolecules* **1994**, *27*, 1274.

111. Ulman, A. *An Introduction to Ultrathin Organic Films*; Academic Press: Boston, 1991.

112. Vahlenkamp, T.; Wegner, G. *Macromol. Chem. Phys.* **1994**, *195*, 1933.

113. Vierheller, T. R.; Foster, M. D.; Schmidt, A.; Mathauer, K.; Knoll, W.; Wegner, G.; Satija, S.; Majkrzak, C. F. *Macromolecules* **1994**, *27*, 6893.

114. Wang, Y. K.; Shu, P. H. C.; Stein, R. S.; Hsu, S. L. *J. Polym. Sci. Polym. Phys. Ed.* **1980**, *18*, 2287.

115. Wang, Y.; Waldman, D.; Lasch, J.; Stein, R. S.; Hsu, S. L. *Macromolecules* **1982**, *15*, 1452.

116. Watanabe, J.; Ono, H.; Uematsu, I.; Abe, A. *Macromolecules* **1985**, *18*, 2141.

117. Watanabe, J.; Takashina, Y. *Macromolecules* **1991**, *24*, 3423.

118. Wegner, G. *Ber. Bunsenges. Phys. Chem.* **1991**, *95*, 1326.

119. Wegner, G. *Thin Solid Films* **1992**, *216*, 105.

120. Weis, R. M. *Chem. Phys. Lipids* **1991**, *57*, 227.

121. Weissbuch, I.; Leveiller, F.; Jacquemain, D.; Kjaer, K.; Als-Nielsen, J.; Leiserowitz, L. *J. Phys. Chem.* **1993**, *97*, 12858.

122. Wilson, E. B.; Decius, J. C.; Cross, P. C. *Molecular Vibrations*; McGraw-Hill: New York, 1955.

123. Woodward, L. A.; Long, D. A. *Trans. Faraday Soc.* **1949**, *45*, 1131.

124. Yase, K.; Schwiegk, S.; Lieser, G.; Wegner, G. *Thin Solid Films* **1992**, *213*, 130.

125. Yokomori, Y.; Uematsu, Y.; Uematsu, I. *Rep. Prog. Polym. Phys. Jpn.* **1972**, *15*, 633.

126. Yokouchi, M.; Chatani, Y.; Tadokoro, H.; Teranishi, K.; Tani, H. *Polymer* **1973**, *14*, 267.

127. Yoon, S. Thesis, University of Massachusetts, 1995.

128. Zachariades, A. E.; Mead, W. T.; Porter, R. S. *Chem. Rev.* **1980**, *80*, 351.